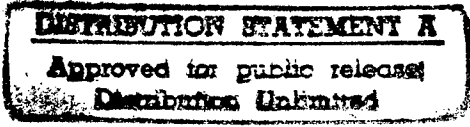


REPORT DOCUMENTATION PAGE			Form Approved OMB No. 0704-0188	
Public reporting burden for this collection of information is estimated to average 1 hour per response, including the time for reviewing instructions, searching existing data sources, gathering and maintaining the data needed, and completing and reviewing the collection of information. Send comments regarding this burden estimate or any other aspect of this collection of information, including suggestions for reducing this burden, to Washington Headquarters Services, Directorate for Information Operations and Reports, 1215 Jefferson Davis Highway, Suite 1204, Arlington, VA 22202-4302, and to the Office of Management and Budget, Paperwork Reduction Project (0704-0188), Washington, DC 20503.				
1. AGENCY USE ONLY (Leave blank)		2. REPORT DATE 17 Jan 97		3. REPORT TYPE AND DATES COVERED
4. TITLE AND SUBTITLE A Study of Mobile Trough Genesis Over The Yellow Sea-East china Sea Region			5. FUNDING NUMBERS	
6. AUTHOR(S) Keith Nickolas Komar				
7. PERFORMING ORGANIZATION NAME(S) AND ADDRESS(ES) Texas A&M University			8. PERFORMING ORGANIZATION REPORT NUMBER 97-001	
9. SPONSORING/MONITORING AGENCY NAME(S) AND ADDRESS(ES) DEPARTMENT OF THE AIR FORCE AFIT/CIA 2950 P STREET WPAFB OH 45433-7765			10. SPONSORING/MONITORING AGENCY REPORT NUMBER	
11. SUPPLEMENTARY NOTES				
12a. DISTRIBUTION AVAILABILITY STATEMENT Unlimited			12b. DISTRIBUTION CODE	
<div style="text-align: center;">  </div>				
13. ABSTRACT (Maximum 200 words)				
<div style="font-size: 2em; font-weight: bold;">19970128 150</div>				
14. SUBJECT TERMS			15. NUMBER OF PAGES 126	
			16. PRICE CODE	
17. SECURITY CLASSIFICATION OF REPORT		18. SECURITY CLASSIFICATION OF THIS PAGE	19. SECURITY CLASSIFICATION OF ABSTRACT	20. LIMITATION OF ABSTRACT

**A STUDY OF MOBILE TROUGH GENESIS OVER
THE YELLOW SEA-EAST CHINA SEA REGION**

A Thesis

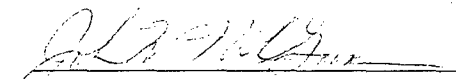
by

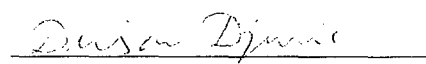
KEITH NICKOLAS KOMAR

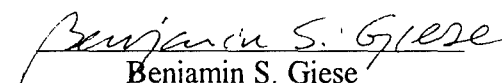
Submitted to Texas A&M University
in partial fulfillment of the requirements
for the degree of

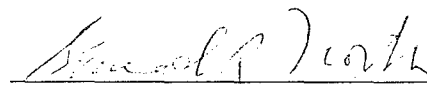
MASTER OF SCIENCE

Approved as to style and content by:


John W. Nielsen-Gammon
(Chair of Committee)


Dusan Djuric
(Member)


Benjamin S. Giese
(Member)


Gerald R. North
(Head of Department)

May 1997

Major Subject: Meteorology

DTIC QUALITY INSPECTED 1

ABSTRACT

A Study of Mobile Trough Genesis over the Yellow Sea-East China Sea Region.

(May 1997)

Keith Nickolas Komar, B. S., Texas A&M University

Chair of Advisory Committee: Dr. John W. Nielsen-Gammon

The purpose of this study was to understand the mechanisms responsible for the formation of mobile troughs over a prolific source region in the Yellow Sea and East China Sea. Two mobile troughs which intensified significantly after formation were analyzed. The troughs were selected from the objective climatology of mobile troughs by Lefevre and Nielsen-Gammon (1995). A quasigeostrophic potential vorticity (QGPV) and associated piecewise tendency diagnosis (PTD) technique developed by Nielsen-Gammon and Lefevre (1995) was used to quantitatively analyze the dynamics of mobile trough formation. The PTD technique involves the inversion of QGPV and QGPV advection. A qualitative approach using dynamical tropopause maps of constant Ertel's potential vorticity (EPV) was utilized in conjunction with the QGPV method.

It was determined that downstream development was the primary mechanism in initiating both mobile troughs. Type A cyclogenesis was not evident in either trough genesis event. A surface cyclone aided the development of one of the mobile troughs, but the cyclone had developed prior to the formation of the mobile trough. Baroclinic processes and large-scale interactions played lesser roles in one trough, but were not

important in the other trough. Barotropic deformation modulated the strength of the second mobile trough by changing the shape of the associated QGPV anomaly. Vertical superposition was important in strengthening the latter stages of the life of the mobile trough, due to two jets superimposing over the mobile trough. Subjective analysis of tropopause maps of both trough genesis events showed the downstream development process as the growth of a new wave by cross-contour advection of potential temperature due to a pre-existing upstream disturbance.

ACKNOWLEDGMENTS

I would like to express my gratitude to Dr. John W. Nielsen-Gammon for his valuable guidance and patience in the preparation of this thesis. I would also like to thank Dr. Dusan Djuric for his expert advice and assistance. I also thank Dr. Giese for his willingness to be on my committee.

I am also grateful for Mr. Robert White's assistance with the department computer resources. The research works of Major Randy Lefevre and Gregory D. McEver laid the groundwork for this study. Also, I thank the United States Air Force for allowing me to further my academic studies here at Texas A&M University.

Lastly, and most important, I would like to thank my wife and true love, Midori, for supporting in too many ways to mention. Her strength of will and her support provided me the motivation to finish this thesis. I also would like to thank her for being a great mother to our newborn daughter, Hannah Mae. May God bless them greatly.

TABLE OF CONTENTS

CHAPTER	Page
I INTRODUCTION.....	1
II BACKGROUND AND MOTIVATION FOR RESEARCH.....	4
1. Knowledge of upper-level mobile troughs.....	4
2. Potential vorticity thinking	9
3. Conceptual models of mobile trough generation	12
4. Motivation for research	15
III DESCRIPTION OF YELLOW SEA-EAST CHINA SEA REGION.....	16
1. Region of study	16
2. Statistical summary of Yellow Sea-East China sea troughs	18
3. Flow regimes associated with trough formation	18
4. Mobile trough paths	20
5. Selection criteria for case studies	22
IV DATA AND METHOD.....	24
1. Data.....	24
2. QGPV height tendency equation.....	25
3. Application of QGPV thinking to piecewise tendency diagnosis.....	27
4. QGPV inversion method	29
5. Basic state and perturbation	30
6. Piecewise inversion method.....	32
7. Application of PTD to case studies.....	33
V CASE STUDY ONE 31 MARCH 1987.....	34
1. Overview of life of mobile trough.....	34
2. Basic state and perturbation fields	40
3. Evaluation of QGPV tendencies	47
4. Piecewise tendencies	49
5. Dynamical tropopause maps.....	71
6. Summary.....	76

CHAPTER	Page
VI CASE STUDY TWO 17 OCTOBER 1988	77
1. Overview of mobile trough.....	77
2. Basic state and perturbation fields	83
3. QGPV tendencies.....	92
4. Tropopause maps.....	95
5. Piecewise tendency diagnosis	100
6. Summary.....	114
VII SUMMARY AND CONCLUSIONS	115
1. Summary.....	115
2. Conclusions.....	117
REFERENCES	119
APPENDIX	123
VITA	126

LIST OF FIGURES

FIGURE		Page
2.1	Frequency of trough genesis during all months throughout the twenty year data set of Lefevre and Nielsen-Gammon's objective climatology of mobile troughs	8
3.1	Map of Yellow Sea-East China Sea region	17
3.2	Map of frequency of mobile troughs that originated in the Yellow Sea-East China Sea region.	21
5.1	The 500 mb geopotential heights and geostrophic vorticity for (a) 870330/0000, (b) 870330/1200, (c) 870331/0000, (d) 870331/1200, (e) 870401/0000, (f) 870401/1200, (g) 870402/0000, (h) 870403/0000.....	35
5.2	The 1000mb heights and 500 mb heights for 870330/0000, 870330/1200, 870331/0000, and 870331/1200.....	39
5.3	Base-state 372 mb QGPV and perturbation 372 mb QGPV for (a) 870331/0000, (b) 870331/1200, (c) 870401/0000, (d) 870401/1200, (e) 870402/0000, (f) 870403/0000.	41
5.4	Base state 372 mb height and perturbation 372 mb height for a) 870331/0000, (b) 870331/1200, (c) 870401/0000, (d) 870401/1200, (e) 870402/0000, (f) 870403/0000	44
5.5	Comparison of observed intensification of trough associated with upper-level small-scale QGPV with intensification rate computed from the quasigeostrophic height tendency equation.....	48
5.6	Quasigeostrophic height tendencies associated with various dynamical processes during the development of the upper-level mobile trough 0000 UTC 31 Mar. 1987 to 0000 UTC 3 Apr. 1987.....	50
5.7	Advections and tendencies associated with downstream development at 00 UTC 31 Mar. 1987.....	52
5.8	Same as for Fig. 5.7, except for 1200 UTC 31 Mar. 1987	53

FIGURE		Page
5.9	Same as for Fig. 5.7, except for 0000 UTC 1 Apr. 1987.....	54
5.10	Same as for Fig. 5.7, except for 1200 UTC 1 Apr. 1987.....	55
5.11	Advections and tendencies associated with baroclinic amplification at 0000 UTC 31 Mar. 1987.	57
5.12	Same as Fig. 5.11, except for 1200 UTC 31 Mar. 1987.....	58
5.13	Same as Fig. 5.11, except for 0000 UTC 1 Apr 1987	59
5.14	Same as Fig. 5.11, except for 1200 UTC 1 Apr 1987	60
5.15	Quasigeostrophic height tendency contribution from total deformation term, barotropic, and superposition	61
5.16	Deformation and tendencies associated with basic state flow at 1200 UTC 31 Mar 1987.....	63
5.17	Same as that for Fig. 5.16, except for 0000 UTC 1 Apr. 1987.....	64
5.18	(a) Same as that for Fig. 5.16a, except for 0000 UTC 2 Apr. 1987; (b) same as that for Fig. 5.16a, except for 0000 UTC 3 Apr. 1987.....	65
5.19	Quasigeostrophic height tendency contributions from the fifth term and sixth term of (4.10), and the sum of the two for the 31 March 1987 case.	66
5.20	Advections and tendencies associated with vortex-vortex interactions at 1200 UTC 1 Apr. 1987	67
5.21	Base state 372 mb heights associated with the full inversion of QGPV; and base state 372 mb QGPV associated with the inversion of upper-level QGPV for (a) 0000 UTC 1 Apr. 1987 and (b) 1200 UTC 1 Apr. 1987	69
5.22	(a) Same as that for Fig. 5.21, except for 0000 UTC 2 Apr. 1987. (b) Small-scale height tendencies at 372 mb at 0000 UTC 2 Apr. 1987 associated with the advection of upper-level base state QGPV by winds associated with full inversion of base state QGPV	70

FIGURE		Page
5.23	Maps of tropopause potential temperature and winds for (a) 0000 UTC 30 Mar. 1987, (b) 1200 UTC 30 Mar. 1987, (c) 0000 UTC 31 Mar. 1987, (d) 1200 UTC 31 Mar. 1987	73
6.1	The 500 mb geopotential heights and geostrophic vorticity for (a) 881017/1200, (b) 881017/1800, (c) 881018/0000, (d) 8810/0600, (e) 881018/1200, (f) 881019/0000, (g) 881019/1200, (h) 881020/0000	78
6.2	The 1000mb heights and 500 mb heights for 881017/1200, 881018/0000, 881018/1200, and 881019/0000	82
6.3	(a) 437 mb QGPV for 1017/1800; (b) 437 mb QGPV base state and perturbation 437 mb QGPV for 881017/1800; (c) same as (a) except for 881018/1800, (d) same as (b) except for 881018/1800; (e) same as (a) except for 881019/0600; (f) same as (b) except for 881019/0600; (g) same as (a) except for 881019/0600; (h) same as (b) except for 881019/1800	84
6.4	Basic state 437 mb height and perturbation 437 mb height for (a) 881017/1800, (b) 881018/0000, (c) 881018/1200, (d) 881019/0000, (e) 881019/0600, (f) 881019/1200	89
6.5	Comparison of observed intensification of trough associated with upper-level small-scale QGPV with intensification rate computed from the quasigeostrophic height tendency equation (4.10)	93
6.6	Perturbation height and perturbation QGPV at 437 mb for 881018/1200	94
6.7	Maps of tropopause potential temperature and winds for (a) 1200 UTC 17 Oct. 1988, (b) 1800 UTC 17 Oct. 1988, (c) 0000 UTC 18 Oct. 1988, (d) 1200 UTC 18 Oct. 1988, (e) 0000 UTC 19 Oct. 1988, (f) 1200 UTC 19 Oct. 1988	96
6.8	Quasigeostrophic height tendencies associated with various dynamical processes during the development of the upper-level mobile trough, 1800 17 Oct. 1988 to 0000 UTC 21 Oct. 1988	101
6.9	Advections and tendencies associated with downstream development at 1800 UTC 17 Oct. 1988	102
6.10	Same as Fig. 6.9, except for 1800 UTC 19 Oct. 1988	103

FIGURE		Page
6.11	Quasigeostrophic height tendency contribution from barotropic, superposition, and the sum of the two.	105
6.12	Deformation associated with basic state upper-level flow at (a) 881018/0000 and (b) 881018/1200	106
6.13	Same as Fig. 6.12 except for (a) 881018/1800, and (b) 881019/1800	107
6.14	Illustration of superposition process.	108
6.15	Advections and tendencies of large-scale interactions for 1800 UTC 19 Oct 1988.....	111
6.16	Advections and tendencies associated with baroclinic amplification at 1800 UTC 17 Oct. 1988	113

CHAPTER I

INTRODUCTION

Weather forecasters scrutinize upper-level weather charts to determine the strengths and tracks of mobile troughs. These mobile troughs are typically seen traveling through the larger scale waves in the atmosphere. An upper-level mobile trough, also known as a short wave, can be defined as an area of relatively high vorticity with maximum amplitude near the tropopause. Short waves and long waves both propagate westward relative to the mean flow. This is a characteristic of a Rossby wave, which is an absolute vorticity conserving motion that depends on β , the variation of the Coriolis force with latitude. Longer Rossby waves propagate upstream faster so they appear to be stationary or moving slowly upstream. Short waves propagate more slowly so they seem to “ride” along with the mean westerlies. A characteristic wavelength of a mobile trough is generally no more than a few thousand kilometers. The vorticity advection associated with moving short waves is greater than that for longer waves (Carlson 1991, p. 44); therefore, these mobile troughs can play a significant role in many observed weather phenomena, from cyclogenesis (Petterssen 1955) to mesoscale convection (Rhea 1966; Maddox 1983).

Recent research into mobile trough climatology (Sanders 1988; Lefevre and Nielsen-Gammon 1995) has shed new light on the characteristics of mobile troughs.

This thesis follows the style and format of the *Journal of the Atmospheric Sciences*.

Obvious geographic biases of trough formation and termination exist. The Yellow Sea-East China Sea region is one of the more prolific trough genesis areas, as identified by Lefevre and Nielsen-Gammon.

Advancement in knowledge of upper-level mobile troughs that form in this region would benefit numerical weather prediction by gaining insight how mobile troughs form. This region is of particular importance because of the large number of cyclones that develop there throughout most of the year (Chen et al. 1991). This region is home to a baroclinic zone with a strong jet for most of the year. Understanding the processes associated with trough formation there would lead to a greater understanding of atmospheric circulation.

The goal of this research is to assess the dominant dynamical processes that cause mobile trough genesis over the Yellow Sea-East China Sea region. This will be accomplished by applying piecewise tendency diagnosis to a number of trough genesis events identified in Lefevre and Nielsen-Gammon's climatology (1995) as forming in that region.

Chapter II provides a brief background of the current knowledge of mobile troughs and discusses the use of potential vorticity inversion in determining the dynamics of mobile trough generation. The chapter then presents issues to be addressed by this work. Chapter III defines the Yellow Sea-East China Sea region and presents a summary of the characteristics of the mobile troughs that form over this area. Chapter IV outlines the method used to calculate QGPV and describes the QGPV height tendency equation. Chapters V and VI investigate two mobile trough genesis events by using the QGPV

height tendency diagnostic technique and by examining tropopause maps. Chapter VII summarizes the major results and conclusions of this research and suggests future work.

CHAPTER II

BACKGROUND AND MOTIVATION FOR RESEARCH

The purpose of this chapter is to provide a basis of what is understood about upper-level mobile troughs and what methods are implemented to study the dynamics of the upper atmosphere. To accomplish this, this chapter briefly gives a chronicle of the body of knowledge concerning upper-level mobile troughs and their relevance to weather. Also, an overview of potential vorticity and the rationale for using it in the study of upper-level mobile trough dynamics is presented. Then, questions are set forth regarding mobile trough genesis over the Yellow Sea-East China Sea.

1. Knowledge of upper-level mobile troughs

a. Early work

Early work on upper-level mobile troughs was primarily limited to their role in cyclogenesis. However, the earliest Norwegian cyclone model of the twentieth century did not explicitly include development in the upper troposphere. Bjerknes (1937) was the first to use sounding data to theorize of the importance of the upper levels of the atmosphere in the development of a surface cyclone. Charney (1947) and Eady (1949) developed baroclinic instability theory, which provided for development at upper and lower levels simultaneously.

However, early observational studies showed that many cyclogenesis events began with a preexisting upper-level mobile trough. Petterssen (1955) noted that over the United States cyclogenesis typically occurred when an area of upper-level cyclonic

vorticity advection associated with an advancing preexisting mobile trough became superposed over a low-level baroclinic zone. Petterssen and Smebye (1971) showed that many cyclogenesis events began with a pre-existing upper-level mobile trough of significant amplitude. They classified this as Type B, to distinguish them from the more classical cyclones which developed simultaneously at all levels (Type A).

b. Recent research

Recent research has shown that Type A cyclogenesis is rare, and likely improbable, in the atmosphere. Sanders (1986) found that upper-level development preceded cyclogenesis in the cases he examined. Wash et al. (1988) detected preexisting vorticity centers of significant amplitude when examining Type A cyclones.

Interest of late in the fundamental aspects of upper-tropospheric mobile troughs has been stimulated by a climatological study by Sanders (1988). He provided the first synoptic climatological study of 500 mb mobile troughs. He subjectively identified and tracked troughs found along the 552 dam geopotential height contour of the 500 mb surface on daily Northern Hemisphere charts. The study of a particular cold season showed a median duration for mobile troughs to be 12 days with a mode of 5 days. Average zonal phase speed was 13 m s^{-1} . Sanders discovered that preferred regions of trough genesis exist over and east of mountain ranges. Trough terminations occurred predominately over the eastern portions of oceans. Additionally, troughs were typically born in large scale northwesterly flow and died in southwesterlies. Sanders speculated that baroclinic and barotropic processes were operating in a detailed study of composited trough genesis episodes.

The theoretical aspects of upper-level mobile trough development were also being examined at that time. Snyder and Linden (1988) and Staley (1988) studied baroclinic instability with energy primarily found at upper levels. Farrell (1989) showed that properly oriented, i.e., elongated, disturbances can be made more compact by large-scale deformation, resulting in an increase in the kinetic energy associated with the disturbance. Rivest and Farrell (1992) described initial conditions that lead to the rapid intensification of upper-level mobile troughs. Within a two-dimensional, periodic system, they found that optimal growth during a specified period of time is achieved by a combination of cross-gradient potential vorticity (PV) advection and superposition. A series of upshear tilted vortices are deformed by the background flow while they excite a Rossby wave along the tropopause. Rivest et al. (1992) modeled the observed long duration of mobile troughs with concentrated PV gradients at the tropopause. Whitaker and Barcilon (1992) considered modal instability as a possible cause of development aloft without appreciable surface intensification. They used basic states with weak baroclinicity at low levels and investigated the effects of a shallow stable layer at the surface and enhanced surface friction. Both effects produced the largest amplitudes at upper levels. Work from Orlanski and collaborators (Orlanski and Katzfey 1991; Orlanski and Chang 1993; Orlanski and Sheldon 1993; and Chang 1993) using energetics showed that upper-level mobile troughs can be generated by transfer of energy from upstream baroclinically growing waves.

Lefevre and Nielsen-Gammon (1995), hereafter LNG, developed an objective climatology of northern hemisphere mobile troughs using the 500 mb pressure surface. The gross results were similar to Sanders'. Locations of trough genesis and termination

were also associated with geography. Preferred genesis regions included the lee of the Rocky Mountains, the Mediterranean Sea, and Southeast Asia. Preferred termination regions were the eastern Pacific Ocean, the Mediterranean Sea, and Southwest Asia. However, LNG found a geometric distribution of life span with a mean of 5.3 days and a median of 4 days. Their objective method was better able to track troughs which formed far from the 552 dam contour of the 500 mb pressure surface.

Figure 2.1 shows the frequency of trough genesis over the Northern Hemisphere from LNG's results. There is a pronounced local maximum of mobile trough formation centered over the Yellow Sea and East China Sea immediately downstream of another maximum over the Mongolian Plateau. The maximum that extends over the Yellow Sea and East China Sea is the only region of enhanced mobile trough formation which is located off the east coast of a significant land mass. Other trough genesis maxima are located either to the lee of large mountain ranges or on the west coasts of continents.

Nielsen-Gammon (1995) conceptualized existing theories on mobile trough formation in terms of the generation of waves along the tropopause potential vorticity discontinuity. These models were then tested on a case of mobile trough formation. It was found that the trough formed primarily by Rossby wave propagation along the tropopause from a cutoff cyclone developing to the west. Both vertical and horizontal propagation contributed to the development. Superposition of potential vortices due to vertical shear and horizontal deformation also aided in the development.

Nielsen-Gammon and Lefevre (1996) diagnosed a particular case of mobile trough genesis using piecewise tendency diagnosis, PTD. PTD is an extension of piecewise

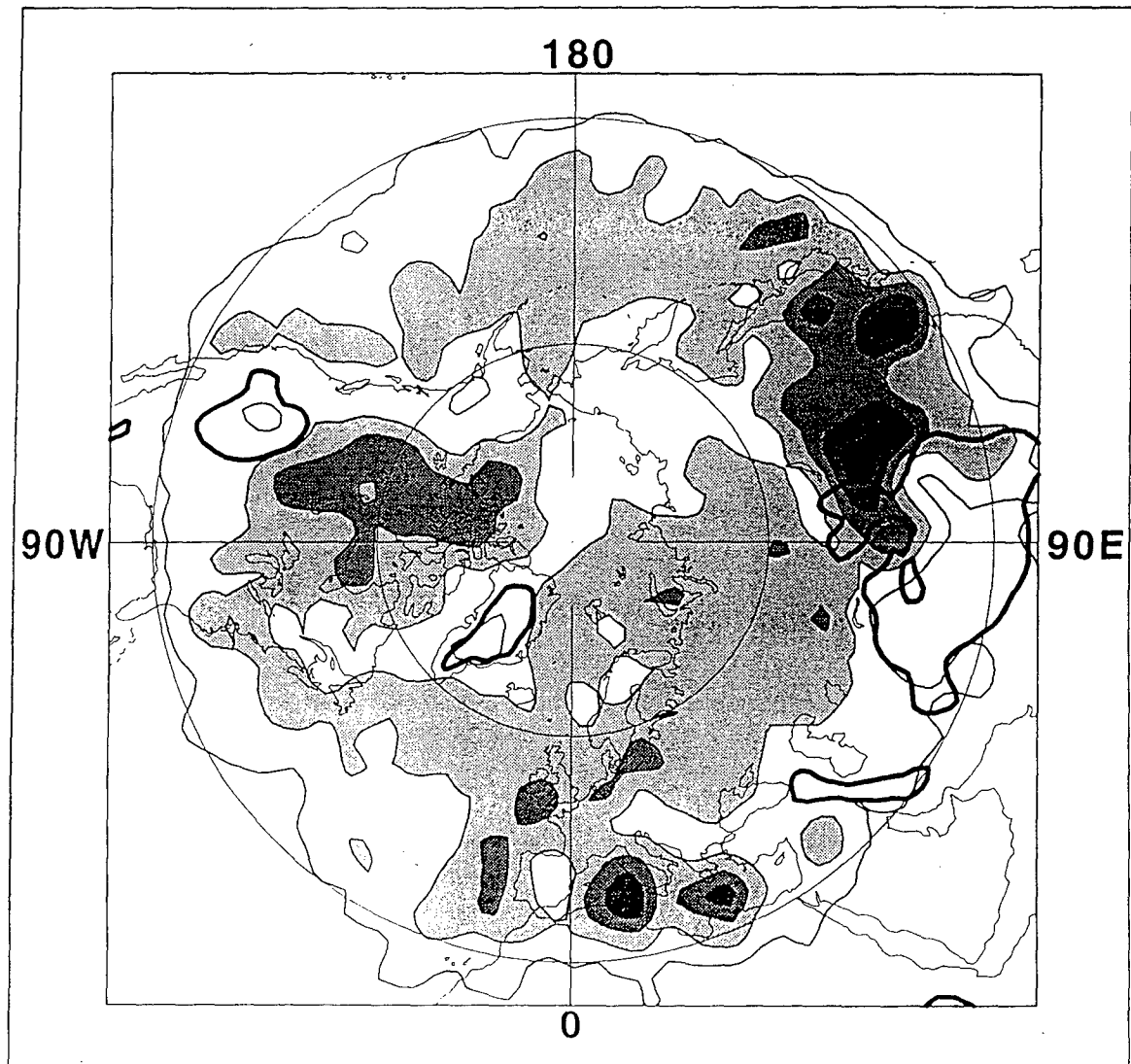


Fig. 2.1. Frequency of trough genesis during all months throughout the twenty year data set of Lefevre and Nielsen-Gammon's objective climatology of mobile troughs. The solid contour shading represents 10, 15, 20, and 25 events per 10^6 km² per year, respectively. The thick contours encircle elevated terrain higher than 2000 meters. (Adapted from Lefevre 1995).

potential vorticity inversion applied to height tendencies, with the forcing terms in the quasigeostrophic height tendency equation partitioned into potential vorticity advection associated with distinct dynamical processes. The trough they studied was formed primarily through downstream propagation of Rossby wave energy and secondarily by deformation. Baroclinic effects played a role later in the life of the trough with the development of a surface cyclone.

Other research under the direction of Nielsen-Gammon used PTD to further investigate mobile troughs and extratropical cyclones. An investigation of mobile trough formation over the Mongolian Plateau (McEver 1996) found that downstream propagation of Rossby wave energy initiated two of the three cases studied. Deformation and superposition also aided development. Cyclogenesis was examined with PTD on three cases, showing that Type B cyclogenesis was evident (Gold 1996). The upper-level dynamics was the primary cyclogenetical forcing.

The importance of understanding mobile troughs apparently cannot be underestimated. As we attempt to learn more about cyclogenesis, understanding how the upper levels of the atmosphere develop appears to be the key factor. Our knowledge of mobile troughs has been greatly expanded in recent years, but much more remains unknown. Variations of downstream development and deformation processes appear to be the predominant factors in a number of mobile trough case studies so far. Might this be a consistent pattern of development?

2. Potential vorticity thinking

This section relies on the theoretical foundation set forth by Hoskins et al. (1985). They applied potential vorticity thinking to the dynamics of observed atmospheric flows.

An explanation of the nature of potential vorticity is given. The two different types of potential vorticity used in this research will be introduced. Then, the rationale for using a potential vorticity framework to assess the dynamics of mobile troughs is explained.

Potential vorticity is a measure of the ratio of the absolute vorticity to the effective depth of the vortex. The advantage of using potential vorticity in examining dynamical phenomena in the atmosphere is that the complete kinematic structure of the atmosphere can be determined by inverting, or solving the potential vorticity equation. The use of potential vorticity allows investigation of mobile trough dynamics which are not so easily addressed using conventional techniques such as the traditional form of the omega equation. The ability to assess and isolate the direct effects of upper-level phenomena and the ability to track potential vorticity anomalies through time makes the use of potential vorticity desirable in this study.

The isentropic coordinate form of potential vorticity is Ertel's potential vorticity

$$(EPV): \quad P = (\zeta_\theta + f) \left(-g \frac{\partial \theta}{\partial p} \right) \quad (2.1)$$

P is potential vorticity, ζ_θ is vorticity in isentropic coordinates, f is the Coriolis parameter, g is acceleration due to gravity, and the stability term, $\frac{\partial \theta}{\partial p}$, is a measure of the effective depth between potential temperatures surfaces measured in pressure coordinates.

A form of potential vorticity can also be derived in the quasigeostrophic framework (Charney and Stern 1962) and can be given as:

$$q \equiv \frac{g}{f_0} \nabla^2 z + f + g f_0 \frac{\partial}{\partial p} \left(\frac{1}{\sigma} \frac{\partial z}{\partial p} \right) \quad (2.2)$$

In (2.2) q is QGPV, z is height in isobaric coordinates, f_0 is the reference Coriolis parameter ($1 \times 10^{-4} \text{ s}^{-1}$), p is pressure, and σ is a measure of static stability. The three parts of the right hand side of (2.2) are respectively relative vorticity, planetary vorticity, and stratification. QGPV is derived from the traditional form of the geopotential tendency equation containing vorticity and thickness advections (Holton p. 164). QGPV and EPV are similar in that the advection of Ertel's potential vorticity on an isentropic surface is approximately proportional to the advection of QGPV on a pressure surface.

The quasigeostrophic (QG) perspective of potential vorticity will be used in this research in a quantitative sense to assess the development of upper-level mobile troughs. The advantage of QG diagnostics is its simplicity. QGPV is conserved following geostrophic motions allowing PV anomalies to be tracked through time and space. The inversion operator is linear allowing for unambiguous attribution of particular troughs to particular PV anomalies. The idea underlying potential vorticity inversion is that the three-dimensional distribution of QGPV, with appropriate boundary conditions, determines the balanced large-scale winds and temperatures of the atmosphere. Therefore, when equation 2.2 is inverted, or solved, for z , the resulting height field will supposedly be an exact replica of the original height field.

For the quantitative work with QGPV, full conservation will be assumed. In the diagnostics presented here, the advection of QGPV is assumed to be the sole forcing in the atmosphere. QGPV diagnostics will then show the intensification of a system by the amplification or redistribution of QGPV.

Since the QGPV inversion is linear, the atmosphere may be easily partitioned. The sum of the effects of the individual levels will equal the total effect of QGPV; hence, piecewise diagnosis is made possible. Therefore, the effects of the upper and lower levels of the atmosphere can be separated and studied in isolation.

The limitations of QGPV are the same as those of the basic quasigeostrophic assumptions. The only vertical or ageostrophic motions allowed are for maintaining thermal wind balance. The ageostrophic motions of the atmosphere must be much smaller than the geostrophic motion. Since QGPV is representative of large-scale geostrophic motions, its use is primarily limited to large-scale dynamics in the atmosphere.

Wavelike patterns in the QGPV field can appear as “troughs” and “ridges”. However, a trough extending southward from the pole in the QGPV field actually corresponds to an area of larger values of QGPV. The reason for the “trough” terminology is that large QGPV anomalies, like vorticity maxima, are usually associated with a trough in the geopotential height field. So “troughs” in the QGPV field are areas of larger values, while “ridges” protruding from the south are areas of lower values. Anomalies with positive values of QGPV imply cyclonic flow while negative anomalies show anticyclonic flow.

3. Conceptual models of mobile trough generation

This section provides the framework for explaining PV thinking. A paradigm of a potential vorticity gradient along the tropopause is used. The models presented here are from Nielsen-Gammon (1995).

Two fundamental processes are responsible for wave generation along potential vorticity gradients. In the first, advective flow induced by PV anomalies “blows” across

the basic state gradient, carrying higher or lower PV with it, and can amplify the perturbations. In the second, the PV anomalies do not grow, but the height field is changed due to the reconfiguration of PV anomalies. Four conceptual models are now cast in terms of "PV thinking."

a. Modal instability

Modal instability builds anomalies with energy extracted from the mean flow. Theoretical models include Charney's (1947) and Eady's (1949) descriptions of baroclinic instability and barotropic instability as proposed by Kuo (1949).

Baroclinic instability requires opposite-signed gradients of potential vorticity, or its surrogate, at different isentropic levels. In the atmosphere, this configuration is seen as a tropopause PV gradient and a surface potential temperature gradient. With a proper phase shift, winds associated with the upper-level Rossby wave act to amplify the wave along the surface frontal zone. The lower-level Rossby wave likewise acts, to a lesser degree, to enhance the PV advections that strengthen the upper wave.

Barotropic instability involves the reversal of the PV gradient within a given isentropic layer. The mechanism of barotropic instability is similar to that of baroclinic instability except that it operates on one particular level, such as the upper troposphere.

b. Non-modal growth

Rivest and Farrell (1992) argued that modal instability is not a significant contributor to atmospheric development. They observe that the most unstable wavelengths tend to be too large and that observed disturbances are capable of growing much more rapidly than the most unstable mode for a finite period of time. They see this

inconsistency as an initial condition problem that can lead to rapid, transient intensification of upper-level mobile troughs.

The process described by Rivest and Farrell can be more easily explained as a vortex interacting with a PV gradient. For example, consider an isolated vortex approaching an upper-level PV gradient from the south. Its associated winds generate a wave along the jet, which grows more and more rapidly as the vortex is drawn closer. The southerlies associated with the developing wave accelerate the vortex northward toward the jet allowing stronger cross-gradient advections but speeding the eventual incorporation of the vortex into the westerlies.

c. Propagation of wave energy

This model involves a preexisting disturbance embedded within a PV gradient. Additional wave crests and troughs will appear downstream, but not upstream, because of the eastward group velocity of Rossby waves in the upper troposphere. As a result of this process, the upstream disturbance will weaken.

A closely related theory is downstream baroclinic development formulated by Orlanski and collaborators (Orlanski and Katzfey 1991; Orlanski and Chang 1993; Orlanski and Sheldon 1993; and Chang 1993). Like the group velocity mechanism, wave energy propagates downstream at upper levels, but the source of energy is the unstable baroclinic growth of an initial, preexisting disturbance.

d. Superposition

Superposition involves the increase of circulation due to a reconfiguration of the PV anomalies, rather than an increase in magnitudes of the anomalies. Farrell (1989) showed that a suitably configured disturbance in deformation flow can undergo energy

growth associated with a change in shape. For a wave on a localized PV gradient, the situation corresponds to an initially small-amplitude wave on an east-west jet which is embedded in diffuence. This diffuence causes the wavelength to decrease while the north-south extent of the wave increases. The anomalous PV becomes more compact allowing the circulations associated with the PV to increase. Thus the kinetic energy associated with the wave increases. If the process continues, the effect reverses, and the wave would become elongated along the north-south axis, hence weakening the kinetic energy of the wave.

4. Motivation for research

The goal of this research will be to ascertain whether there is a common dynamical cause for mobile troughs which form over the Yellow Sea-East China Sea region. Another problem to be addressed is the existence of this local maximum of trough genesis frequency over a predominately marine environment when most maxima are just downstream of major mountain ranges. With an ever-present baroclinic zone, and a high level of upper-level trough formation and surface cyclogenesis, it is plausible that this region would generate Type A cyclogenesis. This research will examine the case studies to see if baroclinic instability is indeed a prevailing factor in upper-level dynamics. Deformation may also be important due to the presence of a strong jet over the study region during the cold season. Another maximum of trough genesis is located approximately thirty degrees longitude upstream of the area of interest (LNG). It is hypothesized that downstream Rossby wave development could be responsible for the downstream region of trough formation.

CHAPTER III

DESCRIPTION OF YELLOW SEA-EAST CHINA SEA REGION

This chapter explains the rationale in selecting the Yellow Sea-East China Sea region to study mobile troughs. To accomplish this objective, the large-scale flow conditions over the region are described. Next, a statistical summary of the mobile troughs that form there are given. Predominant large-scale flow regimes that are associated with mobile trough formation are described. Lastly, a brief synopsis follows of the criteria used in selecting appropriate cases to investigate.

1. Region of study

The Yellow Sea-East China Sea region is defined for this study as the area encompassed by 30° N to 39° N and 120° E to 130° E (Fig 3.1). It includes most of the Korean peninsula, the Yellow Sea, and the northern part of the East China Sea. This region was selected for study because of its pronounced maximum of trough formation as identified by LNG (1995). This region is noted for its prolific cyclogenesis (e.g., Chen et al. 1991).

The Yellow Sea-East China Sea region encompasses a strong baroclinic zone typically from early fall through late spring. This strong thermal contrast is a result of the juxtaposition of the study region between the large, cold northern Asian continent and the warm tropics directly to the south. Thus, an entrance region to the strongest mean jet on earth (over 80 m s^{-1}) is often seen in the study region. Also, the climatological flow at upper levels exhibits confluence from air deflected around the Himalayan

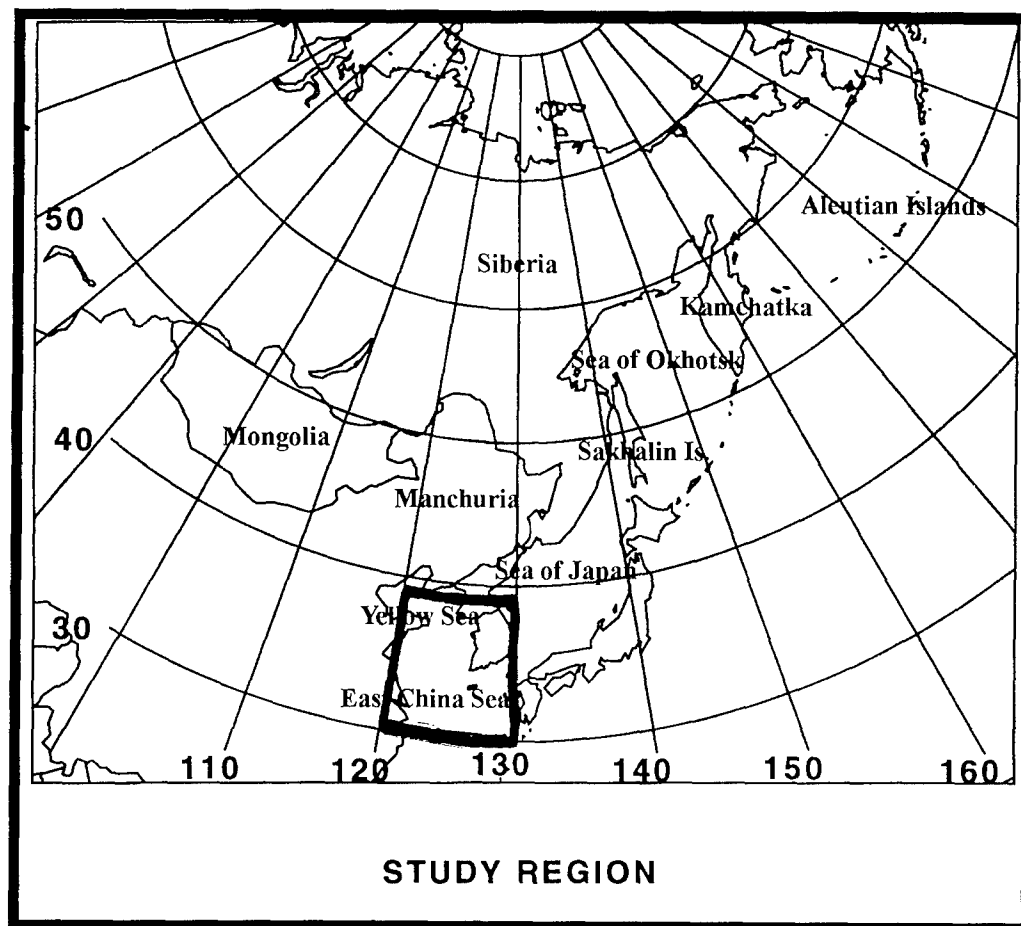


Fig. 3.1 Map of Yellow Sea-East China Sea region. The study region is outlined by the heavy line and is encompassed by 30°N and 39°N and 120°E and 130°E.

highlands (Wallace et al. 1991).

2. Statistical summary of Yellow Sea-East China Sea troughs

LNG's objective climatology (1995) is the basis for the summary statistics provided in this section. Over the 20-year climatology, 456 troughs were initiated in the Yellow Sea-East China Sea region. Based on area, this region is four times more likely than average to initiate a mobile trough.

The mean life span of mobile troughs that form in this region is 5.4 days, which is similar to the hemispheric average of 5.3 days. The longest-lived trough lasted 19.5 days. The median life span was 4 days, the same as that for the complete objective climatology.

Seasonal variations of mobile trough formation were small. Winter (DJF) produced an average of 6.5 troughs. Spring (MAM) averaged 5.6 troughs, summer (JJA), 4.9 troughs, and fall (SON), 5.9 troughs.

3. Flow regimes associated with trough formation

This section describes the patterns of 500 mb flow seen with typical mobile trough formation. The geopotential height and wind fields of thirty-eight different trough genesis events were examined for any evidence of preferential large-scale patterns. A majority of the troughs formed in northwesterly flow and died in southwesterlies. Of course, the variability of the atmosphere will subvert attempts to put particular flow patterns into categorical regimes. However, this section is offered for the reader to grasp the variety of large-scale flow associated with mobile trough genesis over the Yellow Sea-East China sea region.

The nature of the large-scale flows associated with trough formation was best categorized by season. In the cold season, approximately mid-October through early

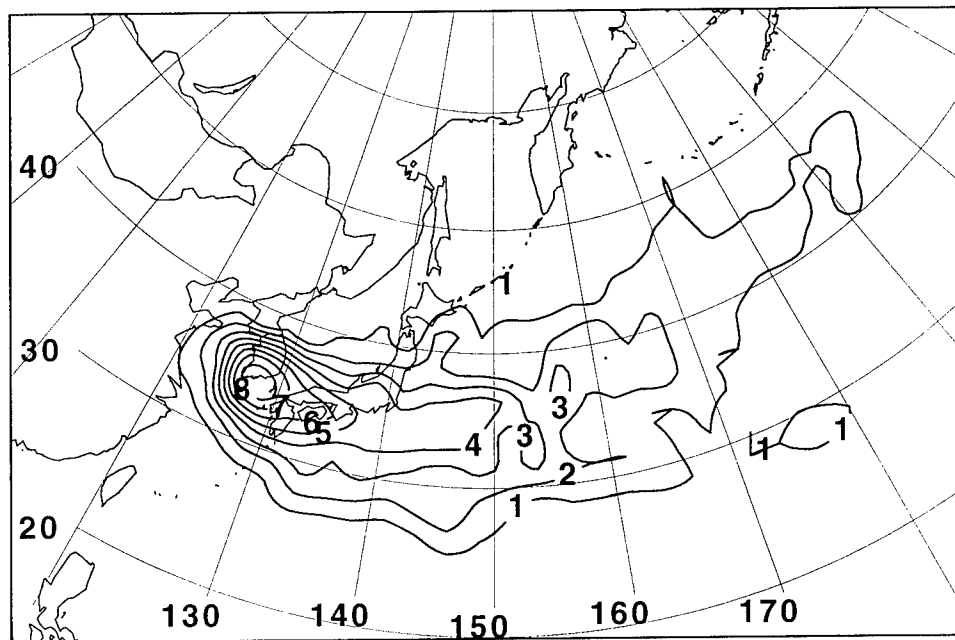
April, two basic flow regimes could be identified in a majority of the mobile trough genesis events examined. The first flow regime was highly meridional due to the presence of a large-scale vortex over eastern Siberia and northern Manchuria. Smaller scale perturbations, or short waves, would develop on the western side of the vortex (over Mongolia and the Yellow Sea-East China Sea region) in large-scale northwesterlies and revolve around the vortex to the east. These short waves would then be ejected out into the zonal flow across the Pacific or track northward towards the Aleutian Islands. Mobile troughs that formed in this flow regime often were associated with surface cyclone development. Some mobile troughs associated with intense surface development evolved into upper-level cyclones over the northern part of the Pacific near the Aleutian Islands.

The second flow regime of the cold season was more zonal in nature. A large-scale trough of weak amplitude was typically located just off the Asian continent. Mobile troughs forming over the study region in this flow regime strengthened little as they traveled to the east over the central part of the Western Pacific. Little surface development was noted with these mobile troughs.

During the warm season the height and temperature gradients weakened considerably. The 500 mb height gradient associated with the polar jet was found farther north and was rarely found to be a factor in trough genesis in the study region. The 500 mb height gradient associated with the subtropical jet was very weak, since the subtropical jet is found at very high altitudes during the warm season. Since mobile troughs require a baroclinic atmosphere, one would expect less mobile trough genesis in the summer. However, in spite of the weaker flow at this time of year, mobile troughs were still being formed.

4. Mobile trough paths

The movement of mobile troughs that formed over the Yellow Sea-East China Sea was tracked to see where a mobile trough travels after it forms. Five years (1984 through 1988) of mobile troughs that formed in the study region were tracked across the Pacific using data from LNG's objective trough tracking algorithm. Figure 3.2 shows a pattern that resembles the mean storm tracks for the Pacific region. The positions of the mobile troughs were available every 12 hours. The paths were made by assuming linear motion between any two 12-hourly positions. The figure was then created by compiling the trough paths and counting the number of times that any path crossed a 2.5° latitude-longitude grid box. The numbers were then contoured. An analysis of the paths of mobile troughs that were born in this area appears to confirm the connections between short waves and surface cyclones. Figure 3.2 is similar to the tracks of coastal cyclones (not shown) detected by Chen et al. (1991).



500 MB TROUGH OCCURRENCES

Fig 3.2. Map of frequency of mobile troughs that originated in the Yellow Sea-East China Sea region. The contours are number of troughs per year computed for a 2.5° by 2.5° grid on a conformal area map.

5. Selection criteria for case studies

This section describes the process that was used to select appropriate cases to investigate. As mentioned previously, 456 troughs were available for study.

Data availability limited the scope of study to troughs that formed during and after 1979. After examining a possible case study from 1979, the analyses to the south of 30° N seem to be filled with anomalous geostrophic vorticity. So, concern with data integrity in the tropics caused the elimination from consideration any troughs that formed before 1984. This left 91 troughs.

The remaining troughs were then evaluated by the strength they possessed through their lifetimes. The measure of trough strength was LNG's Eulerian centripetal acceleration, ECA. Equation 3.1 shows ECA to be the geostrophic wind, V_g , squared, divided by the radius of curvature, R , of the flow.

$$ECA = \frac{V_g^2}{R} \quad (3.1)$$

Any trough that failed to attain $1.0 \times 10^{-3} \text{ m s}^{-2}$ was eliminated. Also, any troughs whose initial ECA was large, over $1.0 \times 10^{-3} \text{ m s}^{-2}$, were discarded to exclude possible instances of trough merger or trough fracture. LNG's tracking algorithm allowed mergers and fractures.

Subjective analyses of 500 mb height and vorticity patterns were used to further filter the total number of possible case studies to eleven. The criteria used at this stage were subjective. If any mobile trough appeared to exist at 500 mb prior to its initialization over the Yellow Sea-East China Sea region, then it was eliminated. This test eliminated possible tracking algorithm errors and cases where interpretations of trough

merger or trough fracture were considered as true trough genesis. These eleven remaining trough genesis events were further evaluated by conducting preliminary partitioning of base state and perturbation height fields.

The two cases to be presented in this research (31 March 1987 and 17 October 1988) represent the two flow regimes noted during cold season mobile trough genesis over the Yellow Sea-East China Sea region.

CHAPTER IV

DATA AND METHOD

This chapter describes the data used in this research and explains the method developed by Nielsen-Gammon and Lefevre (1996) to invert (solve) the QGPV equation. Then, a discussion of the QGPV height tendency equation and the piecewise method used to obtain height tendencies for the selected case studies follows.

1. Data

The data to be used in the March 1987 case study was prepared and maintained as DS082.0 by the Data Support Section, Scientific Computing Division, National Center for Atmospheric Research (NCAR). The twice daily (0000 UTC and 1200 UTC) geopotential height data were extracted from National Center for Environmental Prediction (NCEP) final analyses (Kanamitsu 1989). The final analyses were prepared using 12 vertical levels and an R24 rhomboidal spherical harmonic truncation. Global data at each of ten pressure levels (1000, 850, 700, 500, 400, 300, 250, 200, 150, 100 mb) were archived on a 2.5° by 2.5° rectangular longitude-latitude grid. Data from the northern hemisphere was used in this research. Each time of the data set consists of three-dimensional geopotential height values in a 145 by 37 by 10 matrix.

A second data set was available in the October 1988 case study. The National Center for Environmental Prediction (NCEP) and the National Center for Atmospheric Research (NCAR) are cooperating in a project to produce a 40-year record of global analyses of atmospheric fields (Kalnay et al. 1996). This effort involves the recovery of

data from many different platforms and sources. This data is then put through a quality control procedure and assimilated with a model that is kept unchanged over the analysis period, 1957-96. The model has a T62 triangular spherical harmonic truncation (horizontal resolution of about 210 km) with 28 vertical levels. The availability of these data provides a unique opportunity to compare the results of two different data sets in the same study. The data from the reanalysis project used in this research consisted of Gaussian grids of 192 by 94 global grid points of temperature and specific humidity at 28 sigma levels and surface pressure fields and surface geopotential height fields. Data were available four times daily, every six hours (00, 06, 12, 18 UTC). Geopotential height fields were calculated at sigma boundaries using the hydrostatic and hypsometric equations. The geopotential heights were then interpolated to twelve pressure surfaces (1000, 925, 850, 700, 600, 500, 400, 300, 250, 200, 150, and 100 mb).

2. QGPV height tendency equation

The QGPV height tendency equation developed here follows the method of Nielsen-Gammon and Lefevre (1996). A Laplacian-like operator, \mathbf{L} , is defined as the functional relationship between ϕ and q in (2.2), with the exception that the Coriolis parameter, f , is subtracted from the total QGPV equation. ($\phi = gz$ in the following derivations.)

$$\mathbf{L}(\phi) = q - f = \frac{1}{f_0} \nabla^2 \phi + f_0 \frac{\partial}{\partial p} \left(\frac{1}{\sigma} \frac{\partial \phi}{\partial p} \right) \quad (4.1)$$

The operator \mathbf{L} may be inverted to obtain the geopotential height distribution from the quasigeostrophic potential vorticity, q , distribution.

$$\phi = L^{-1}(q - f) \quad (4.2)$$

The boundary conditions are specified using the boundary potential temperature θ to calculate the vertical gradient of the geopotential.

$$\frac{\partial \phi}{\partial p} = -\frac{R}{p} \left(\frac{p}{p_o} \right)^{\frac{R}{c_p}} \theta \quad (4.3)$$

Nielsen-Gammon and Lefevre (1996) found that the 1000 mb temperature seemed to be hydrostatically inconsistent over high terrain in the DS082.0 data set. They then computed the mean temperature between 850 mb and 1000 mb using $\ln p$. The lower boundary was set at 922 mb. A similar computation was performed on the upper boundary making 122 mb the upper bound. A height tendency equation may be derived by taking the local time derivative of (4.2) and inverting together with the time derivative of (4.3):

$$\frac{\partial q}{\partial t} = \frac{1}{f_o} \nabla^2 \left(\frac{\partial \phi}{\partial t} \right) + f_o \frac{\partial}{\partial p} \left(\frac{1}{\sigma} \frac{\partial}{\partial p} \left(\frac{\partial \phi}{\partial t} \right) \right) = L \left(\frac{\partial \phi}{\partial t} \right) \quad (4.4)$$

$$\frac{\partial \phi}{\partial t} = L^{-1} \left(\frac{\partial q}{\partial t} \right) \quad (4.5)$$

$$\frac{\partial}{\partial p} \left(\frac{\partial \phi}{\partial t} \right) = -\frac{R}{p} \left(\frac{p}{p_o} \right)^{\frac{R}{c_p}} \left(\frac{\partial \theta}{\partial t} \right) \quad (4.6)$$

In the quasigeostrophic framework the local rate of change of q is given by geostrophic advection of q , as well as frictional and diabatic generation. The lower boundary condition (4.6) reduces to topographic forcing, cooling and heating by upslope and downslope flow. As in the previous research, diabatic friction and topographic processes will be neglected as this study will focus the upper levels of the atmosphere, where such

processes are typically small. Any variations produced by heating and friction will affect the height field in a manner equivalent to adiabatically generated q or θ variations, so errors will not accumulate. In other words, for each synoptic time, the analysis height field will be used to calculate the QGPV and QGPV height tendencies.

With the focus of this research on upper levels, equations (4.5) and (4.6) may be rewritten:

$$g \frac{\partial z}{\partial t} = \frac{\partial \phi}{\partial t} = L^{-1}(-V_g \cdot \nabla q) \quad (4.7)$$

$$g \frac{\partial}{\partial p} \left(\frac{\partial z}{\partial t} \right) = \frac{\partial}{\partial p} \left(\frac{\partial \phi}{\partial t} \right) = -\frac{R}{p} \left(\frac{p}{p_o} \right)^{\frac{R}{C_p}} (-V_g \cdot \nabla \theta) \quad (4.8)$$

The geostrophic wind vector is V_g , and z is geopotential height. Equation (4.7) is known as the QGPV height tendency equation. The right hand side of (4.8) contains the effects of both absolute vorticity and stratification. The use of (4.8) as a boundary condition satisfies the analogy between interior q and boundary θ (Bretherton 1966). Both q and boundary θ are conserved following geostrophic motion. Thus, the right-hand sides of (4.7) and (4.8) may be regarded as “forcing” the height tendencies.

3. Application of QGPV thinking to piecewise tendency diagnosis

This section illustrates the application of equation (4.7) to upper-tropospheric systems. The relationship between QGPV thinking and height tendencies motivates the use of piecewise tendency diagnosis, PTD. PTD will be useful in differentiating dynamical processes occurring in the formation of mobile troughs. This discussion of PTD closely follows that presented by Nielsen-Gammon and Lefevre (1996).

Partitioning the total flow into basic state and perturbation makes practical the describing the dynamics of wavelike phenomena. The partitioning may be calculated in a number of ways. Common schemes include time mean vs. time-varying, zonal mean vs. zonally-varying, and small zonal wavenumbers vs. large zonal wavenumbers. The basic states are represented here with overbars, and the perturbations with primes. Partitioning (4.7) leaves the result:

$$\frac{\partial \phi}{\partial t} = \frac{\partial \bar{\phi}}{\partial t} + \frac{\partial \phi'}{\partial t} = L^{-1}(-\bar{v} \cdot \nabla \bar{q}) + L^{-1}(-\bar{v} \cdot \nabla q') + L^{-1}(-v' \cdot \nabla \bar{q}) + L^{-1}(-v' \cdot \nabla q') \quad (4.9)$$

Since the focus of this research is only on upper-tropospheric systems, one can partition the height field into elements due to upper-level and lower-level potential vorticity and potential temperature. The linearity of QGPV allows the evaluation of upper-level potential vorticity associated with upper-level flow separately from the lower levels. The effects of the winds induced by the lower-level QGPV will be incorporated into (4.10) through the fourth and sixth terms:

$$\begin{aligned} \frac{\partial \phi'_U}{\partial t} = & L^{-1}(-\bar{v} \cdot \nabla \bar{q}_U)' + L^{-1}(-\bar{v} \cdot \nabla q'_U)' + L^{-1}(-v'_U \cdot \nabla \bar{q}_U)' \\ & + L^{-1}(-v'_L \cdot \nabla \bar{q}_U)' + L^{-1}(-v'_U \cdot \nabla q'_U)' + L^{-1}(-v'_L \cdot \nabla q'_U)' \end{aligned} \quad (4.10)$$

The terms, v'_U and v'_L represent the upper- and lower-level winds associated with perturbation potential vorticity respectively. The term v'_L is computed by inverting the low-level QGPV, using the observed θ' as the lower boundary condition and $\theta'=0$ as the upper boundary condition on the vertical derivative of height. The large-scale wind field, \bar{v} , is left unpartitioned to avoid the large cancellations found by Holopainen and Kaurola

(1991) between winds induced by the basic state upper-level and lower-level QGPV gradients.

The interpretation of each of the forcing terms on the right hand side of (4.10) is based on the partitioning of the full geostrophic wind and of the inversion of potential vorticity. The first term represents the nonlinear basic state interactions onto the perturbation scale. The second term represents the advection of small-scale PV by the large-scale flow. The third term represents advection of large-scale PV by the perturbation winds associated with the inversion of the upper-level PV anomaly, which includes group velocity effects and downstream development. The fourth term, the baroclinic amplification term, is the advection of upper-level basic state potential vorticity by winds associated with the low level q' anomalies including surface θ' anomalies. The term baroclinic amplification is used instead of baroclinic instability because fundamentally similar growth can occur through this basic advection process even when normal mode baroclinic instability is not possible (Rotunno and Fantini 1989). The fifth and sixth terms represent the perturbation scale interaction among vortices and anomalies, and can grow in importance as the complexity and amplitude of the system increases.

4. QGPV inversion method

The inversion method described here is that of Nielsen-Gammon and Lefevre (1996). For the March 1987 case study, the data were separated into two levels: main and intermediate. The eight main levels were separated by 100 mb between 172 mb and 872 mb. The intermediate levels were set between 122 mb and 922 mb also separated by 100 mb.

With the availability of data at 28 sigma levels for the October 1988 case, I decided to include a greater number of input pressure levels to compute QGPV. The $\ln p$ average of 1000mb and 925 mb, 962 mb, was used as the lower boundary, while the upper boundary remained 122 mb. The QGPV was then calculated at twelve main levels separated by 70 mb between 927 mb and 157 mb.

The height data for both case studies was interpolated to their respective main levels using cubic splines and used in the calculation of the stratification term. The stratification term required the vertical finite differencing of the static stability at the intermediate levels. The stratification term was then transformed into spherical harmonic space using SPHEREPACK (written by John Adams and Paul Swarztrauber of NCAR). The vorticity term was calculated in spherical harmonic space while the Coriolis parameter, f , was put into spherical harmonic space. The QGPV was then calculated with spherical harmonics by summing the coefficients of the stratification term, the vorticity term, and the Coriolis parameter. The result was transformed back into grid space.

5. Basic state and perturbation

The partition between basic state and perturbation must be meaningful if an analysis is to be valid. The basic state should represent the mean flow in which the anomaly of interest, here an upper-level mobile trough, is embedded. The perturbation should represent the synoptic-scale flow associated with the mobile trough. The precision of QGPV dynamics and of the piecewise tendency diagnosis requires that the phenomenon of interest be placed in the perturbation scale. For the method used here, the intensity of the mobile trough is defined as a local minimum value of perturbation height, and the rate of intensification is equal to the height tendency at the height minimum.

Therefore, the mobile trough should not be incorporated with the basic state. A climatological mean would not suffice for a basic state because it is typically not representative of the mean large-scale flow near the mobile trough. This was noted in Chapter III where a variety of large-scale flow regimes were associated with mobile trough formation over the Yellow Sea-East China Sea region. A time-mean basic state also presents difficulties. The time evolution of the large-scale flow could corrupt the perturbation quantity causing the diagnosis method to fail.

Nielsen-Gammon and Lefevre (1996) and McEver (1996) use a spherical harmonic wavenumber truncation (low-pass basic state) which separates the small-scale mobile trough from the large-scale basic state. Nielsen-Gammon and Lefevre transform the total QGPV from grid point space into spherical harmonic space at each level. They then filter the QGPV into its small- and large-scale parts by using zonal wavenumbers 0-6 and total wavenumbers 0-9 as the large-scale. The small scale is calculated by subtracting the large-scale QGPV from the total QGPV. The same procedure is used at the boundaries. To solve for the height coefficients, an 8×8 (12×12 for the reanalysis data) matrix is solved using a tridiagonal solver routine (Press et al 1992). Further, if piecewise inversion was used, Nielsen-Gammon and Lefevre set the QGPV coefficients at certain levels to zero before solving the equation.

The partitioning method used in this research was an extension of the above method. I placed the time-mean component of the perturbation field back into the large-scale basic state. This required an additional computation to calculate the perturbation time-mean component, encompassing the entire lifetime of the mobile trough. This was done after examining the perturbation fields of several cases. Some small-scale height

perturbations remained stationary throughout the time period investigated. This suggested a limitation of the spherical harmonic truncation to accurately represent the background flow. The mathematical details of this low-pass basic state with a time-mean perturbation component can be found in the Appendix.

6. Piecewise inversion method

To use the QGPV height tendency equation (4.10) to evaluate mobile trough genesis, a method of piecewise inversion of QGPV must be developed. Nielsen-Gammon and Lefevre (1996) followed a similar method to that developed by Holopainen and Kaurola (1991), except that Nielsen-Gammon and Lefevre set the QGPV to zero at levels away from the point of interest. One can isolate the q coefficients of interest by setting the other levels to zero. Nielsen-Gammon and Lefevre found that the 372 mb level had the greatest amount of QGPV information. This is because of the large PV gradients of the tropopause typically located near this level. A natural break was apparent between upper-level and lower-level QGPV near 500 mb. Upper-level QGPV was defined as 472 mb and above and the lower-level QGPV was as 572 mb and below. The pieces thus divided will still total the sum, owing to the linearity of the QGPV operator. The QGPV for the reanalysis data case study was partitioned in the vertical by defining the top six layers as upper levels, 507 mb and above. The lower layers consisted of 577 mb and below.

The method used to calculate piecewise tendencies is also identical to that of Nielsen-Gammon and Lefevre's. For example, to compute the height tendency for $\mathbf{L}^{-1}(-\mathbf{v}_L' \cdot \nabla q_U')$, the term associated with the low-level perturbation winds advecting

perturbation upper -level QGPV, one must solve for q' by setting zonal (0-6) and total wavenumbers (0-9) to zero. (For the October case study the base state was composed of zonal wavenumbers up to 5 and total wavenumbers to 8). Then, to calculate v'_L , q' must be partitioned by setting the upper-level values of q' and upper boundary perturbation thickness to zero. The lower-level perturbation height (z') and perturbation wind (v'_L) are calculated in spherical harmonic space; next, q' and v'_L are transformed into grid point space. The advection of q' by v'_L is then computed at upper levels. The resulting advection is then filtered again to eliminate any large-scale effects by setting all large-scale wavenumbers to zero and inverting it for the height tendency. The filtered forcing, advectons, and height tendencies are then transformed back to a latitude-longitude grid.

7. Application of PTD to case studies

Nielsen-Gammon and Lefevre's (1996) strategy of using piecewise tendency diagnosis on the QGPV height tendency equation was shown to be useful in assessing dynamical processes that lead to the formation of a mobile trough over the western United States. The QG framework did indeed reveal the mobile trough genesis processes of the atmosphere. McEver (1996) also applied this method to case studies of trough formation over the Mongolian plateau. The results from the previous studies provide a measure of confidence for this research. Two case studies were chosen using the process described in Chapter III. The PTD method described above will be applied to these two cases of mobile trough formation in the Yellow Sea-East China Sea region.

CHAPTER V

CASE STUDY ONE

31 MARCH 1987

This purpose of this chapter is to explain the development of a mobile trough that forms over the Yellow Sea-East China Sea region on 0000 UTC 31 March 1987. A synoptic overview of the mobile trough and its development is given. Nielsen-Gammon's and Lefevre's (1996) PTD technique is used to determine the mechanisms governing the development of the mobile trough. The downstream development mechanism will be shown to contribute most to development. Baroclinic processes and large-scale interactions play lesser roles during the formation of the trough. Additionally, the development of the mobile trough will be described using dynamical tropopause maps constructed with a constant value of isentropic potential vorticity.

1. Overview of life of mobile trough

The mobile trough develops over the Yellow Sea in northwest flow associated with a polar vortex north of Sakhalin Island (Fig 5.1). The precursor conditions consisted of strong northwesterly flow across Mongolia and a general increase in curved flow just upstream of the Yellow Sea (Fig 5.1a-b). The incipient mobile trough formed on 0000 UTC 31 March 1987 (Fig. 5.1c). Another mobile trough can be seen just downstream of the trough studied here. The two prominent maxima appear in the 500 mb vorticity field on 0000 UTC 31 March 1987. Twelve hours later, only one vorticity maximum is present just east of Honshu (Fig 5.1d). This vorticity maximum is associated with our mobile

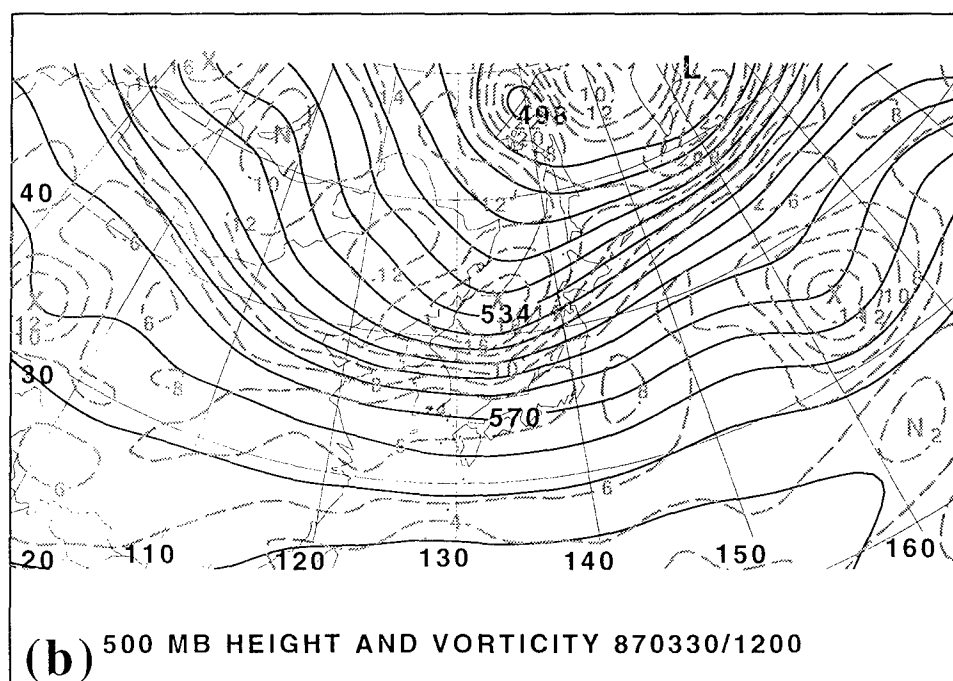
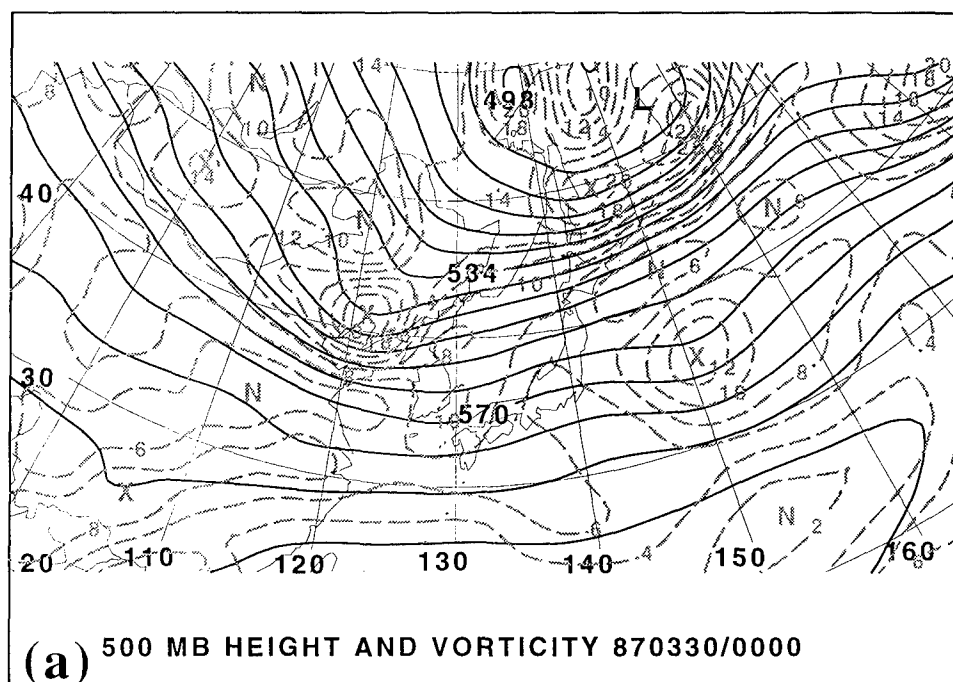


Fig. 5.1. The 500 mb geopotential heights (black, contour interval 6 dam) and geostrophic vorticity (gray dashed, contour interval $2 \times 10^{-5} \text{ s}^{-1}$) for (a) 870330/0000, (b) 870330/1200, (c) 870331/0000, (d) 870331/1200, (e) 870401/0000, (f) 870401/1200, (g) 870402/0000, (h) 870403/0000.

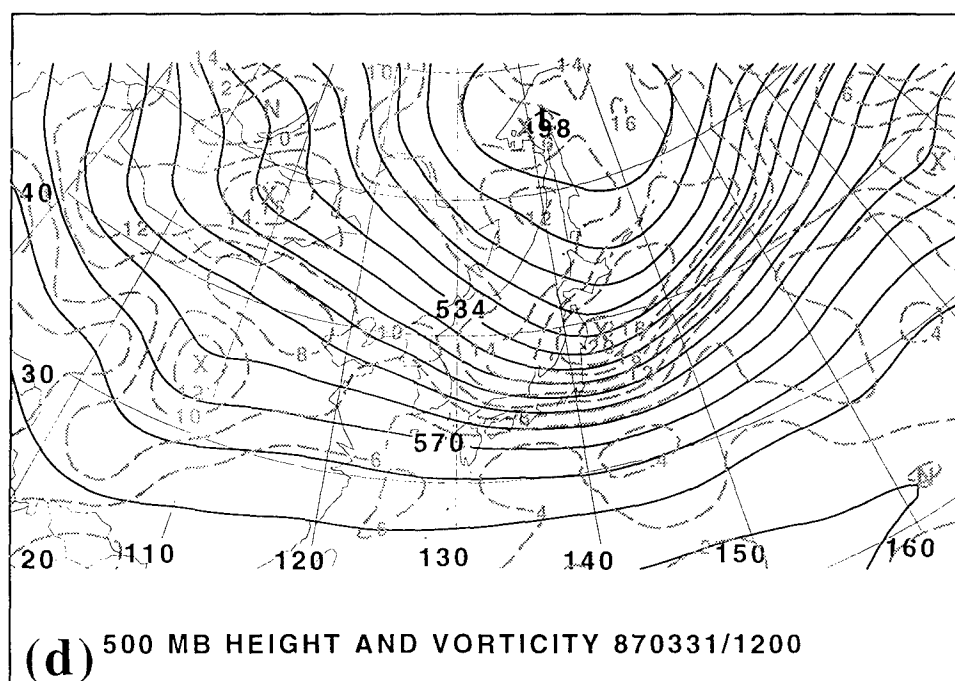
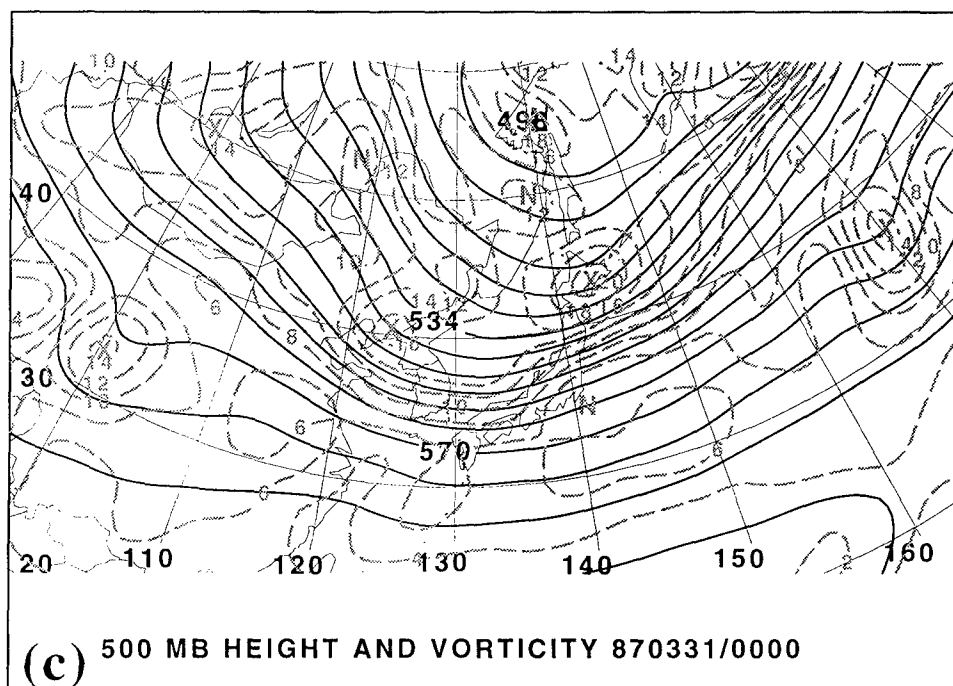


Fig. 5.1, continued.

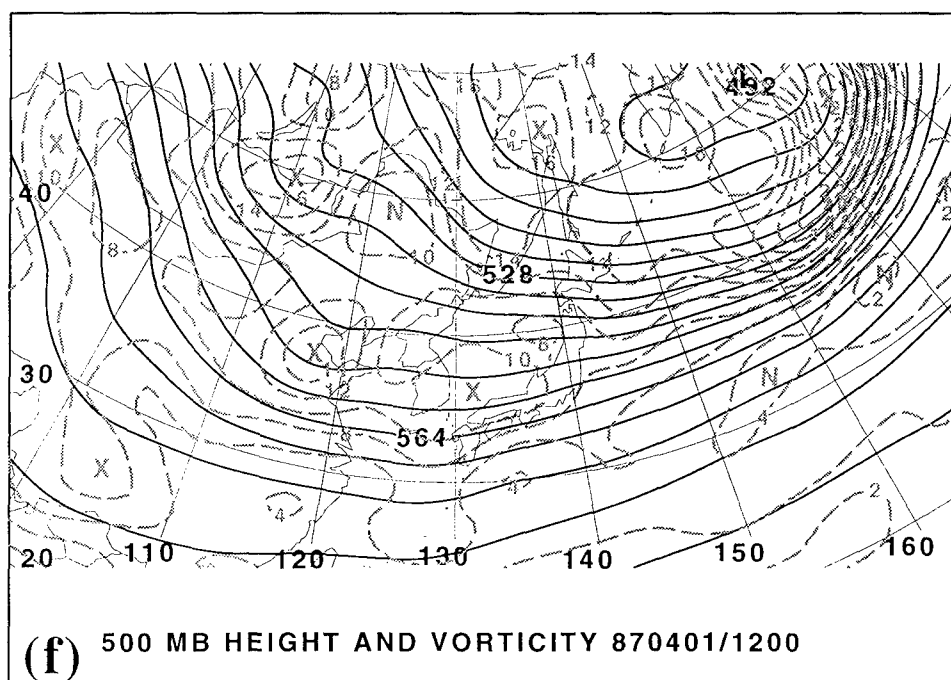
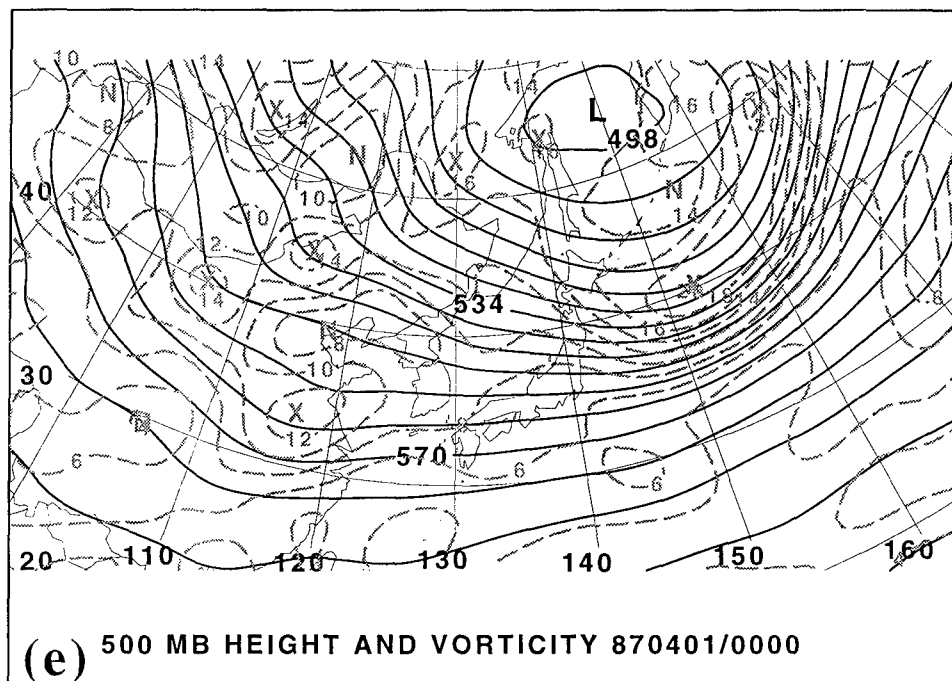


Fig. 5.1, continued.

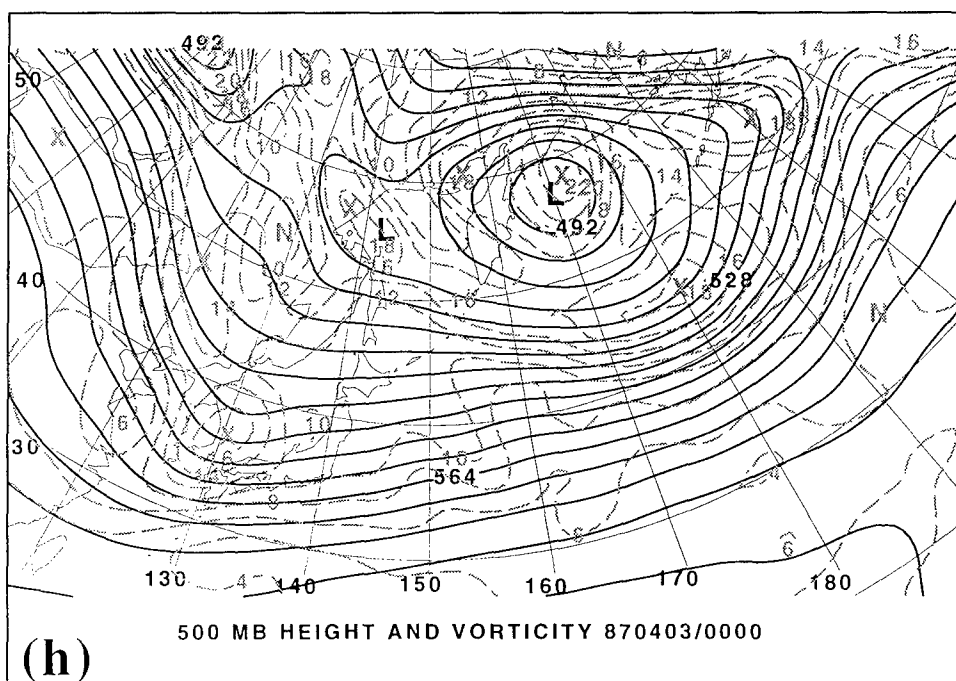
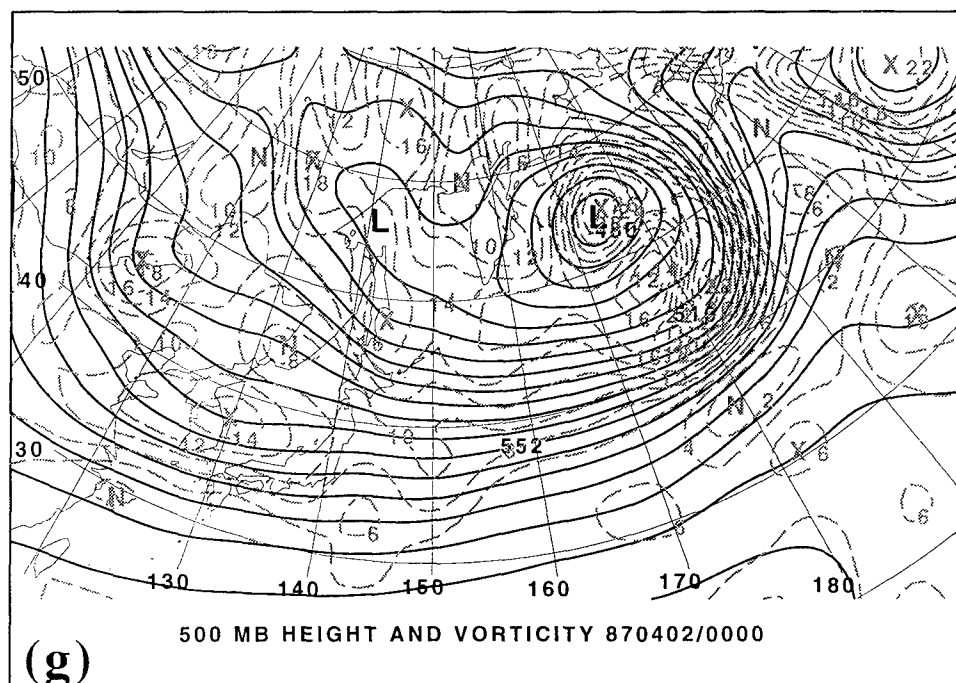


Fig. 5.1, continued.

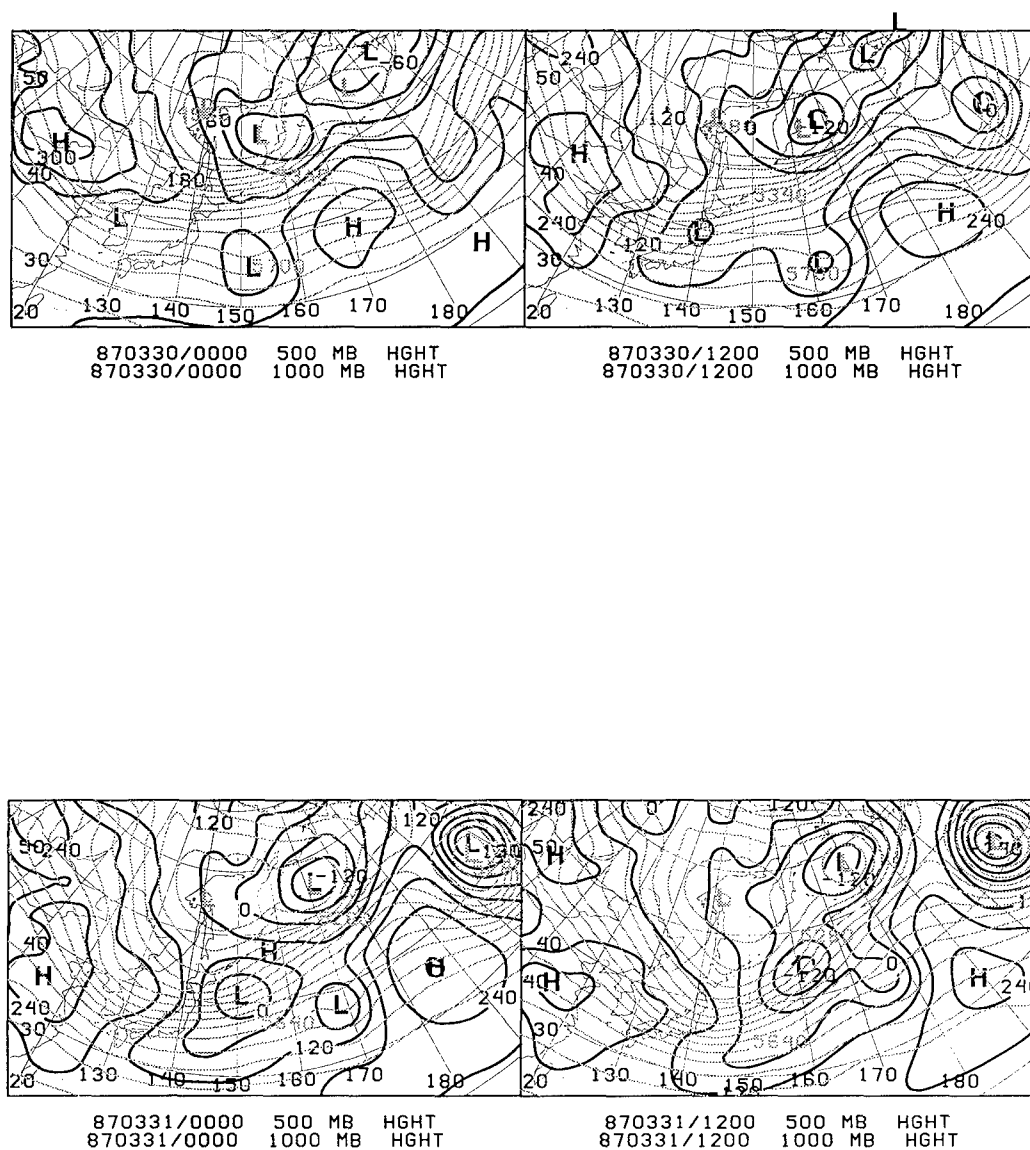


Fig. 5.2. The 1000mb heights (black) and 500 mb heights (gray) for (upper left) 870330/0000, (upper right) 870330/1200, (lower left) 870331/0000, (lower right) 870331/1200. Contour interval for both fields is 60 m.

trough since the advection by the mean flow would have carried the downstream trough farther to the east. The vorticity fields of the two troughs merge. The downstream trough weakens as the vorticity contours associated with it become elongated along the mean flow. However, by 0000 UTC 1 April (Fig. 5.1e), two weak vorticity maxima can be seen over the western North Pacific. Over the next two days (Fig. 5.1f-h), our mobile trough moves to the northeast where it weakens and then slows down, becoming quasi-stationary near the Aleutian Islands after 0000 UTC 3 April.

A low-level cyclone develops over the Sea of Japan and can be seen over the island of Honshu on 1200 UTC 30 March. The low-level cyclone forms in association with the previously mentioned downstream trough (Fig 5.2). As will be pointed out later, this cyclone still plays a small role in the development of the case study mobile trough.

2. Basic state and perturbation fields

In this case study, 372 mb will be the focal point of the investigation. Nielsen-Gammon and Lefevre (1996) found that the QGPV field at 372 mb had the greatest influence on the 500 mb heights. This finding also held for the current case. Likewise, the perturbation height field is correspondingly largest at 372 mb.

Figure 5.3 shows the evolution of perturbation and basic state QGPV fields from 0000 UTC 31 March through 0000 UTC April 3. The base state is composed of spherical harmonic wavenumbers (0-6) zonal and (0-9) total and the time-mean component of the small-scale wavenumbers (7-15) averaged over the lifetime of the mobile trough (0331/0000-0404/1200). The perturbation QGPV fields are commensurate to the spatial and temporal evolution of the mobile trough. The perturbation QGPV associated with the mobile trough reaches a maximum at 0401/1200.

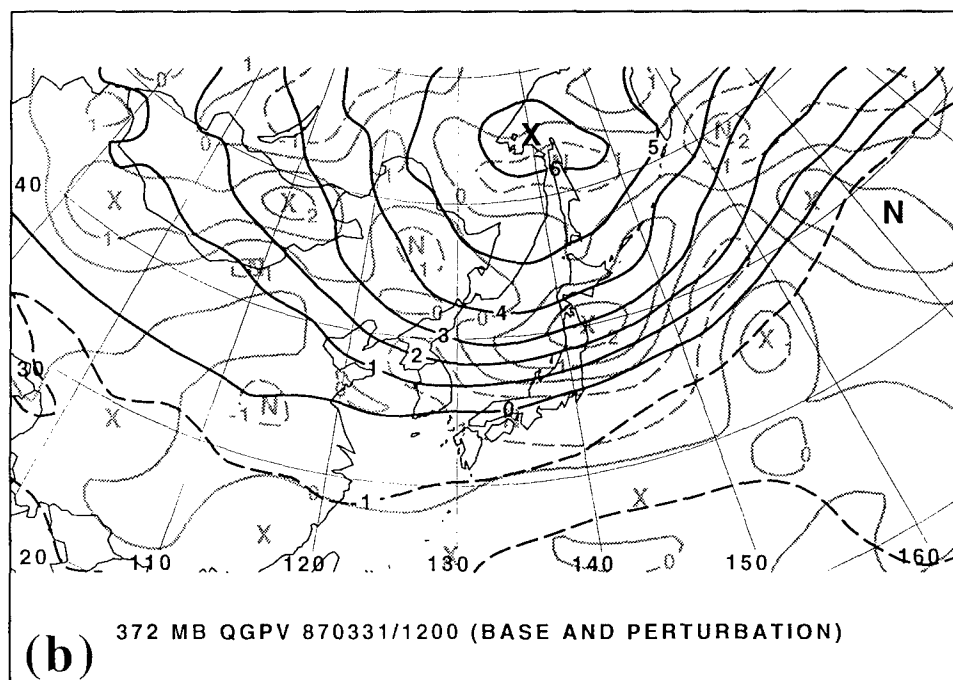
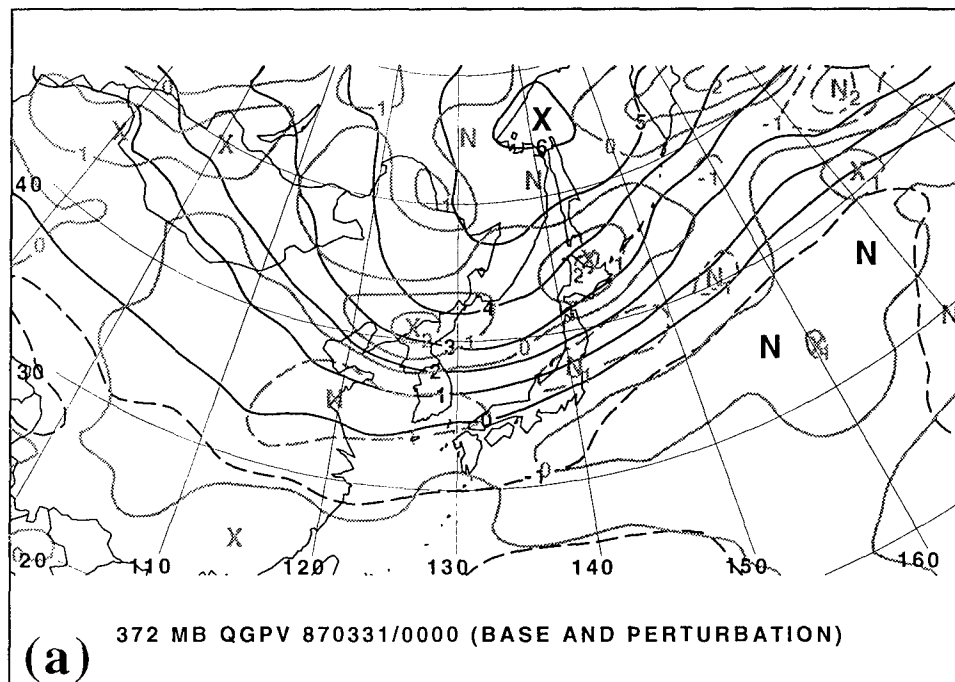


Fig 5.3. Base-state 372 mb QGPV (black, $\times 10^{-4} \text{ s}^{-1}$) and perturbation 372 mb QGPV (gray, $\times 10^{-4} \text{ s}^{-1}$) for (a) 870331/0000, (b) 870331/1200, (c) 870401/0000, (d) 870401/1200, (e) 870402/0000, (f) 870403/0000. Negative contours are dashed. Positive and negative QGPV anomalies are marked with X's and N's, respectively.

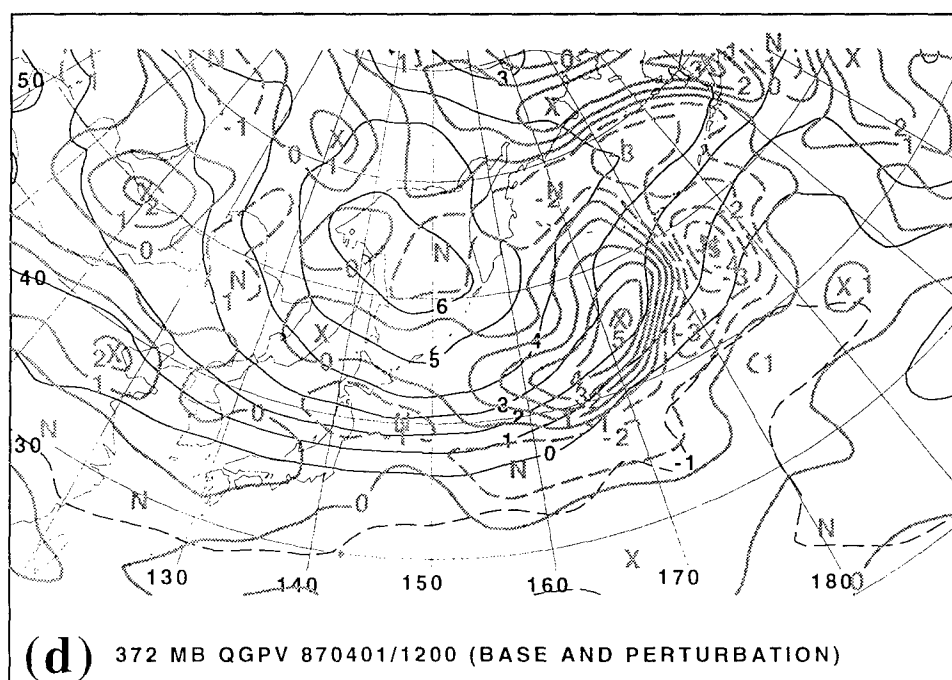
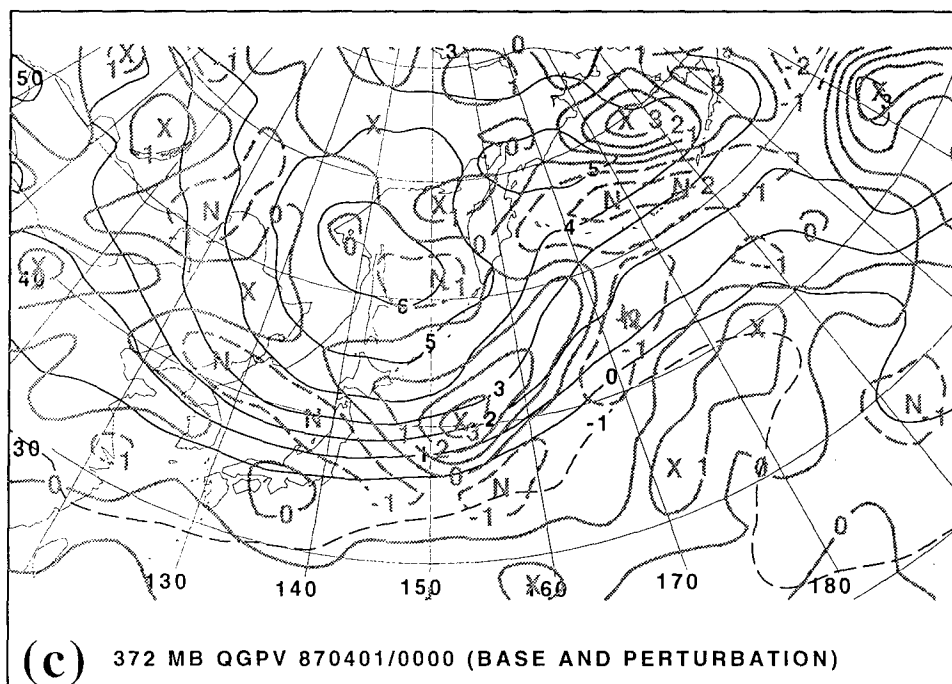


Fig. 5.3, continued.

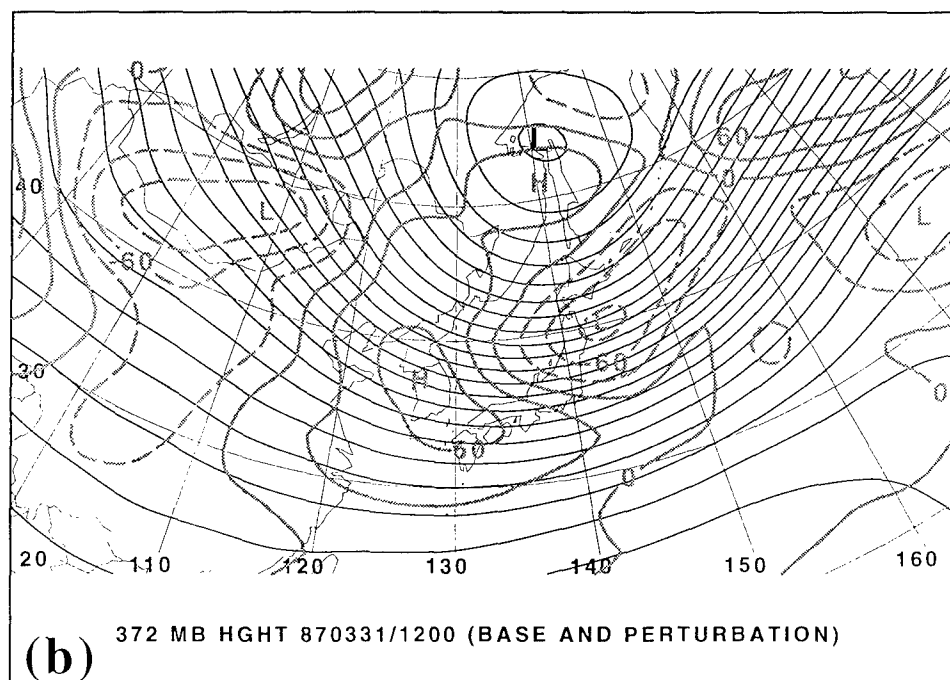
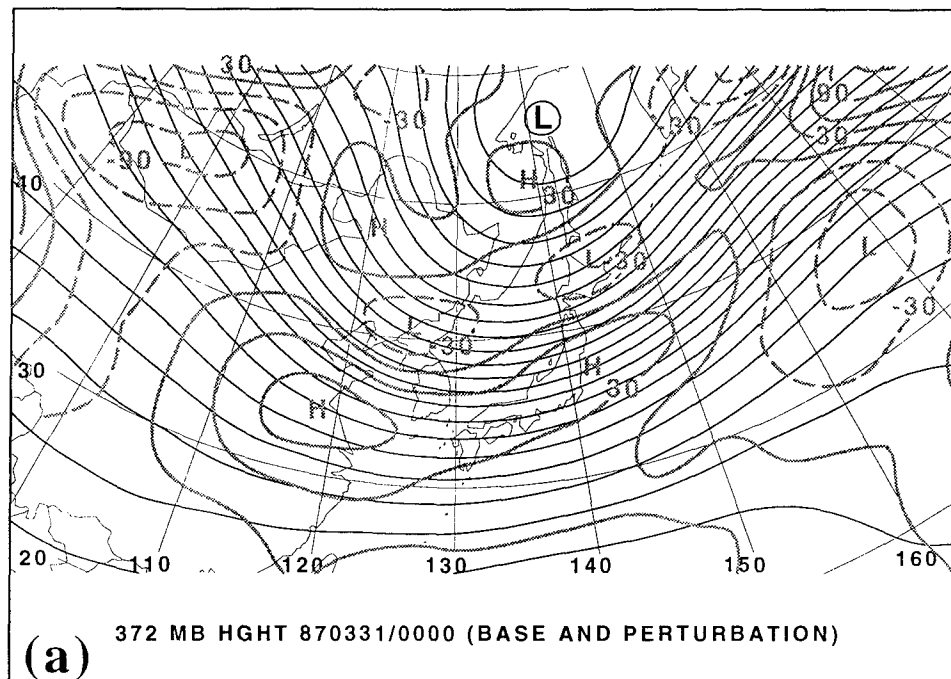


Fig. 5.4. Base state 372 mb height (black, contour interval 6 dam) and perturbation 372 mb height (gray, contour interval 30 m) for a) 870331/0000, (b) 870331/1200, (c) 870401/0000, (d) 870401/1200, (e) 870402/0000, (f) 870403/0000.

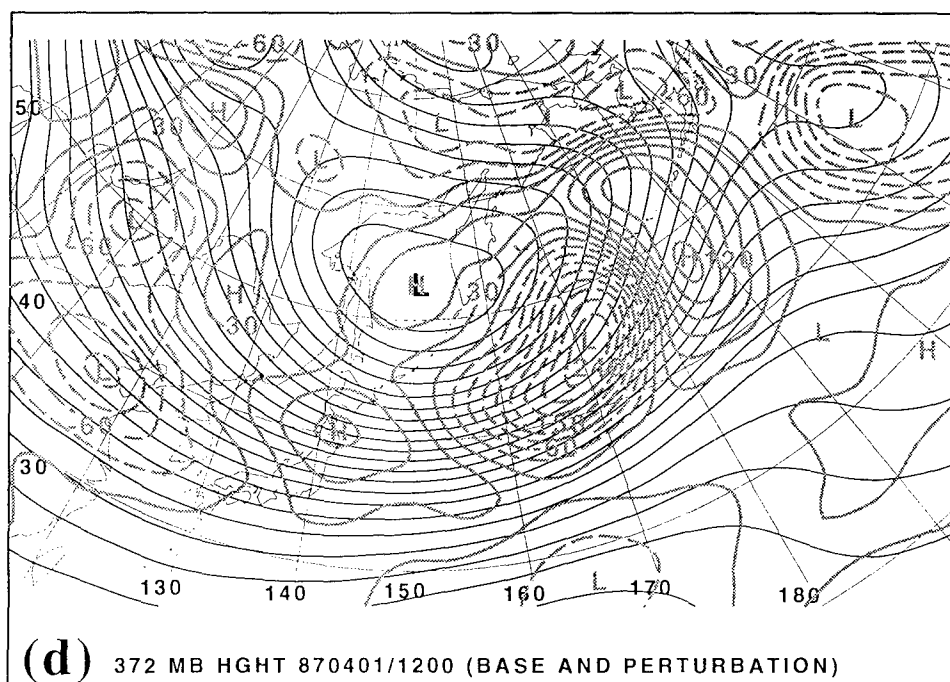
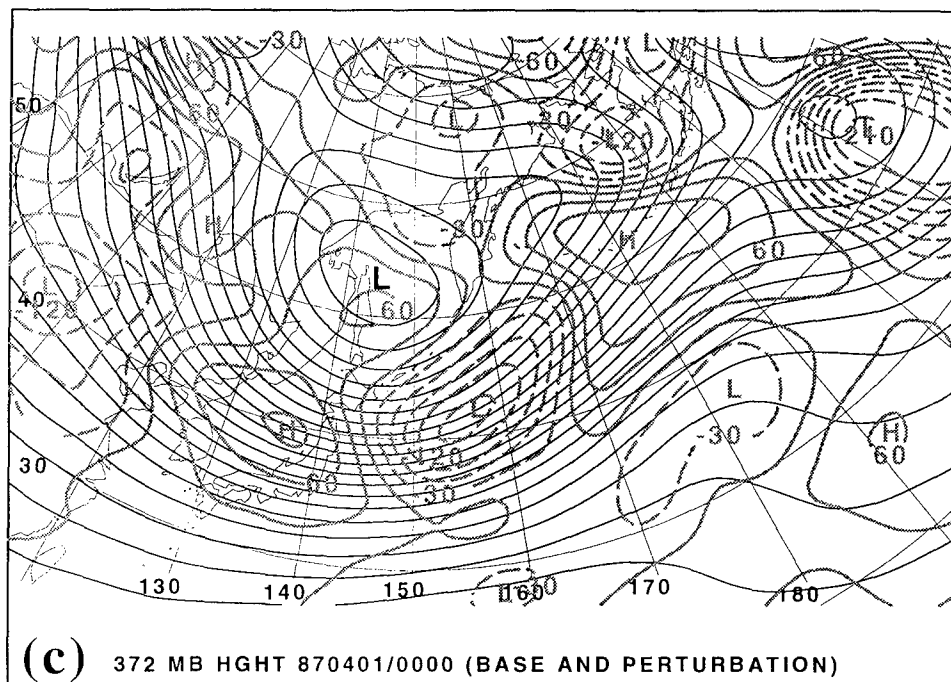


Fig. 5.4, continued.

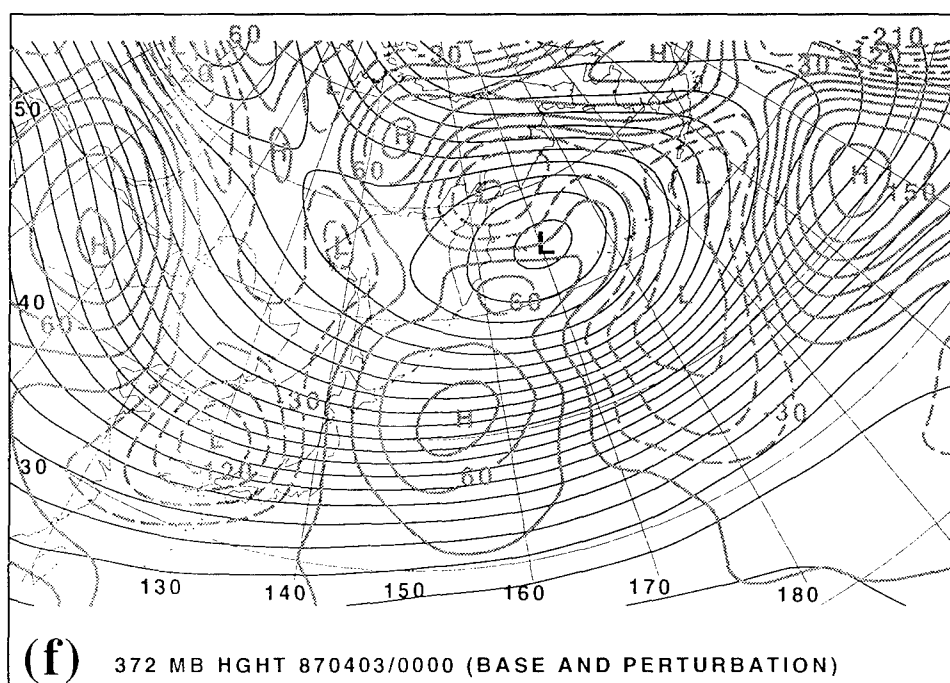
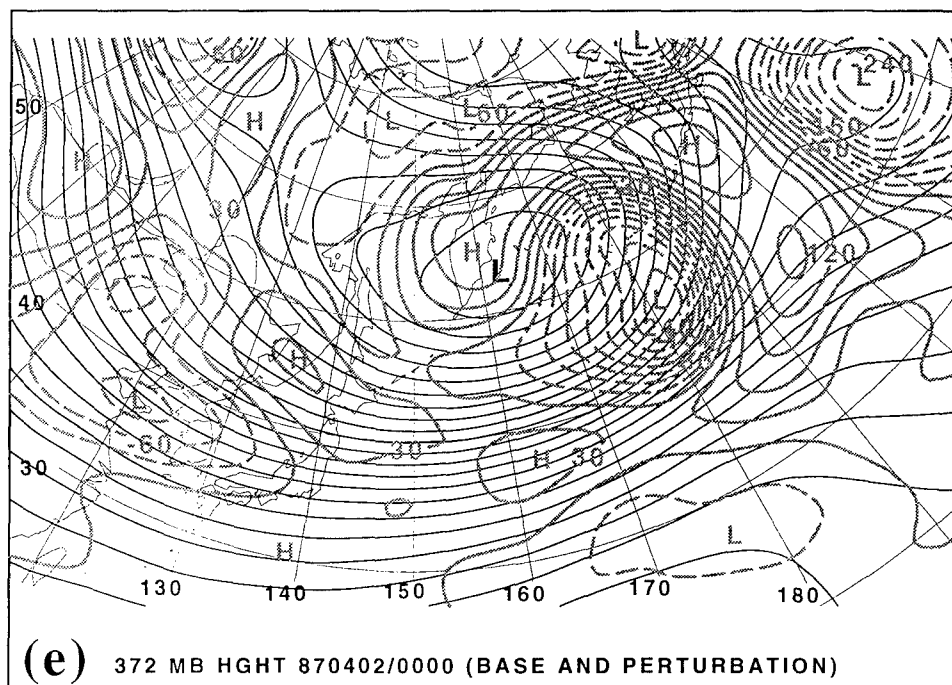


Fig. 5.4, continued.

Figure 5.4 shows the time evolution of the perturbation and base state height fields. The 372 mb perturbation height fields (associated with the upper-level perturbation potential vorticity) correspond to the 500 mb vorticity patterns of the mobile trough. The maximum in strength of the 372 mb height perturbation occurs at the time of greatest extent and magnitude of geostrophic vorticity of the 500 mb mobile trough.

The low-pass basic state with a time-mean perturbation component slowly evolves in time but appears to partition the essential large-scale features into the base state. The partitioning scheme explained in Chapter IV proved robust for this case study. Realistic height and QGPV gradients are contained in the basic state fields.

3. Evaluation of QGPV tendencies

QGPV tendencies for the first four days are investigated (0331/0000-0403/0000) to determine what mechanisms were most important in the genesis of the trough and subsequent intensification. Figure 5.5 shows a comparison of tendencies between those calculated using the QG tendency equation (4.10) and those calculated by centered finite differencing of the upper-level height perturbation.

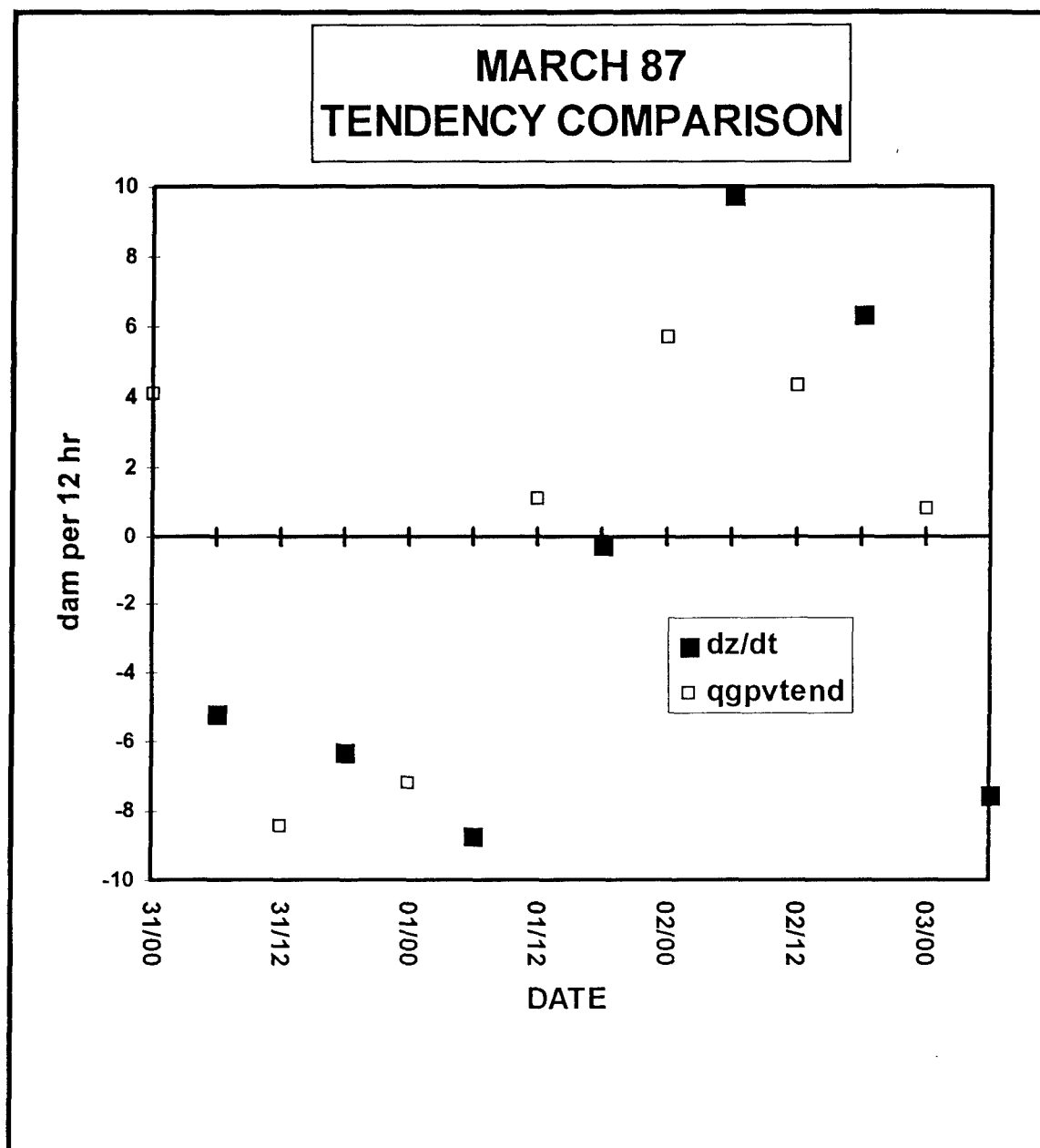


Fig. 5.5. Comparison of observed intensification of trough associated with upper-level small-scale QGPV (filled squares; computed as a 12-hour finite difference of minimum heights) with intensification rate computed from the quasigeostrophic height tendency equation (4.10) (open squares; defined as instantaneous height tendency at location of minimum height).

The two tendencies are similar overall with minor exceptions. The QGPV tendency overestimates intensification on 0331/1200. It also prematurely predicts the trough to weaken at 0401/1200. The premature filling may be due to neglecting diabatic and friction effects. The effects of heating and friction are presumably significant at that time since a mature extratropical cyclone is associated with the case by 0401/0000. The QGPV tendencies from the case study by Nielsen-Gammon and Lefevre (1996) also showed premature filling of the mobile trough very similar to the results obtained here.

The first instantaneous QGPV tendency on 0331/0000 shows a filling rate of 4.1 dam per 12 hrs. However, twelve hours later, the QGPV tendency becomes negative (-8.4 dam per 12 hr). The observed tendency (filled squares) between the two times was 5.1 dam per 12 hr. The large difference between the two QGPV tendencies suggests significant changes in atmospheric flow which caused the rapid intensification of the trough.

4. Piecewise tendencies

The sum of the individual terms of (4.10) will equal the total QG tendency at the trough. Figure 5.6 shows the contributions of the terms of (4.10). The fifth and sixth terms of (4.10) were summed in the figure and were labeled as VORTEX-VORTEX terms.

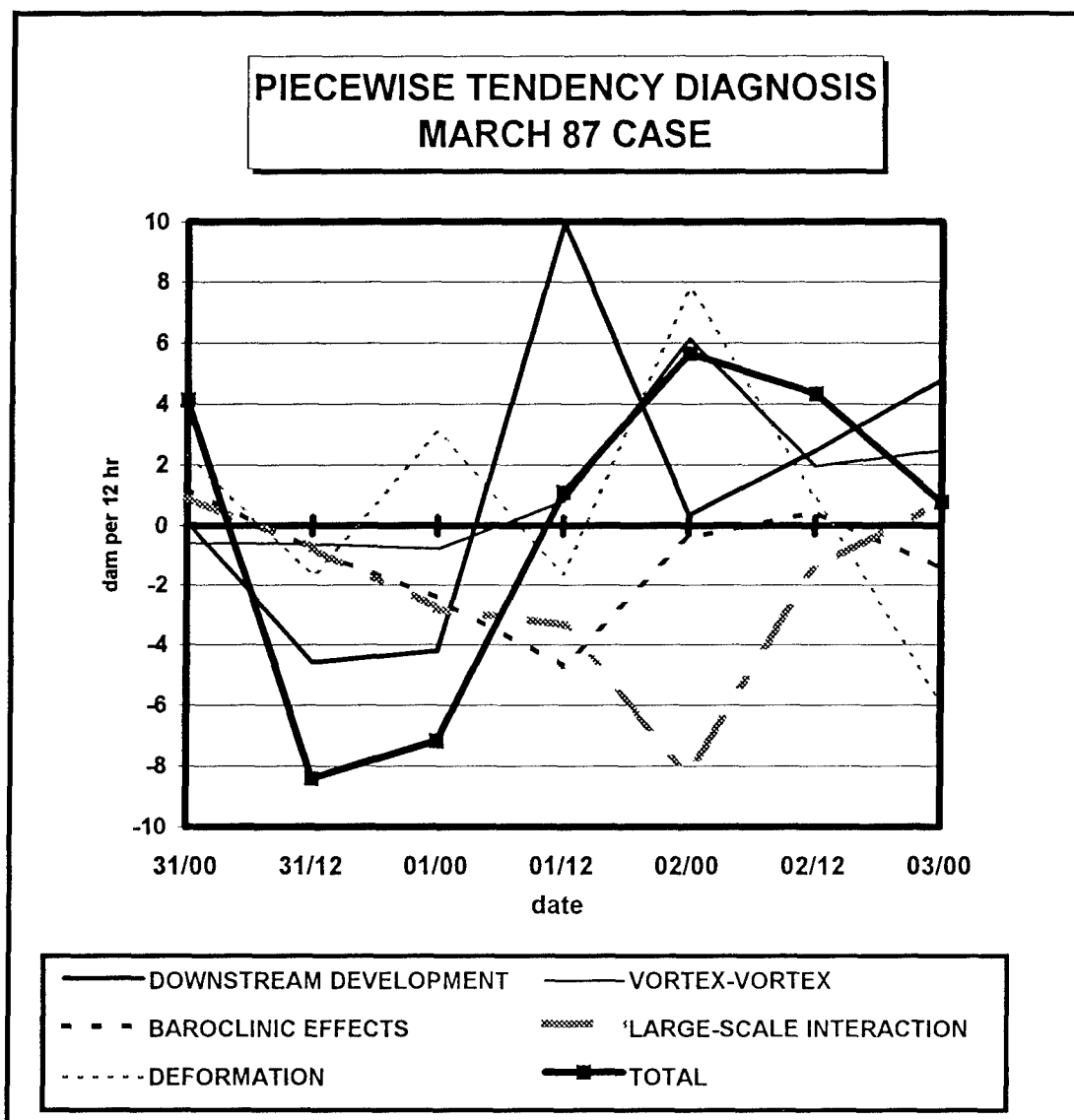


Fig. 5.6. Quasigeostrophic height tendencies associated with various dynamical processes during the development of the upper-level mobile trough, 0000 UTC 31 Mar. 1987 to 0000 UTC 3 Apr. 1987.

a. Downstream development

The downstream development, $L^{-1}(\mathbf{v}'_u \bullet \nabla \bar{q}_u)'$, provides the largest contribution in strengthening the trough during the first 24 h. This term then becomes strongly positive on 0401/1200, contributing to weakening of the trough. The term remains positive throughout the rest of the episode investigated.

Figures 5.7 through 5.10 illustrate the evolution of the effect of the downstream development term on the mobile trough. The upper panel of each figure shows 372 mb large-scale QGPV, 372 mb small-scale QGPV, and the wind associated with upper-level small-scale QGPV. The lower panel of each figure shows 372 mb height tendencies due to the downstream development term and 372 mb small-scale height perturbations. Nielsen-Gammon and Lefevre (1996) investigated the downstream development mechanism by examining the proximity of nearby negative QGPV anomalies, and their resultant positive height perturbations. A negative anomaly to the north-northwest of the trough on 0331/1200 (Fig 5.8) is causing positive QGPV advection into the trough. The circulation due to the negative QGPV perturbation causes slight height falls over the western portion of the upper-level height perturbation. The process continues and strengthens. Positive QGPV advection by perturbation-scale winds increases through 0401/0000 (Fig. 5.9).

The process quickly reverses on 0401/1200 (Fig. 5.10). The negative QGPV advection associated with the QGPV anomaly dominates the advection pattern causing height rises over two-thirds of the height perturbation, thereby weakening the trough.

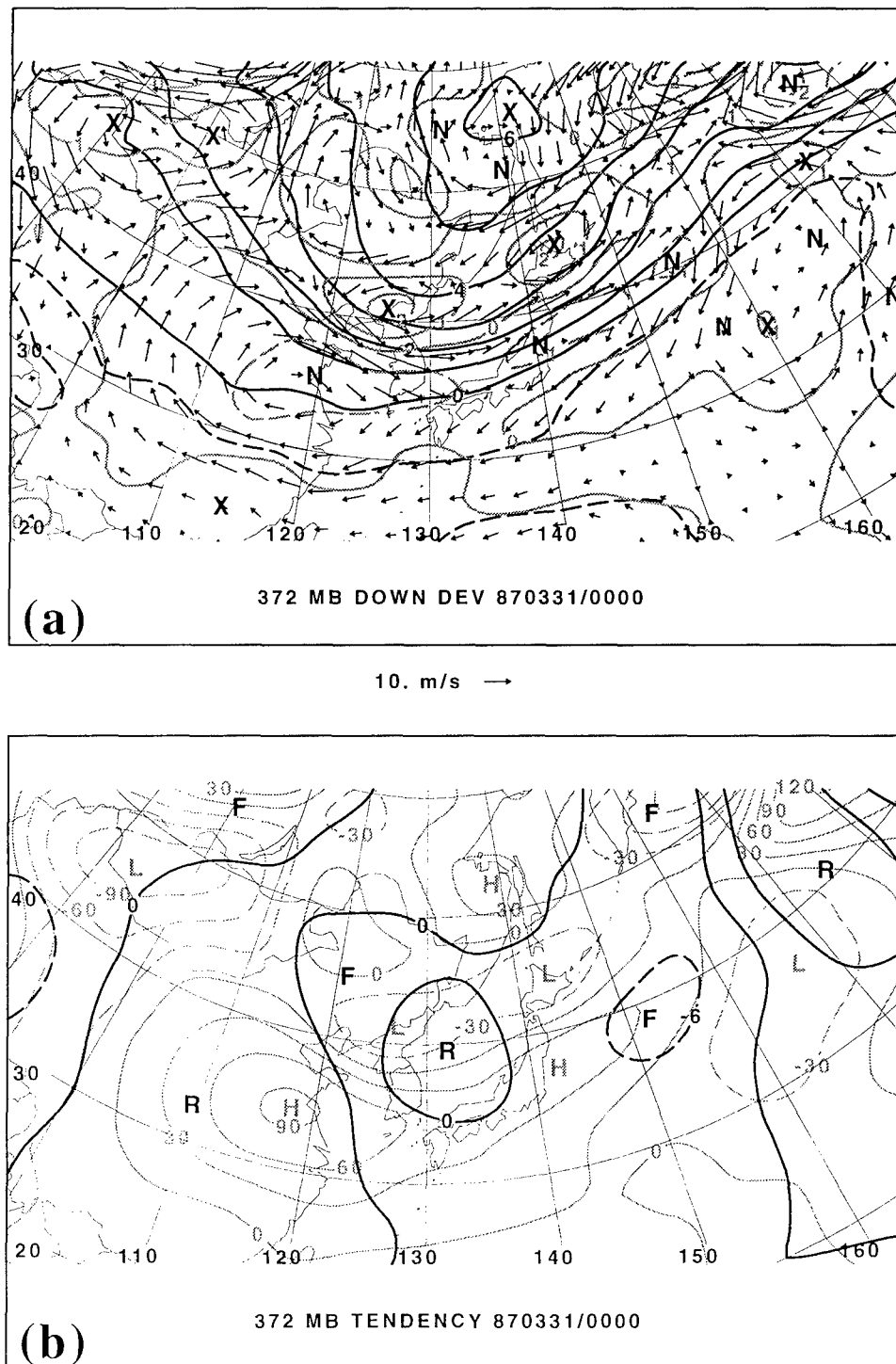
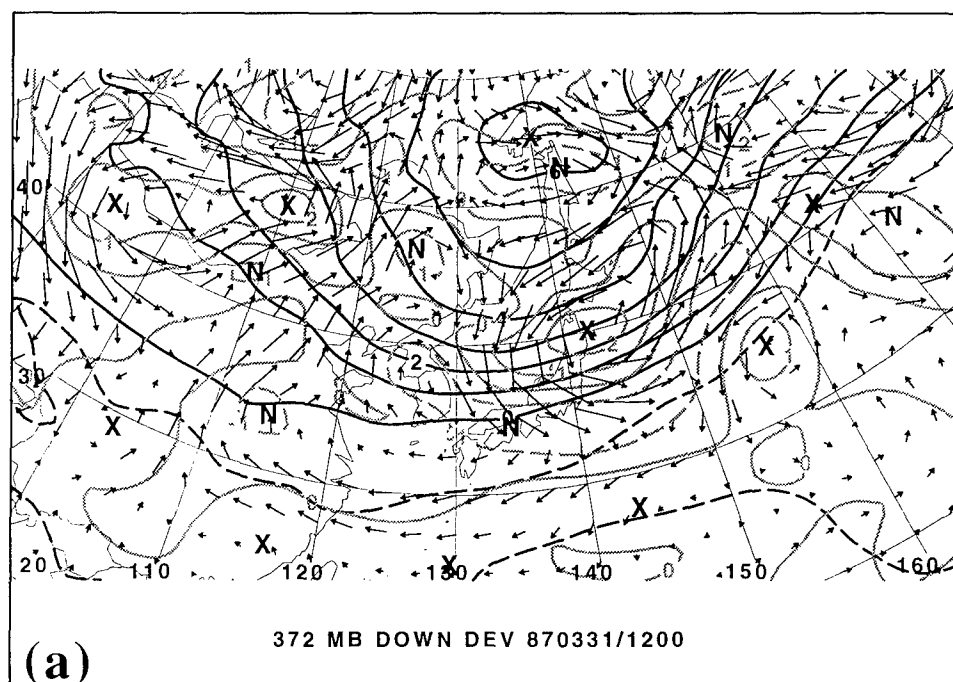


Fig 5.7. Advections and tendencies associated with downstream development at 00 UTC 31 Mar. 1987. (a) Large-scale 372 mb QGPV (black, $\times 10^{-4} \text{ s}^{-1}$); perturbation 372 mb QGPV (gray, $\times 10^{-4} \text{ s}^{-1}$); and 372 mb winds associated with upper-level perturbation QGPV. (b) Small-scale height tendencies associated with advection of upper-level large-scale potential vorticity by winds associated with upper-level perturbation QGPV (black, dam per 12 hr; and 372 mb heights associated with upper-level perturbation QGPV (gray, dam).



10. m/s →

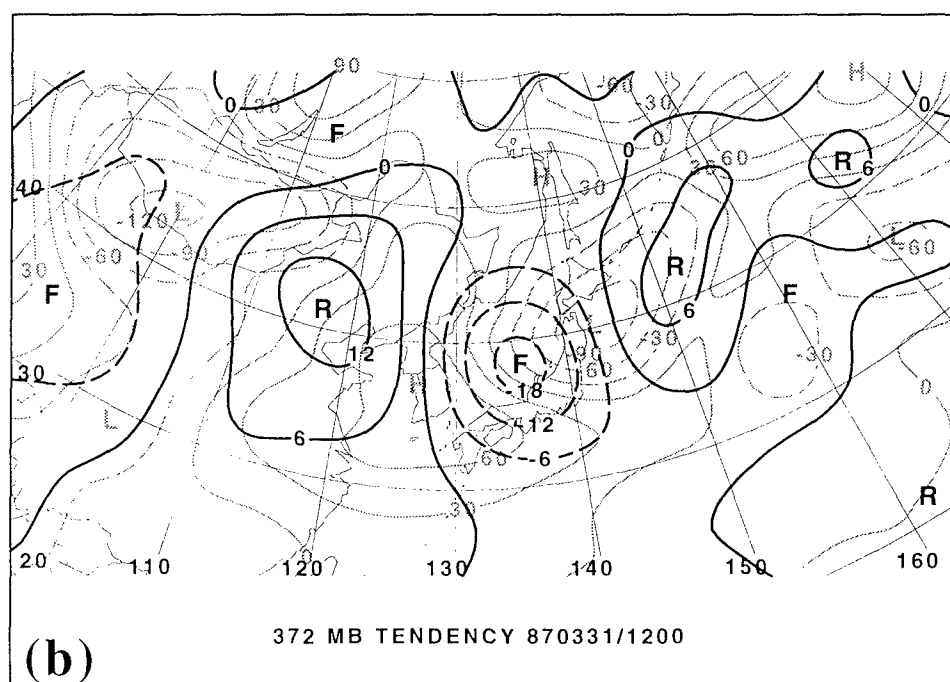
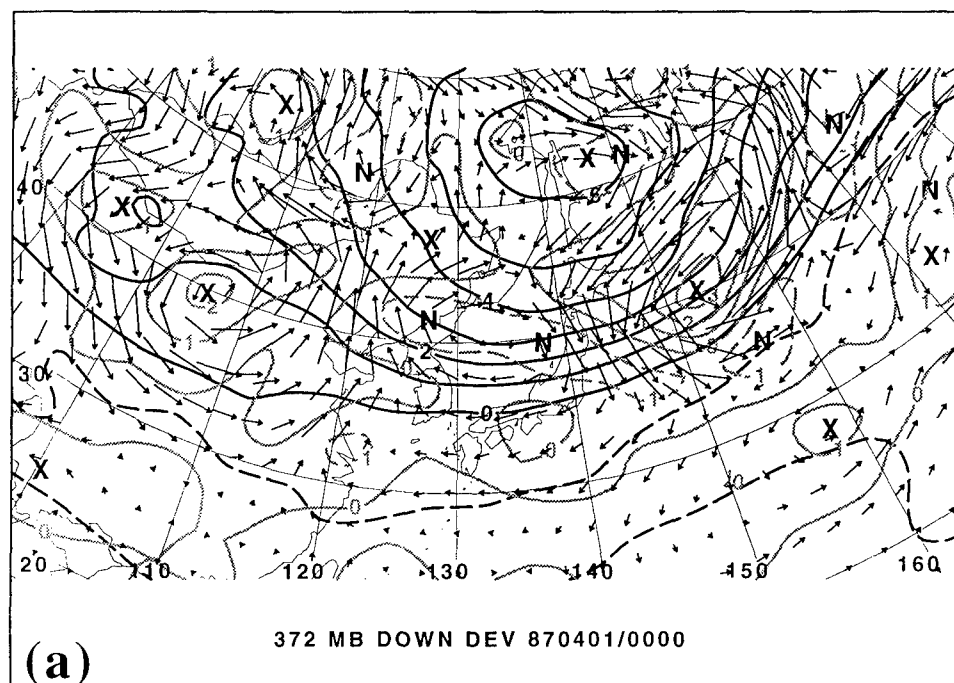


Fig. 5.8. Same as for Fig. 5.7, except for 1200 UTC 31 Mar. 1987.



10. m/s →

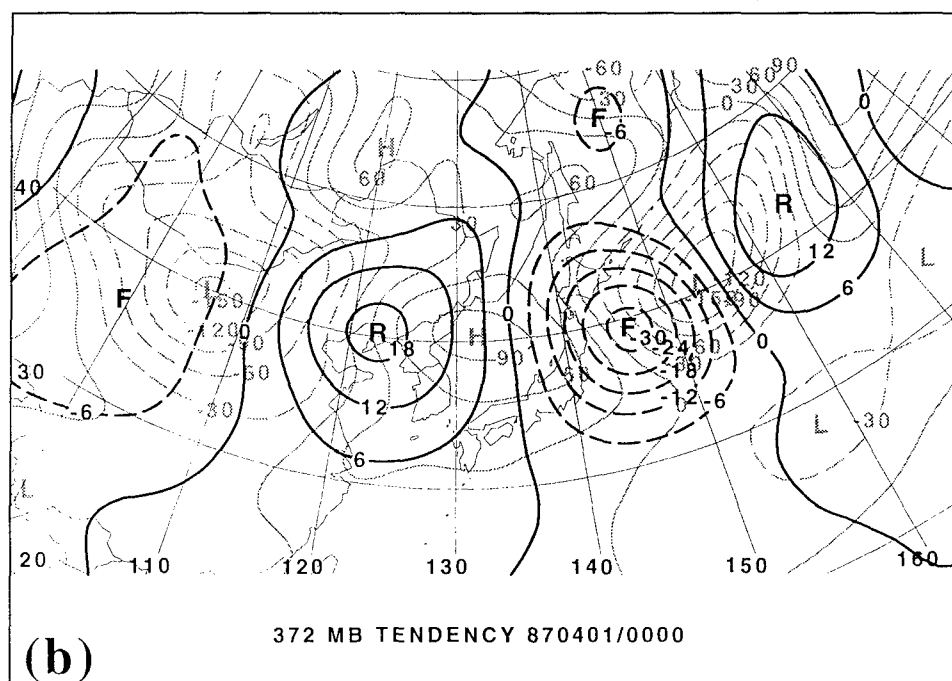


Fig. 5.9. Same as for Fig. 5.7, except for 0000 UTC 1 Apr. 1987.

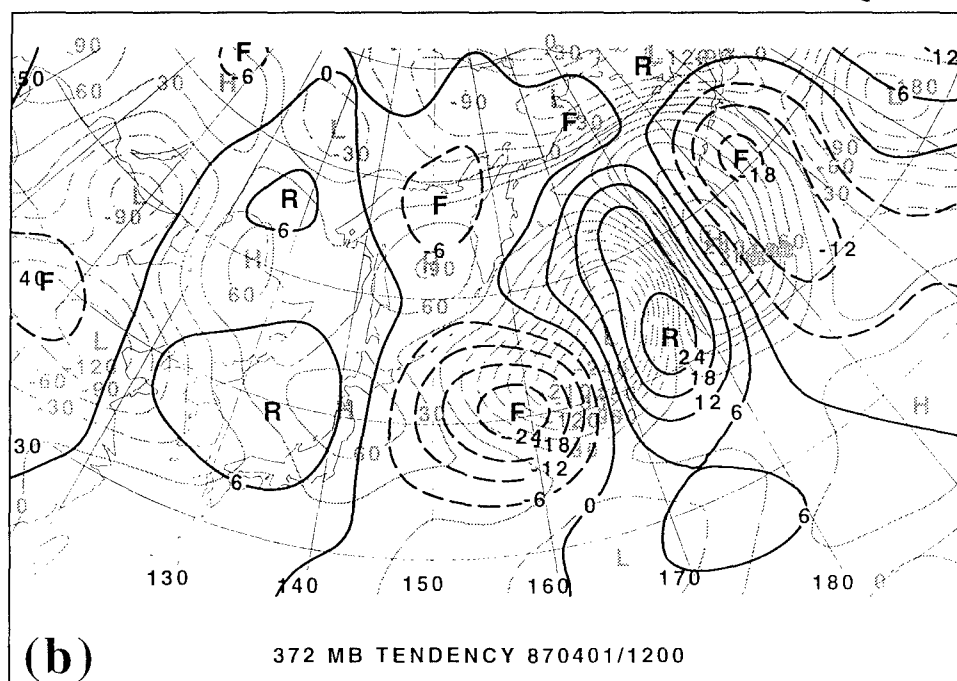
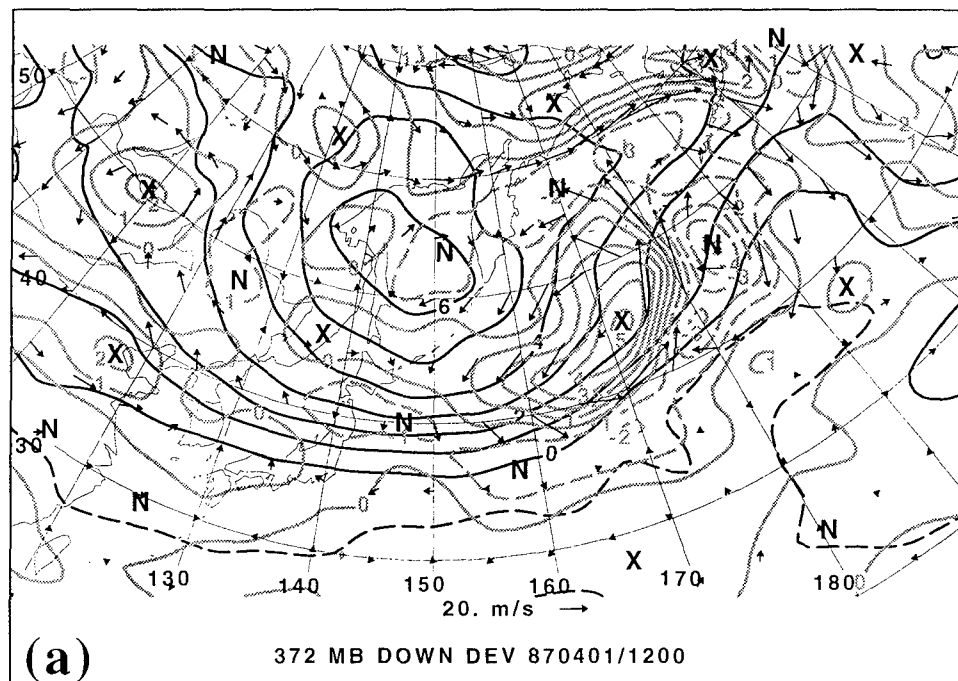


Fig. 5.10. Same as for Fig. 5.7, except for 1200 UTC 1 Apr. 1987.

Also, the dominant positive height perturbation is now located downstream of the mobile trough. Thus, the process that once provided for the development of the trough has begun to drain energy away.

b. Baroclinic amplification

The baroclinic term, $L^{-1}(-v'_L \bullet \nabla \bar{q}_U)'$, strengthens the trough from 0331/1200 to 0402/0000. A surface cyclone develops to the east of the mobile trough (see Fig. 5.2) in association with a trough downstream of our mobile trough. Figures 5.11-5.14 show the effect of the lower-level perturbation-scale winds on the upper-level basic state QGPV field. Initially, the strength of the circulation associated with this term is significantly less than the downstream development term. However, as the low-level cyclone matures, the associated circulation increases, and accordingly the effect on the upper levels grows. The greatest strengthening due to the baroclinic term was noticed at 0401/1200. However, the overall tendency by that time was positive, as competing processes were acting to weaken the trough.

c. Deformation

This term, $L^{-1}(-\bar{v} \bullet \nabla q'_U)'$, may involve horizontal (barotropic) deformation and vertical deformation by the vertical wind shear of the basic state (superposition). The contributions from this term were highly erratic throughout the period of the investigation. There were alternating periods of positive and negative height tendencies.

In order to separate the total deformation into horizontal deformation and deformation due to vertical shear, a procedure first developed by Nielsen-Gammon and Lefevre (1996) was incorporated. To calculate the horizontal (barotropic) deformation

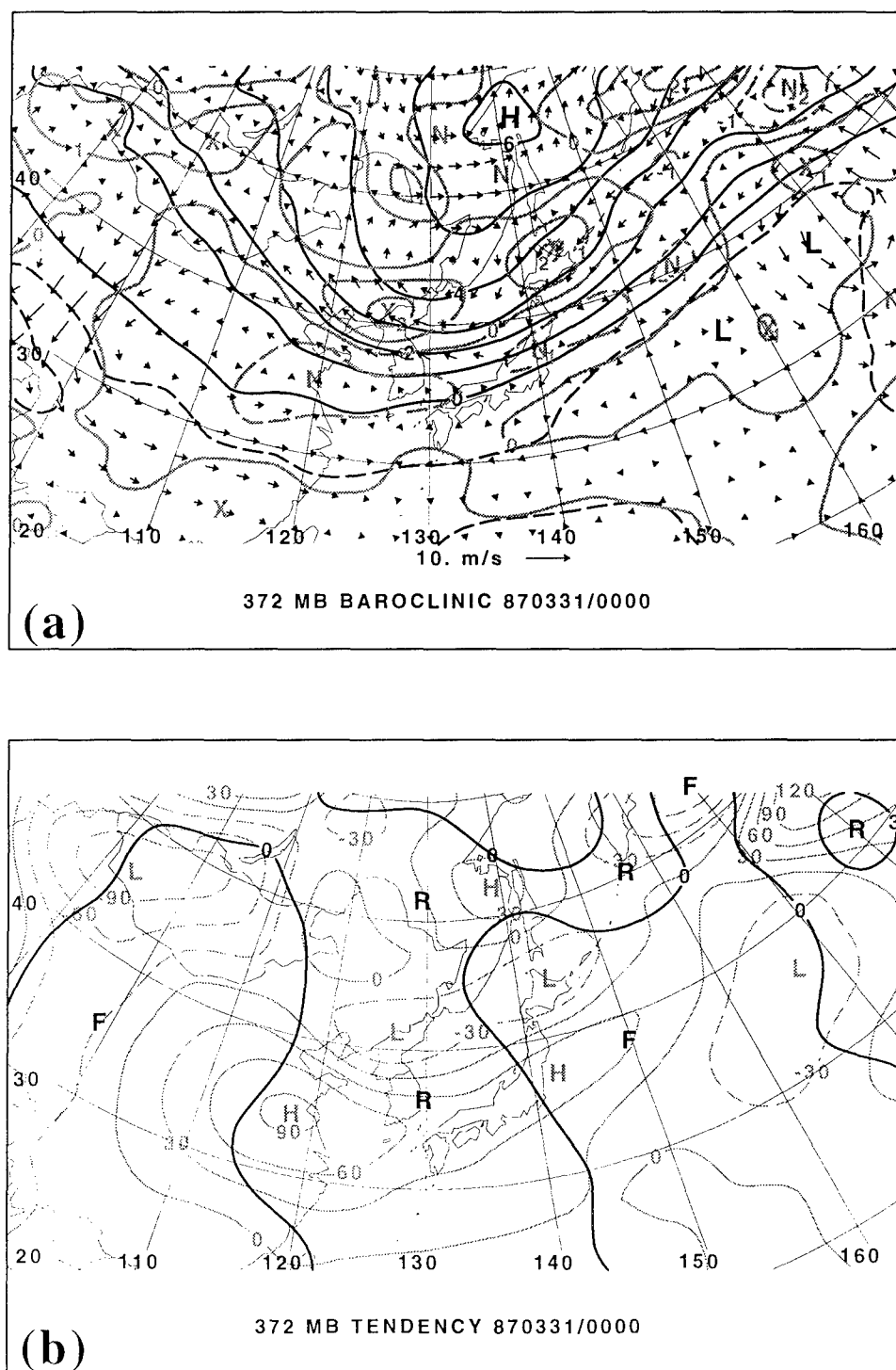


Fig. 5.11. Advections and tendencies associated with baroclinic amplification at 0000 UTC 31 Mar. 1987. (a) Base state 372 mb QGPV (black, $\times 10^{-4} \text{ s}^{-1}$); perturbation 372 mb QGPV (gray, $\times 10^{-4} \text{ s}^{-1}$); and 372 mb winds associated with lower-level perturbation QGPV. (Reference vector shown.) (b) Small-scale 372 mb height tendencies associated with advection of upper-level base state QGPV by winds associated with lower-level perturbation QGPV (black, contour interval 3 dam per 12 hr); and 372 mb heights associated with upper-level perturbation QGPV (gray, dam).

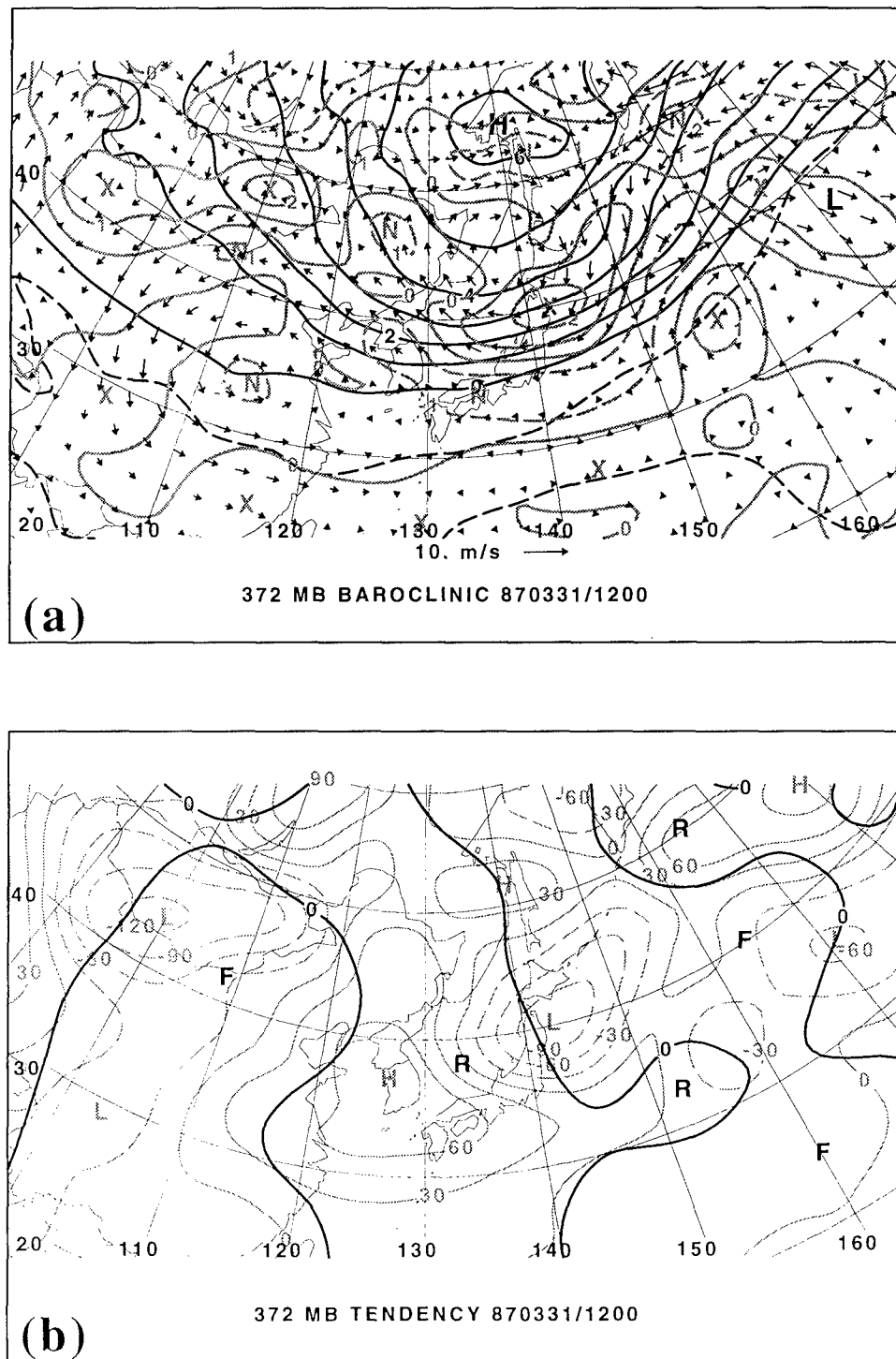


Fig. 5.12. Same as Fig. 5.11, except for 1200 UTC 31 Mar. 1987.

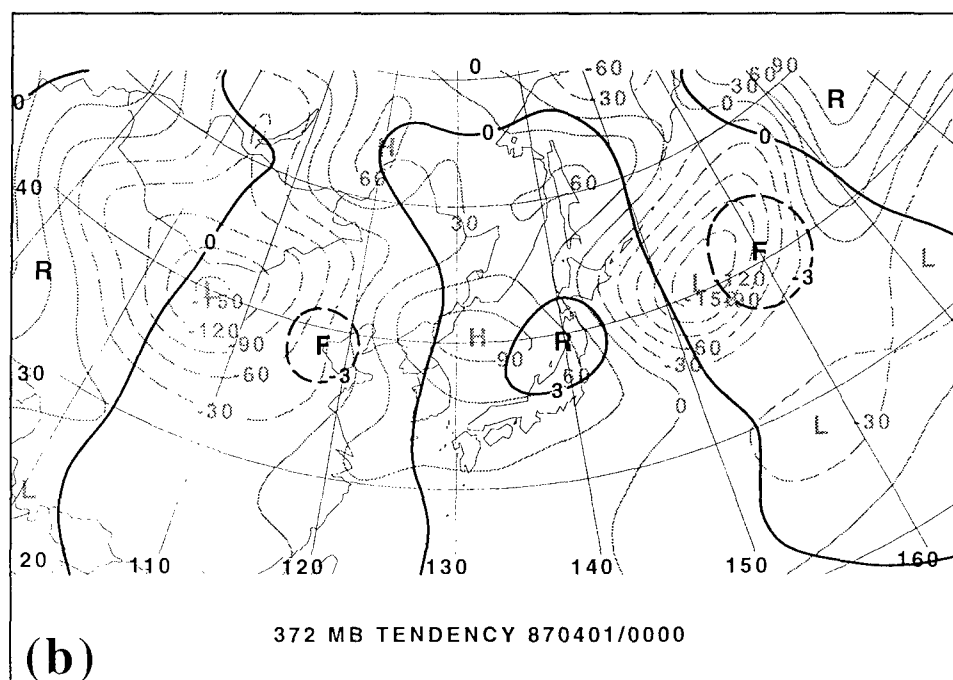
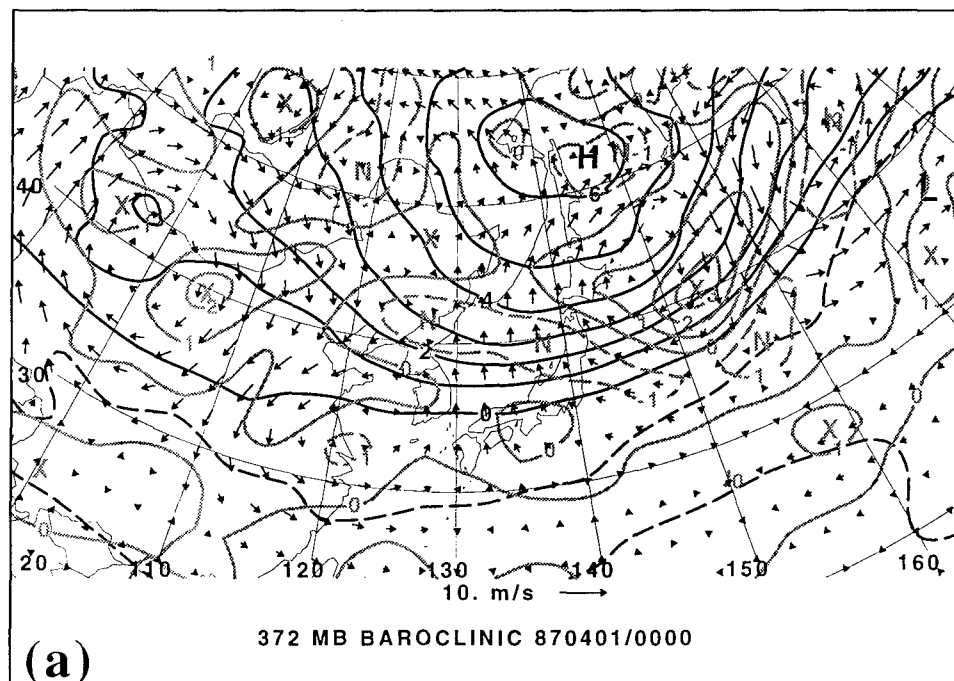


Fig. 5.13. Same as Fig. 5.11, except for 0000 UTC 1 Apr 1987.

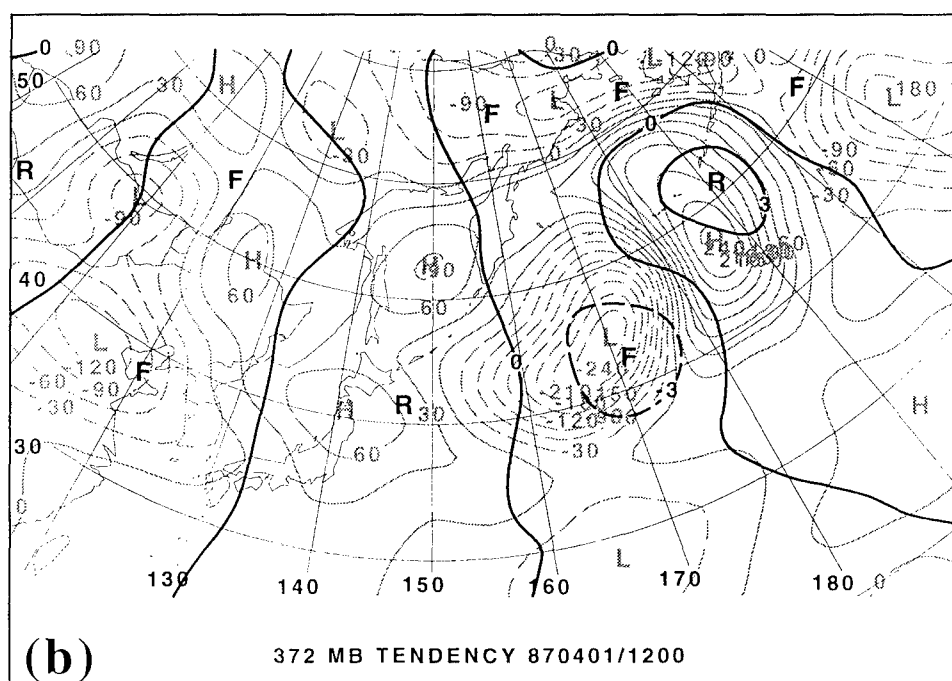
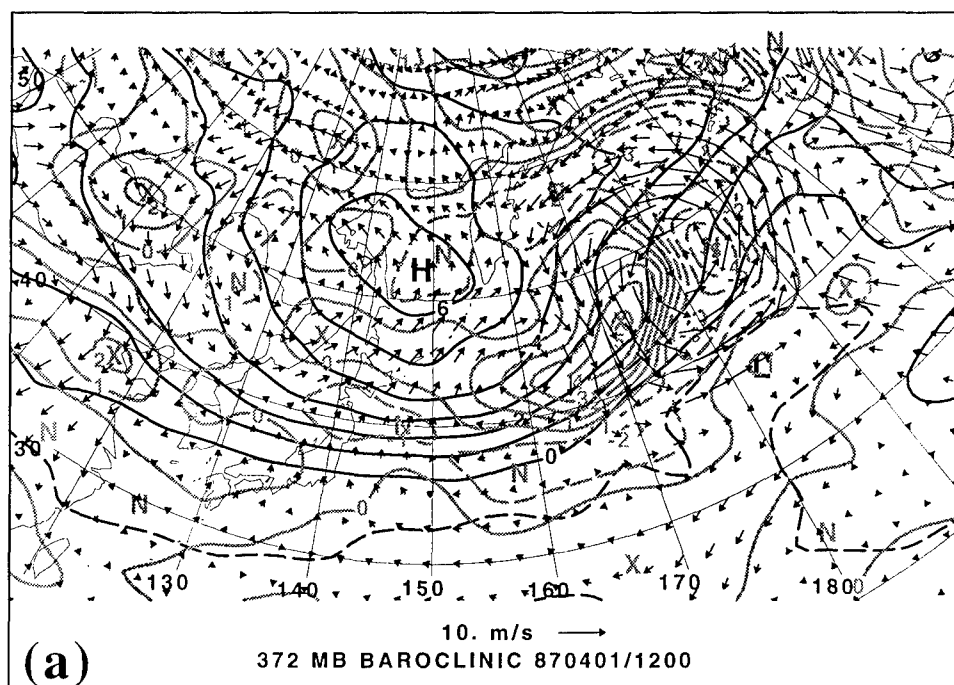


Fig. 5.14. Same as Fig. 5.11, except for 1200 UTC 1 Apr 1987.

the 372 mb wind was used to advect the QGPV at all levels. The difference between the full term and the horizontal deformation term is attributed to deformation due to basic state vertical wind shear. Figure 5.15 displays the tendencies from superposition (vertical shear), barotropic deformation (horizontal), and the total deformation term (second term of the right hand side of (4.10)).

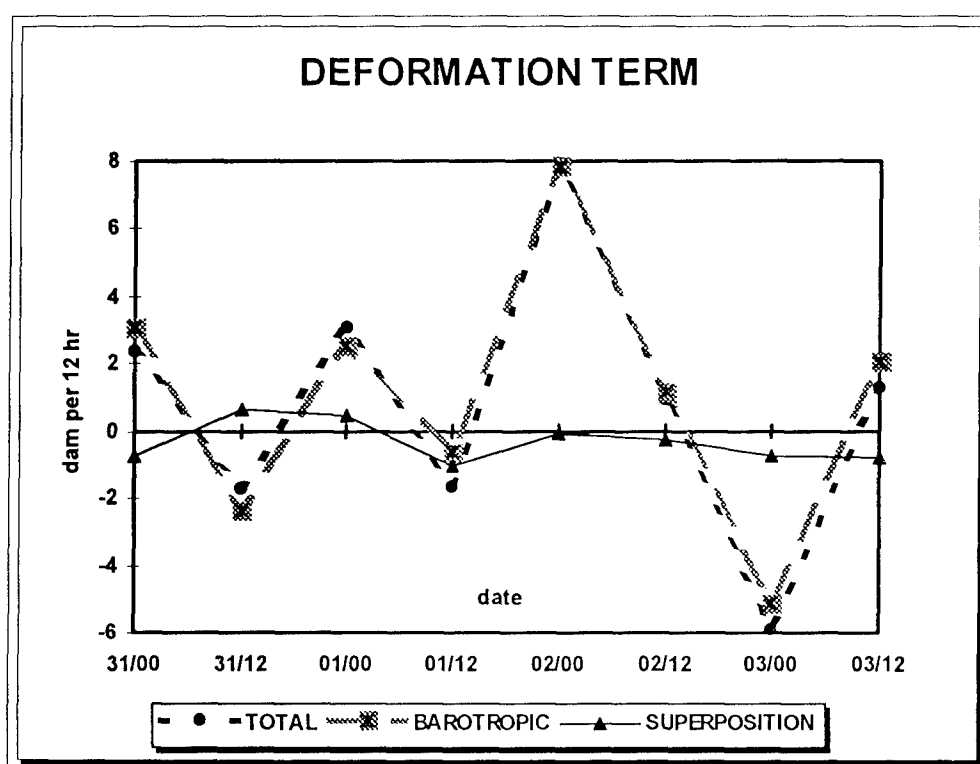


Fig. 5.15. Quasigeostrophic height tendency contribution (dam per 12hr) from total deformation term (black dots, dotted), barotropic (gray squares, dashed), and superposition (black triangles, thin line).

Barotropic deformation is the dominant component of the deformation term, while the tendencies due to superposition were always near zero. On 0331/1200 the trough was slightly strengthened due to barotropic deformation (-1.7 dam/12 hr). Figure 5.16a shows the QGPV perturbation associated with the trough in the base of a large-scale trough over Honshu. Axes of dilatation and large-scale heights are plotted to show the mechanism of strengthening. The western half of the positive QGPV perturbation is stretched as shown by the axes of dilatation oriented nearly parallel to the major axis of the perturbation. This stretching results in height rises (Fig 5.16b). The eastern side is experiencing stretching along the minor axis. This results in height falls due to the compacting of the anomaly, with an increase in circulation.

Twelve hours later (Fig. 5.17), the perturbation QGPV is on the eastern side of the long wave trough and is stretched more along its major axis (southwest-northeast). A height rise/fall couplet is centered over the anomaly; however, height rises dominate much of the anomaly.

The deformation term is most positive at 0402/0000 (7.8 dam/12 hr) and is the largest factor in trough decay at the time. The term attempts to strengthen the trough again as the trough nears the Aleutians (Fig 5.18) at 0403/0000 (-5.9 dam/12 hr) but other competing processes dominate and act to weaken the trough.

d. Vortex-vortex

The small-scale vortex-vortex interaction terms, $L^{-1}(-\mathbf{v}'_L \bullet \nabla \mathbf{q}'_U)'$ and $L^{-1}(-\mathbf{v}'_U \bullet \nabla \mathbf{q}_U)'$, contribute weakly to development early on but predominately act to weaken the trough later.

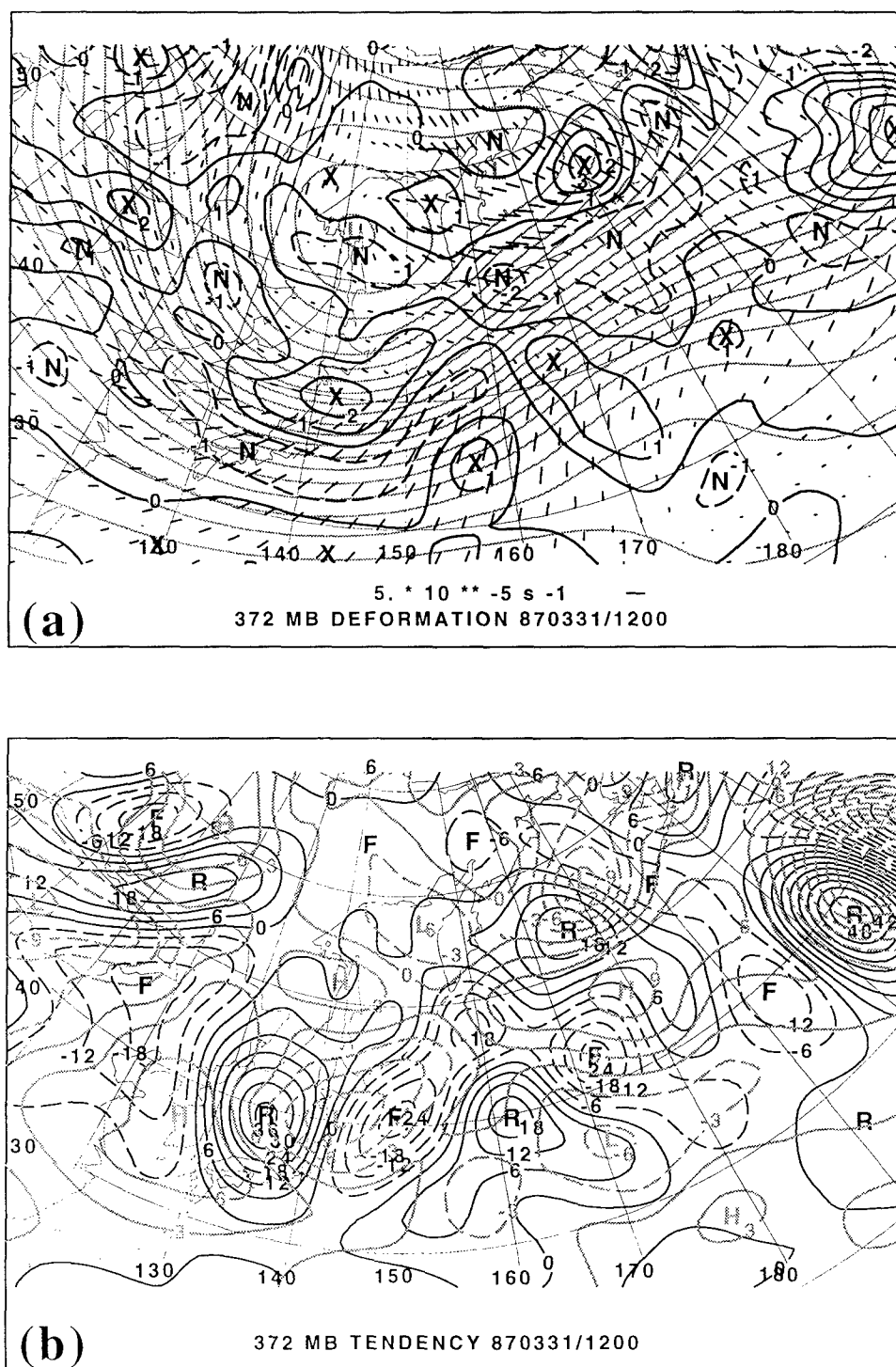


Fig. 5.16. Deformation and tendencies associated with basic state flow at 1200 UTC 31 Mar 1987. (a) Perturbation 372 mb QGPV (black, $\times 10^{-4} \text{ s}^{-1}$); base state 372 mb heights (gray, contour interval 6 dam); and 372 mb axes of dilatation associated with base state deformation (lengths of axes are proportional to the magnitude of deformation, scaled as shown); (b) small-scale 372 mb height tendencies associated with advection of upper-level perturbation QGPV by base state winds (black, dam); and 372 mb heights associated with upper-level perturbation QGPV (gray, contour interval 3 dam, negative contours dashed).

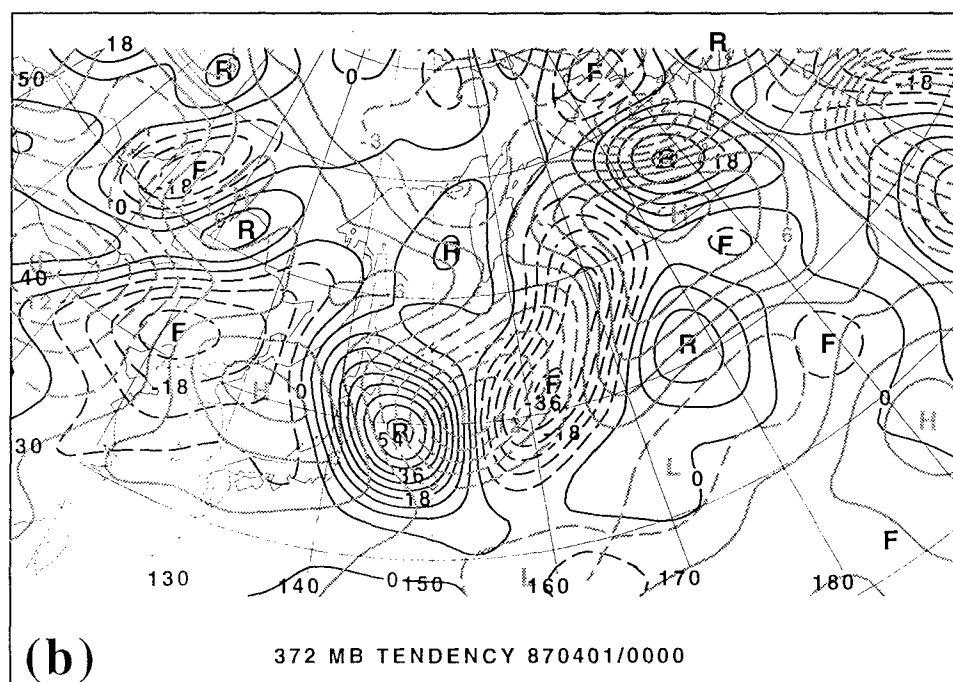
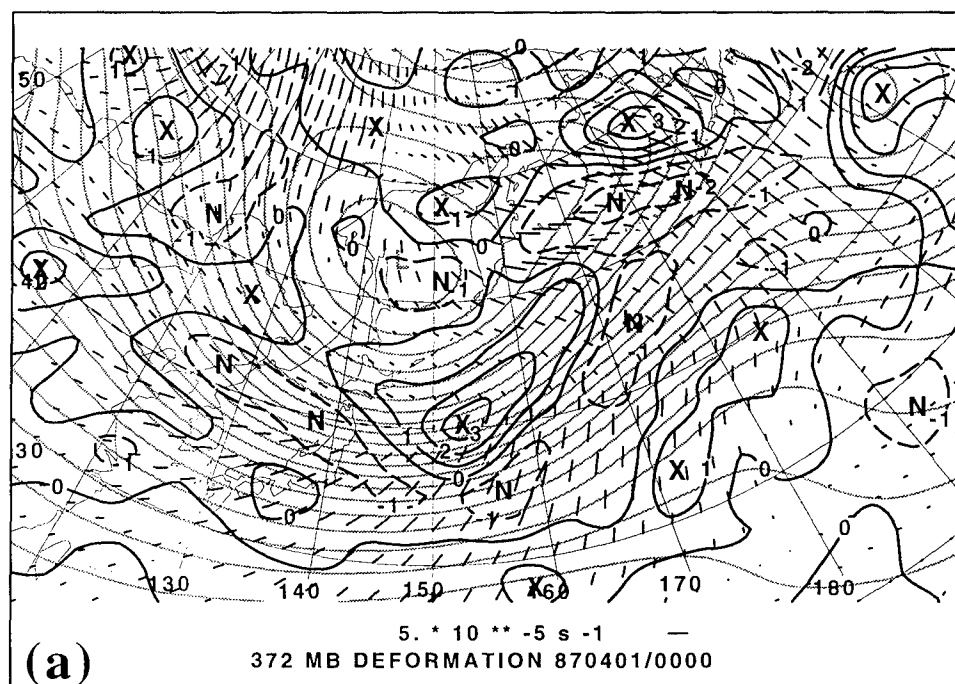


Fig. 5.17. Same as that for Fig. 5.16, except for 0000 UTC 1 Apr. 1987.

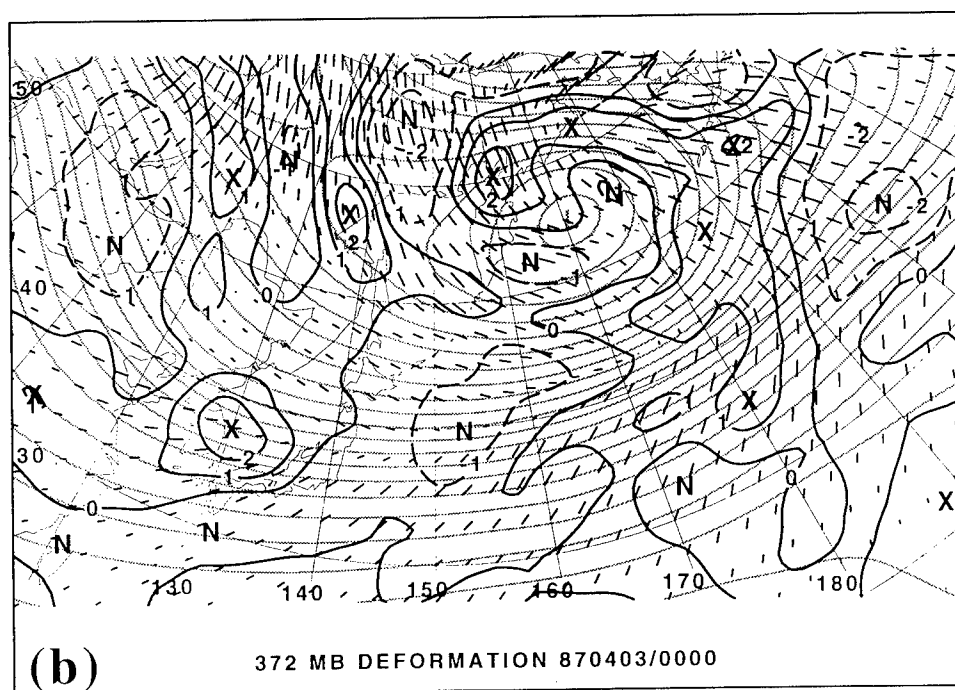
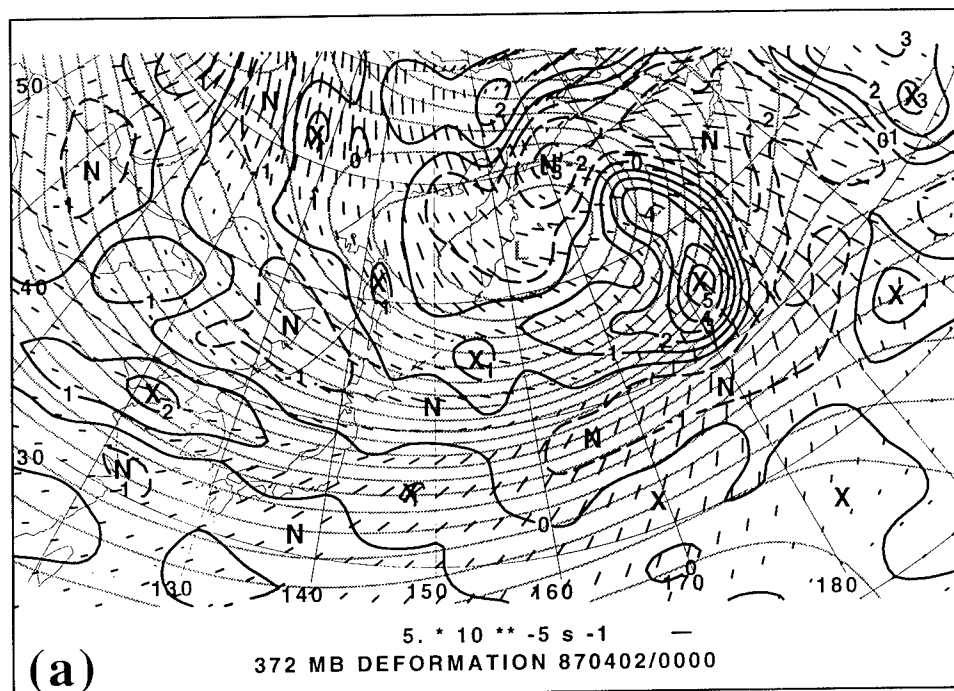


Fig. 5.18. (a) Same as that for Fig. 5.16a, except for 0000 UTC 2 Apr. 1987; (b) same as that for Fig. 5.16a, except for 0000 UTC 3 Apr. 1987.

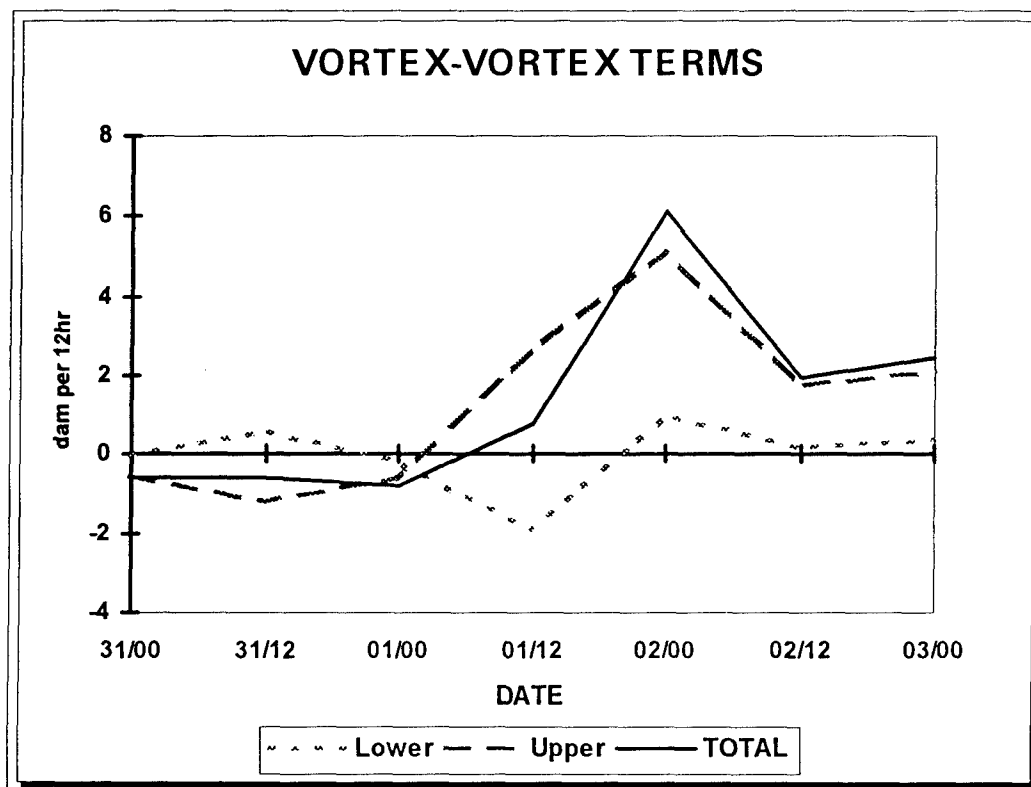


Fig 5.19. Quasigeostrophic height tendency contributions (dam per 12 hr) from the fifth term (Upper) (black, dashed) and sixth term (Lower) of (4.10) (gray, dotted), and the sum of the two (black solid) for the 31 March 1987 case.

Figure 5.19 shows the individual contributions of lower and upper vortex-vortex terms and their sum. The upper vortex-vortex term contributes most to development (-1.2 dam/12 hr) at 0331/1200. At this time, the circulation around the height perturbation is slightly smoother than the perturbation QGPV. This is due in part to the 472 mb QGPV perturbation center which is shifted slightly to the south of the perturbation at 372 mb (not shown). This effect is short-lived. The upper vortex-vortex term acts to weaken the trough after 0401/0000.

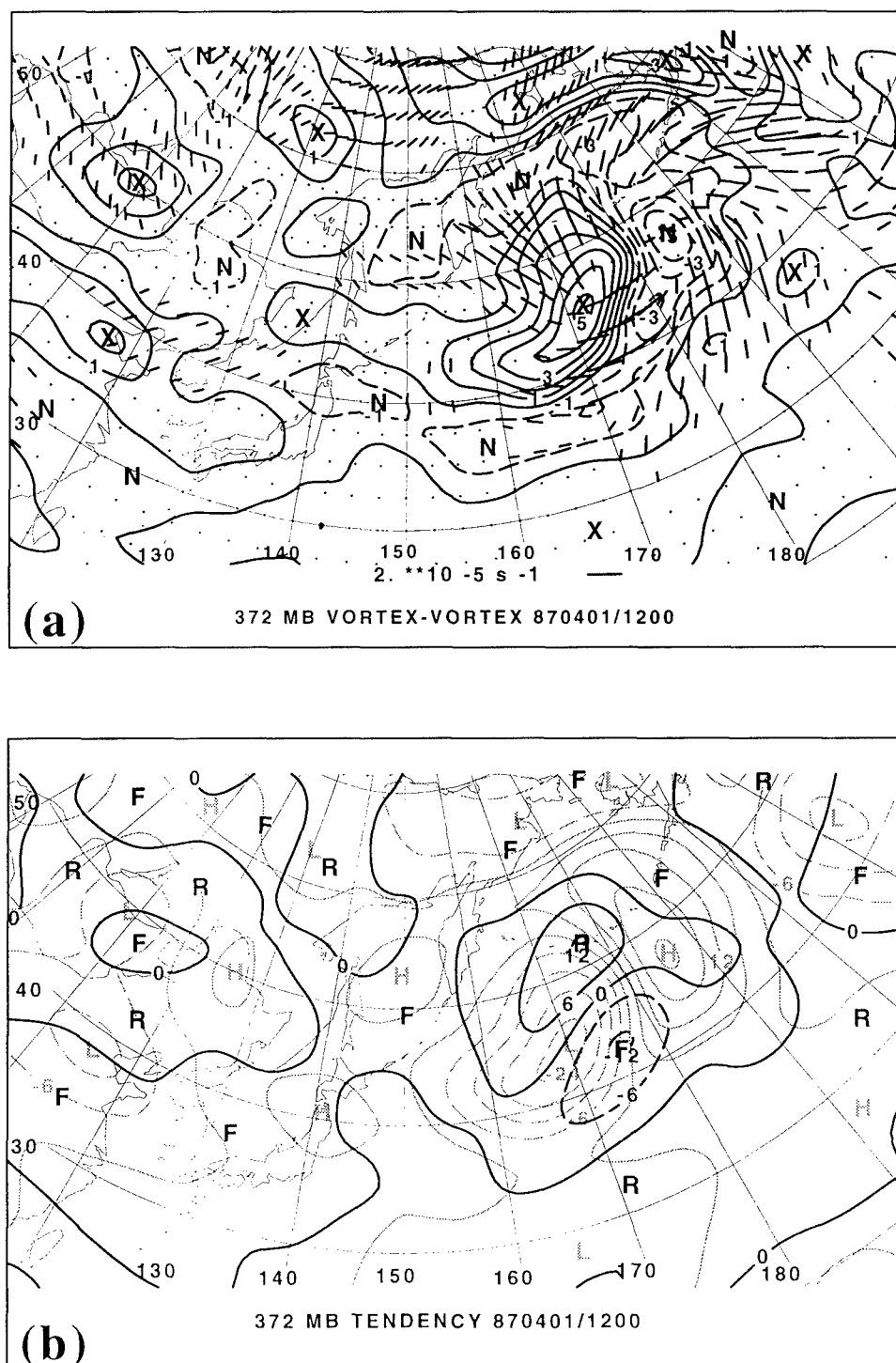


Fig. 5.20. Advections and tendencies associated with vortex-vortex interactions at 1200 UTC 1 Apr. 1987. (a) Perturbation 372 mb QGPV (black, $\times 10^{-4} \text{ s}^{-1}$); and 372 mb axes of dilatation associated with small-scale deformation due to *lower-level* perturbation QGPV (lengths of axes are proportional to magnitude of deformation, scale at bottom). (b) Small-scale height tendencies associated with advection of upper-level perturbation QGPV by winds associated with perturbation *lower-level* QGPV (black, dam per 12 hr); and 372 mb heights associated with upper-level perturbation QGPV (gray, m).

The lower vortex-vortex term generally had a weaker influence on the trough. At the time of the term's greatest strengthening at 0401/1200 (Fig. 5.20), a mature surface cyclone was situated to the northeast of the mobile trough. The deformation due to the lower vortex-vortex term elongates the PV perturbation along its minor axis, resulting in increased circulation and thereby strengthening.

e. Interactions due to the base states of height and QGPV

The large-scale interaction term, $L^{-1}(-\bar{\mathbf{v}} \bullet \nabla \bar{q}_U)'$, represents the effect of the base state winds advecting the base state QGPV. This term intensifies the mobile trough in five of the seven time periods investigated. The phase difference between the large-scale height and the large-scale QGPV can lead to positive QGPV advections in the vicinity of the trough. Figure 5.21 shows the base states of height and QGPV at 0401/0000 and 0401/1200. The nonlinear interaction between basic states of height and QGPV causes a projection onto the perturbation scale of height. This same effect was detailed in a case study by McEver (1996). The largest contribution to development due to this interaction was at 0402/0000. The flow associated with the base state height is advecting air with higher values of QGPV accounting for height falls of nearly 8 dam per 12hr at the trough center (Fig. 5.22). However, other terms are counteracting the effects of the large-scale tendency. The overall tendency shows weakening of the trough.

The differences in structure between the base state heights and QGPV may be caused partly by the inversion method. The calculation of the large-scale geopotential height requires the full inversion of large-scale QGPV (inversion of all q including boundary conditions). This includes the large-scale thickness. The large-scale thickness

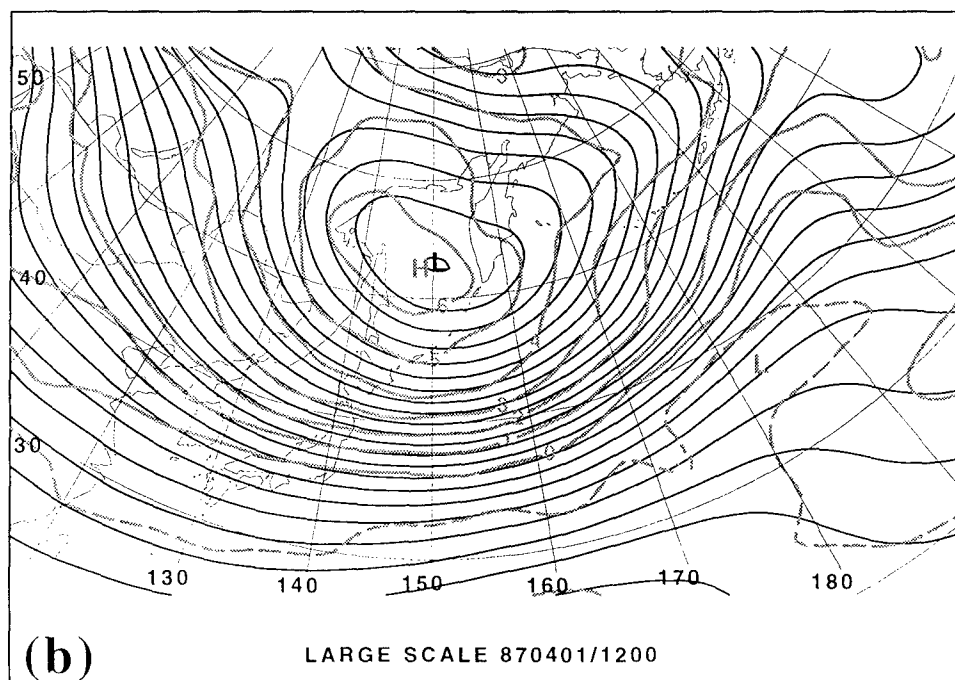
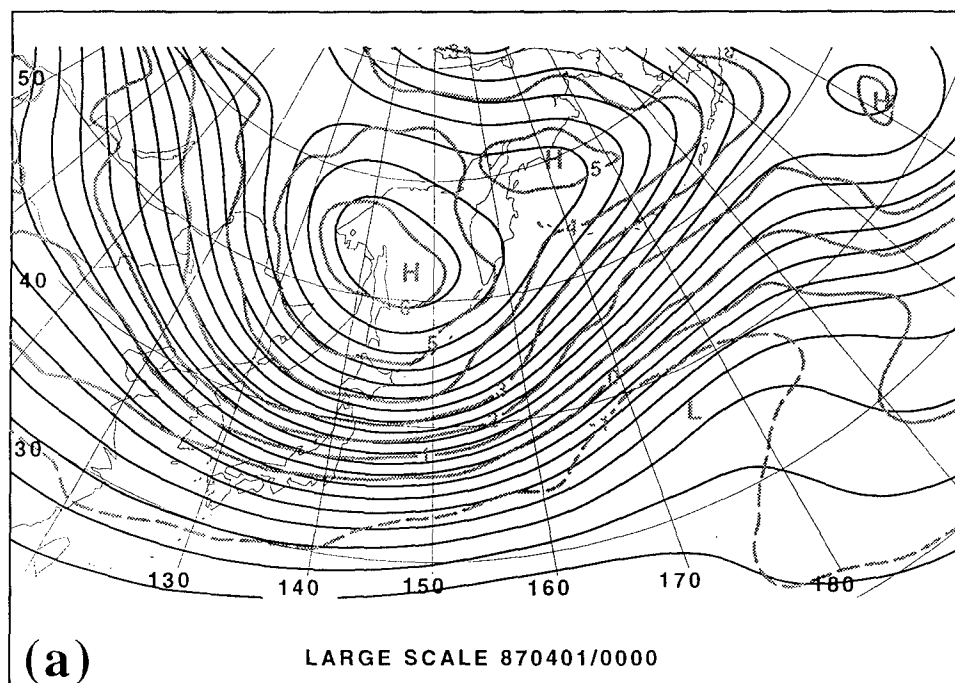


Fig. 5.21. Base state 372 mb heights associated with the full inversion of QGPV (black, contour interval 6 dam); and base state 372 mb QGPV associated with the inversion of upper-level QGPV (gray, dashed, $\times 10^{-4} \text{ s}^{-1}$) for (a) 0000 UTC 1 Apr. 1987 and (b) 1200 UTC 1 Apr. 1987.

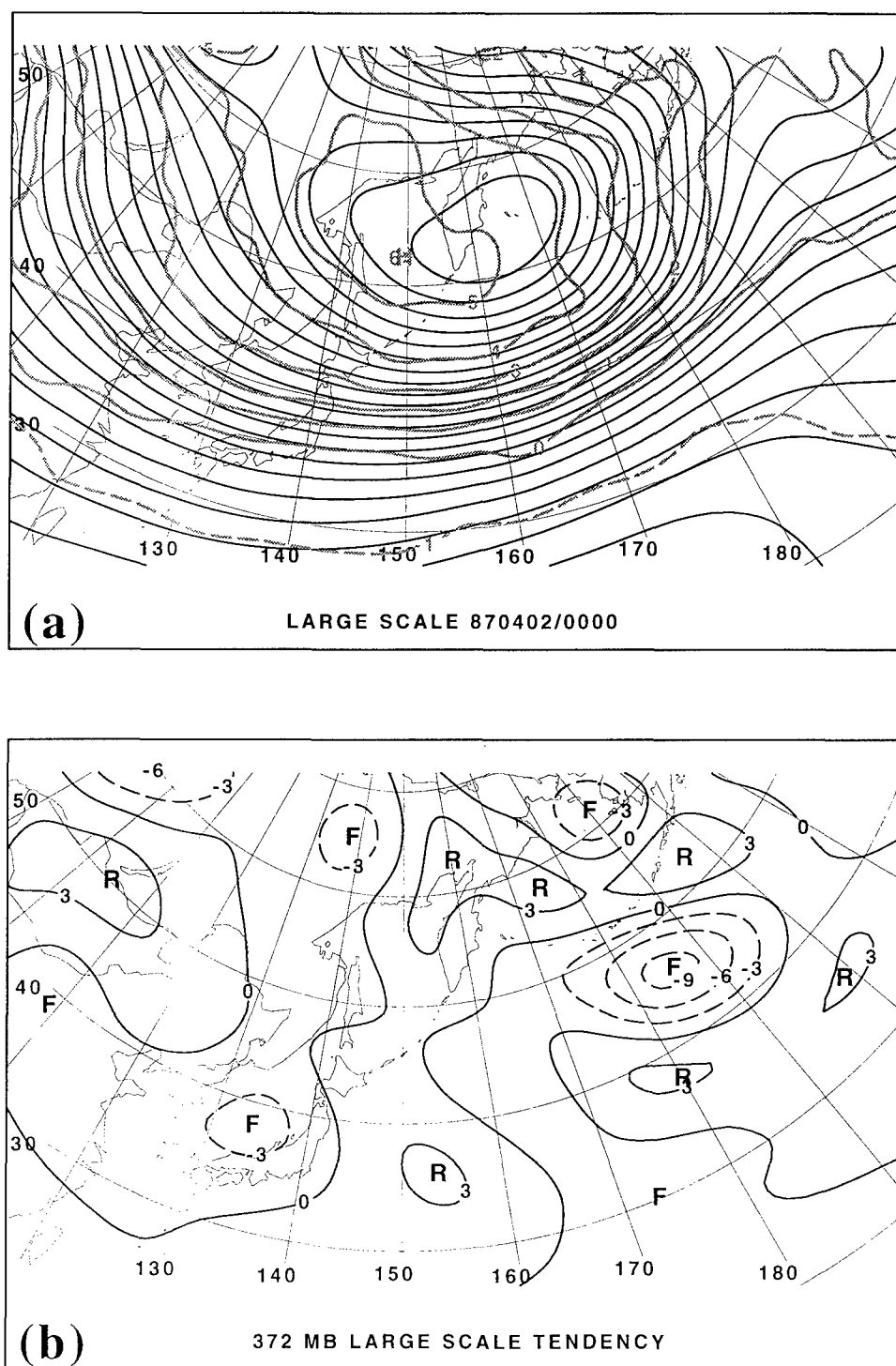


Fig. 5.22. (a) Same as that for Fig. 5.21, except for 0000 UTC 2 Apr. 1987. (b) Small-scale height tendencies at 372 mb at 0000 UTC 2 Apr. 1987 associated with the advection of upper-level base state QGPV by winds associated with full inversion of base state QGPV (contour interval 3 dam per 12 hr).

gradient during the cold season off the coast of Asia is typically oriented from southwest to northeast, the result of a large-scale surface warm anomaly to the southeast of Japan. When taking this into account, this may cause the large-scale height to be shifted slightly to the southeast, resulting in a slight phase difference between the large-scale height and QGPV fields. Also, the base state fields used in this research contain a time-mean component of the perturbation-scale fields. Therefore, some small-scale effects of the base-state interactions are to be expected.

5. Dynamical tropopause maps

Further insight into the development of the mobile trough can be gained by examining dynamical tropopause maps of the event. Dynamical tropopause maps have been used to study synoptic-scale variability of the atmosphere (e.g., Hoskins and Berrisford 1988, Thorncroft et al. 1993). Recently, Bosart et al. (1996) demonstrated the value of dynamical tropopause maps, in conjunction with QGPV maps, in the examination of large-scale antecedent conditions associated with the "Superstorm '93" over eastern North America. When inspecting dynamical tropopause maps, the analogous conceptual model would be the Eady model representation of the troposphere with a fixed top (here, represented by the tropopause map) and bottom (ground) boundaries. The assumption that the upper-level potential vorticity gradient begins at the tropopause is essential to encapsulate the dynamics of the upper-troposphere into the motion and influence of a single-contour or tightly-packed set of contours (Nielsen-Gammon 1995).

The dynamical tropopause maps used in this research were constructed by interpolating atmospheric variables (θ , u , v , p) to the 1.5 PVU surface ($1 \text{ PVU} = 10^{-6} \text{ m}^2 \text{ s}^{-1}$

K kg^{-1} .) Potential temperature on a tropopause surface (θ_T) is conserved for adiabatic and frictionless flow. Regions of baroclinicity and strong jet streams are easily identified by tight θ_T and pressure contours. Waves in the potential temperature field on the tropopause are analogous to waves of potential vorticity on isentropic surfaces or waves of QGPV on a pressure surface. Cold anomalies at the tropopause surface tend to induce cyclonic circulation, while anticyclonic circulations are associated with warm anomalies. With the both winds and potential temperatures plotted, it is possible to infer the advection, propagation, and evolution of upper-level features. Where waves in the potential temperature field are amplifying, the corresponding height perturbations are amplifying as well.

Figure 5.23 displays the evolution of the tropopause before and during the formation of the mobile trough. The maps show the distribution of potential temperature and wind on the tropopause. The prominent features on these charts are two ribbons of concentrated contours of potential temperature extending across the east Asian continent. The northern ribbon is associated with polar jet, while the southern one (seen over central China through southern Japan) is associated with the subtropical jet stream.

Figure 5.23a-b shows a well-developed ridge-trough system at the tropopause upstream of the area where the studied mobile trough formed at 500 mb. This wave system is separated somewhat from the main jet ribbon. A warm anomaly (maximum contour value of 305K) is evident over northern Mongolia at 1200 UTC 30 March, inducing anticyclonic circulation around it. The northerlies associated with the warm anomaly are causing significant advection of potential temperature into an isolated cold

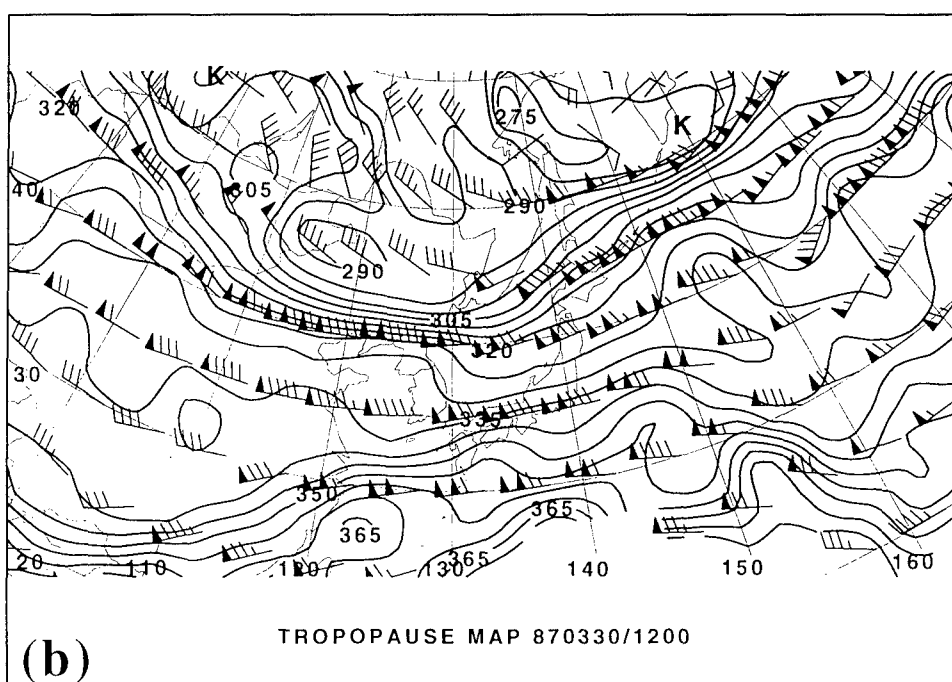
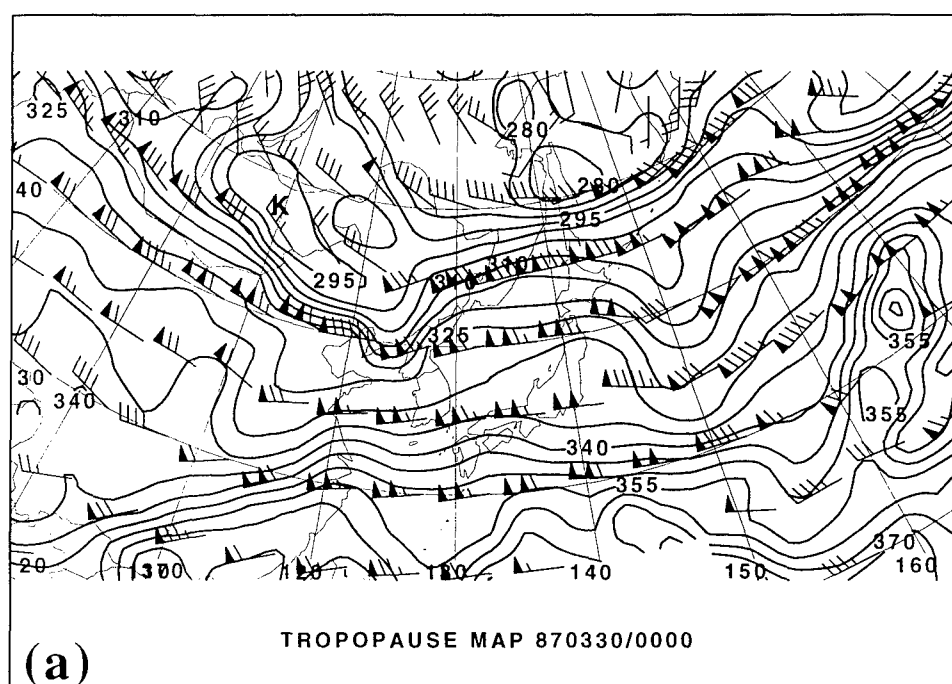


Fig. 5.23. Maps of tropopause potential temperature (contour interval 5K) and winds (with one pennant, full barb, and half barb denoting 25, 5, 2.5 m s^{-1} , respectively) for (a) 0000 UTC 30 Mar. 1987, (b) 1200 UTC 30 Mar. 1987, (c) 0000 UTC 31 Mar. 1987, (d) 1200 UTC 31 Mar. 1987.

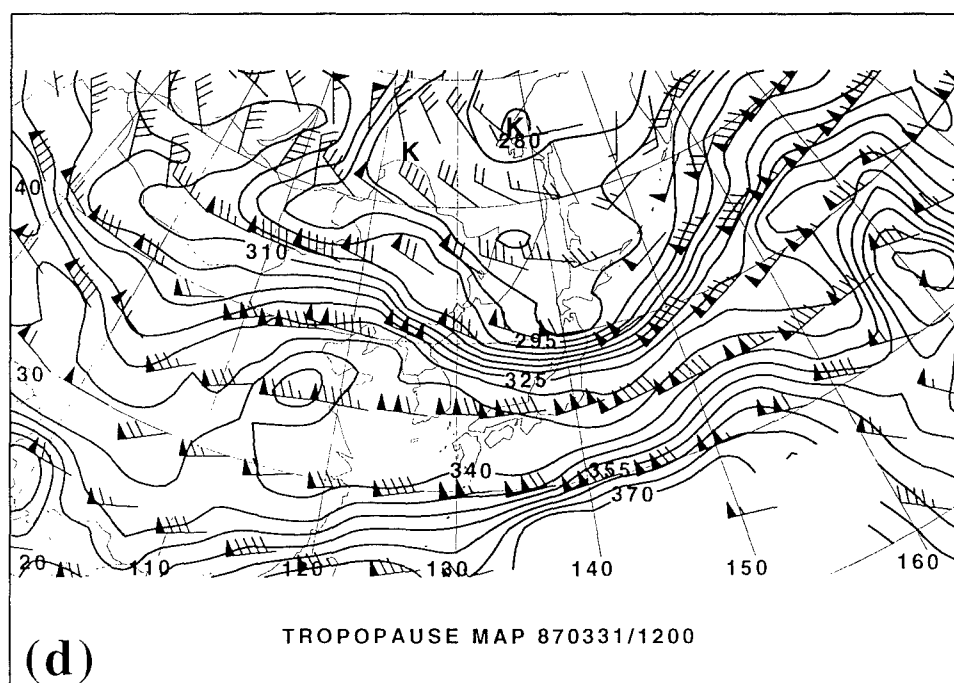
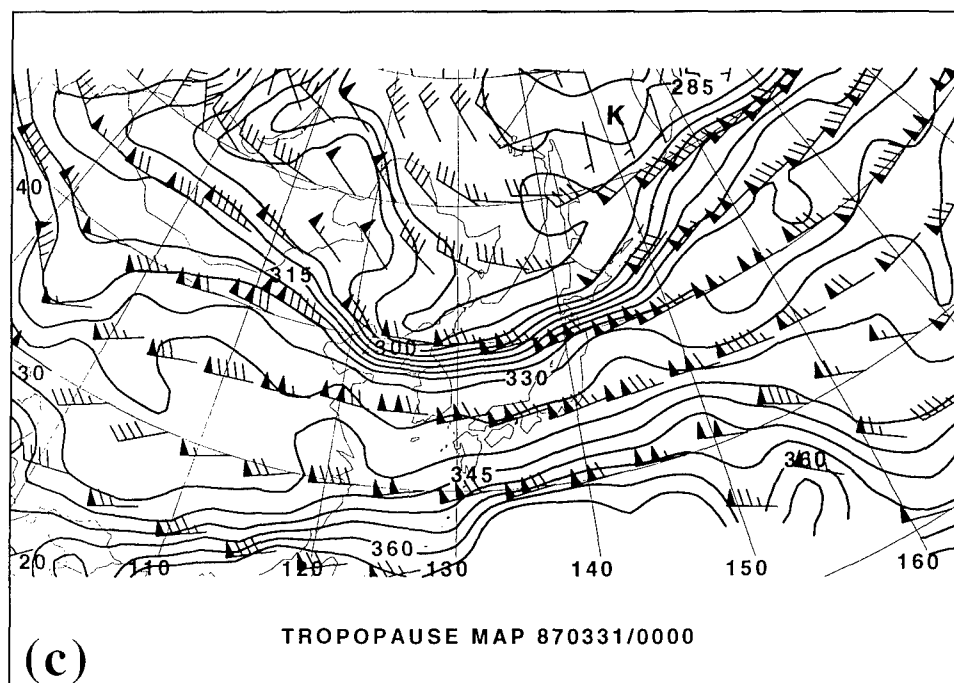


Fig. 5.23, continued.

anomaly (minimum contour value of 290K) just downstream over Manchuria. These two potential temperature anomalies were tracked back in time to 0325/0000 where they appear to form by being "pinched off" the polar potential temperature ribbon over north-central Russia (not shown).

Twelve hours later, (Fig. 5.23c) the polar jet gradient is strengthening. A wave in the potential temperature contours can be seen over the region where the mobile trough develops. It may be noticed that the cold anomaly no longer exists. The anticyclonic circulation associated with the upstream warm anomaly has weakened, but potential temperature advection continues. Therefore, continual strengthening of the wave is expected.

The wave arrives over Honshu on 0331/1200 (Fig. 5.23d) and extends over 45K of the potential temperature field. The wave at this time, ridge-to-ridge, encompasses over 40 degrees of longitude. The precursor upstream vortices have weakened considerably. They are now indistinguishable from the background flow, as potential temperature advection has decreased considerably.

The above subjective analysis of the development of the tropopause wave associated with the mobile trough fits the pattern associated with the propagation of a group of Rossby waves. Downstream propagation requires an upstream disturbance. The disturbance must be capable of producing flow across pre-existing potential vorticity isopleths. This requirement is met in this case with the upstream wave seen on the tropopause maps. As soon as northerlies associated with the upstream ridge strengthened, the cross-contour flow began in earnest, thereby forming a trough. The upstream wave weakened as our mobile trough strengthened.

6. Summary

In summary, the genesis of this mobile trough, as diagnosed using piecewise tendency diagnosis on the QGPV height tendency equation, involved three primary processes. It was found that downstream development was the primary mechanism responsible for mobile trough formation. Baroclinic effects and large-scale interactions played lesser roles during development. A surface cyclone developed *prior* to the formation of the mobile trough, therefore simultaneous development at upper-level and lower-levels is discounted (Type A cyclogenesis). A combination of downstream development and barotropic deformation contributed to the decay of the mobile trough.

Analysis of dynamical tropopause maps also showed that development of the mobile trough was primarily due to the downstream development process. This mechanism was evident in the cross-contour flow associated with a pre-existing wave causing the development of a wave downstream.

CHAPTER VI

CASE STUDY TWO

17 OCTOBER 1988

This purpose of this chapter is to explain the development of a mobile trough that formed over the Yellow Sea-East China Sea region on 1800 UTC 17 October 1988. A brief synoptic overview of the development of the mobile trough is given. Then, this case will be examined using dynamical tropopause maps. Also, Nielsen-Gammon's and Lefevre's (1996) PTD technique will be used to ascertain the dynamical mechanisms that governed the development of the mobile trough. The downstream development mechanism will be shown to contribute most to initiation of the trough. Superposition of potential vorticity at different levels contributes the most strengthening in the later stages. Barotropic deformation modulates the strength of the mobile trough throughout the later stages of its life.

1. Overview of mobile trough

This mobile trough developed on the northwest side of a weak amplitude, long wave situated over the Yellow Sea-East China Sea region. The large-scale flow regime was predominately zonal. Figure 6.1 shows the initial development of the trough. Enhanced positive geostrophic vorticity advection is evident just west of the Yellow Sea on the western flank of the large-scale trough on 17 October 1200 UTC (Fig. 6.1a). One might argue that the mobile trough formed at this time. However, six hours later, the vorticity advection becomes more pronounced near 35 N, 120 E, and the mobile trough is

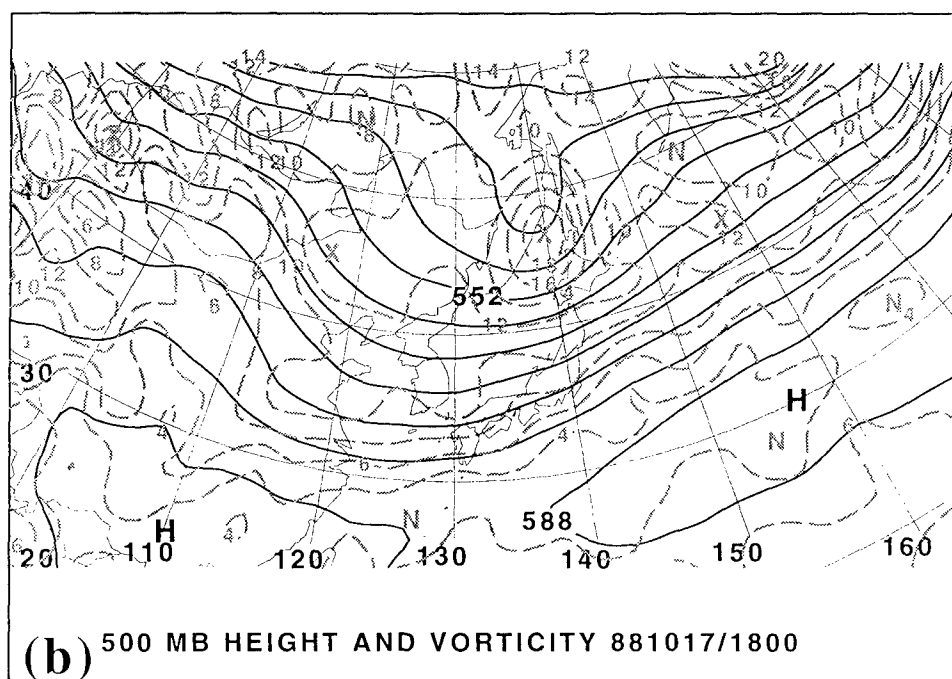
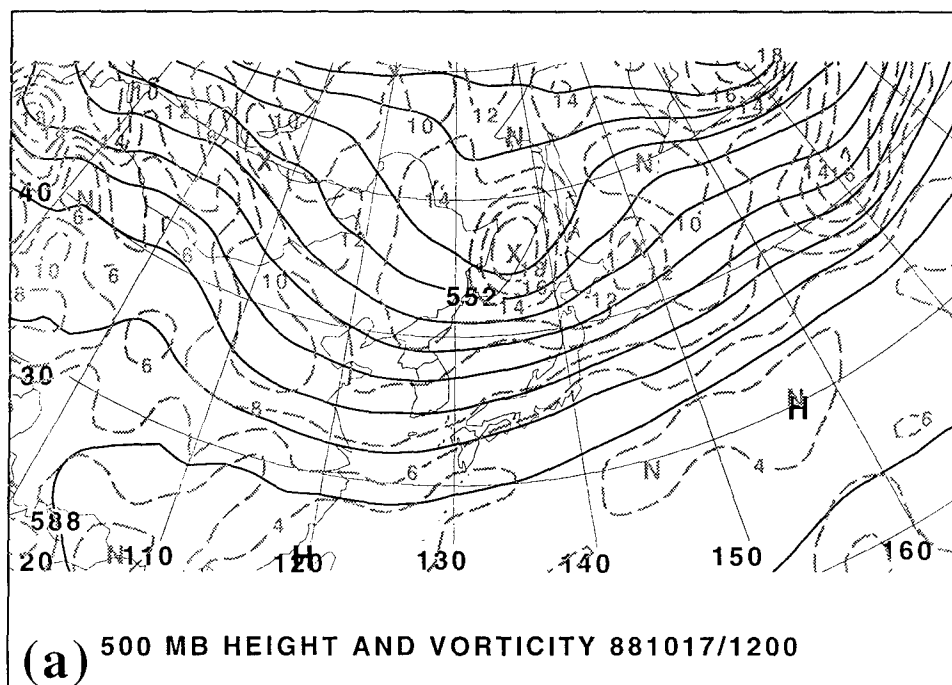


Fig. 6.1. The 500 mb geopotential heights (black, contour interval 6 dam) and geostrophic vorticity (gray dashed, contour interval $2 \times 10^{-5} \text{ s}^{-1}$) for (a) 881017/1200, (b) 881017/1800, (c) 881018/0000, (d) 8810/0600, (e) 881018/1200, (f) 881019/0000, (g) 881019/1200, (h) 881020/0000.

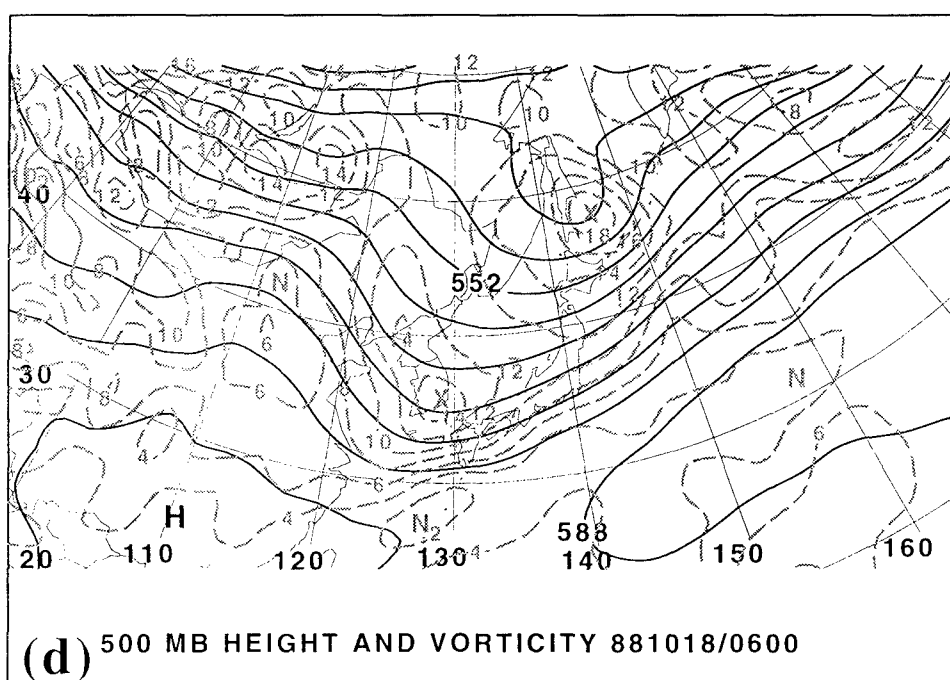
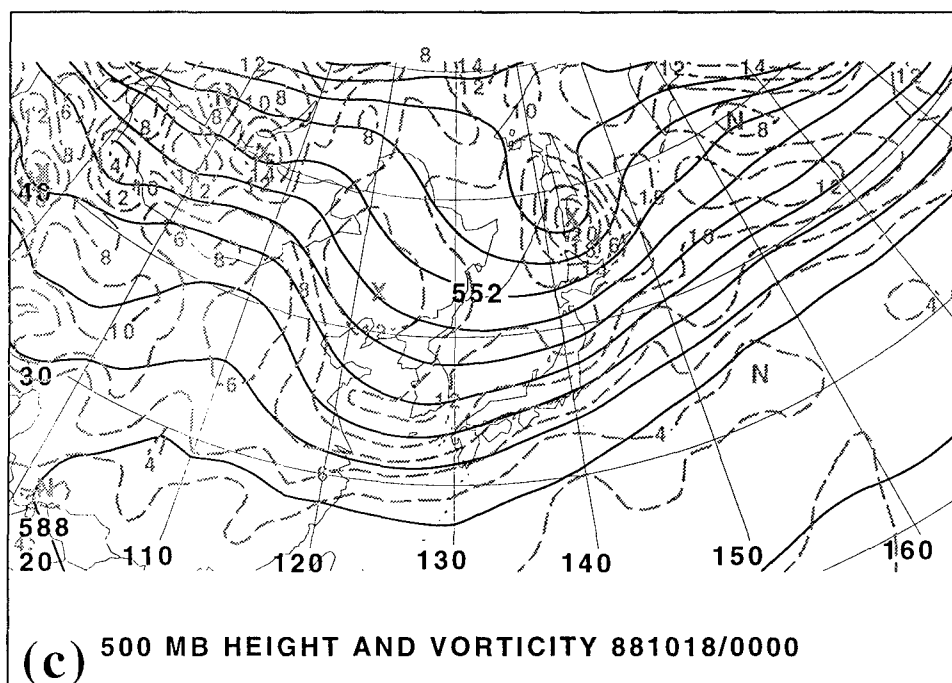


Fig. 6.1, continued.

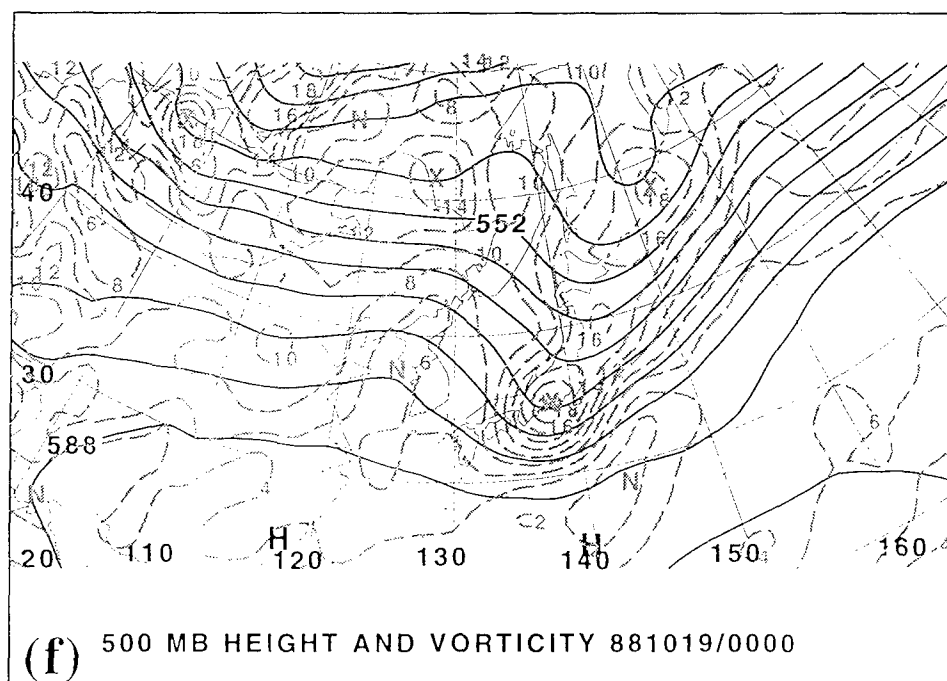
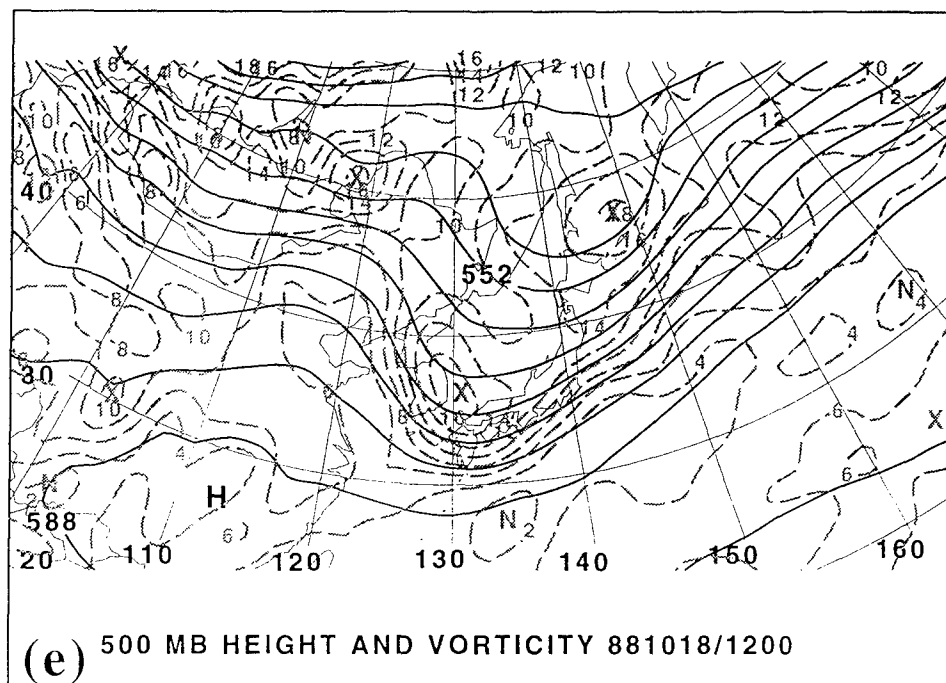


Fig. 6.1, continued.

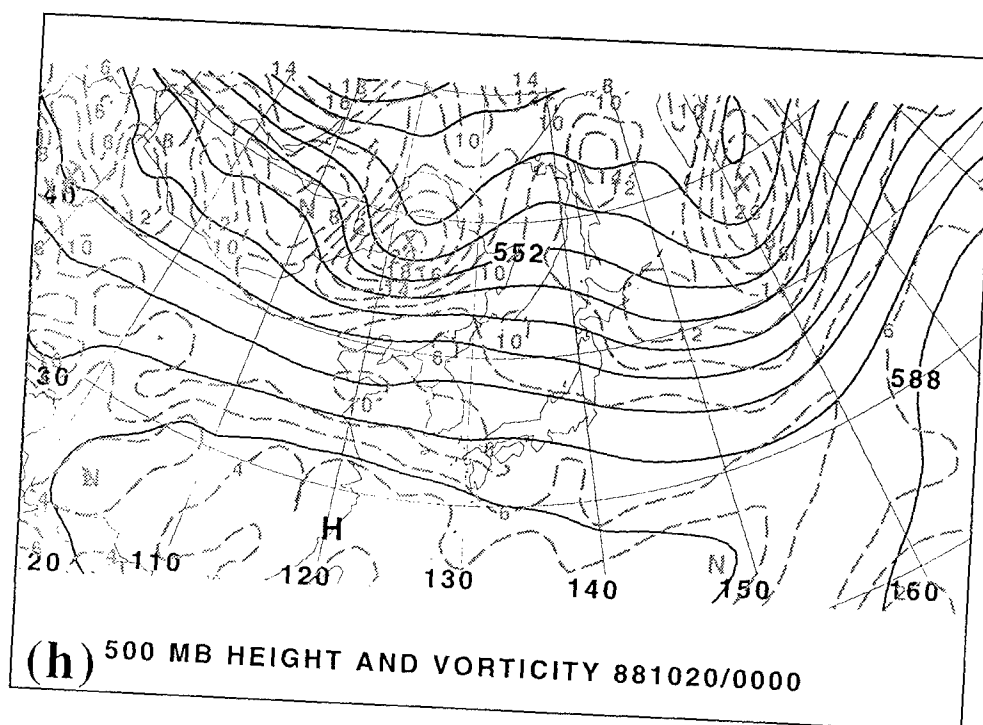
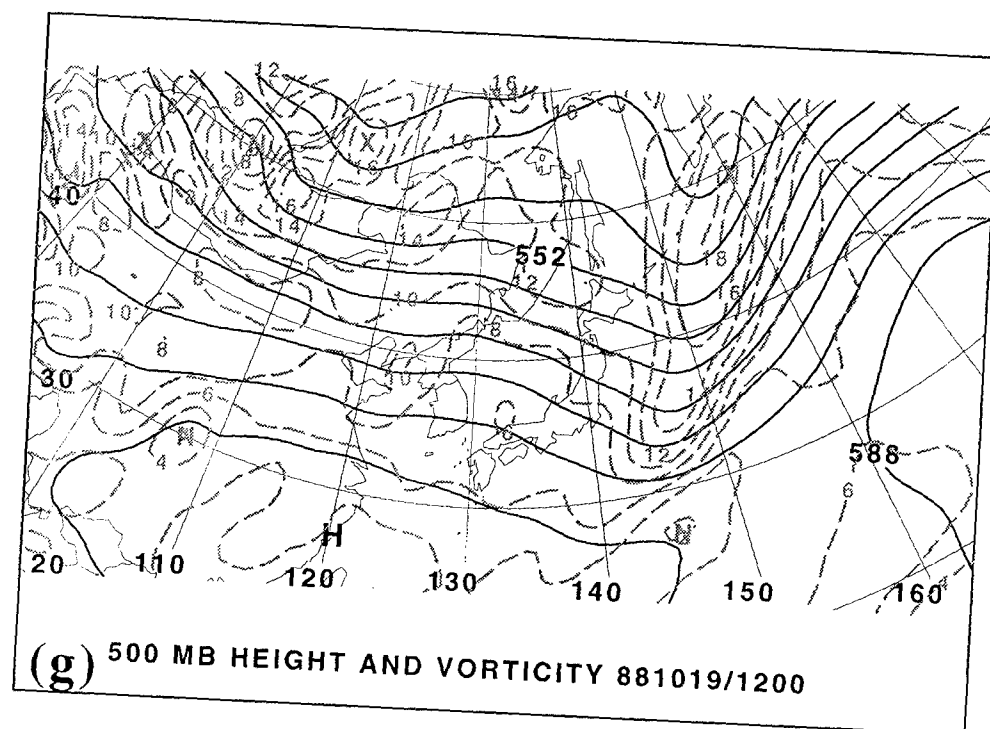


Fig. 6.1, continued.

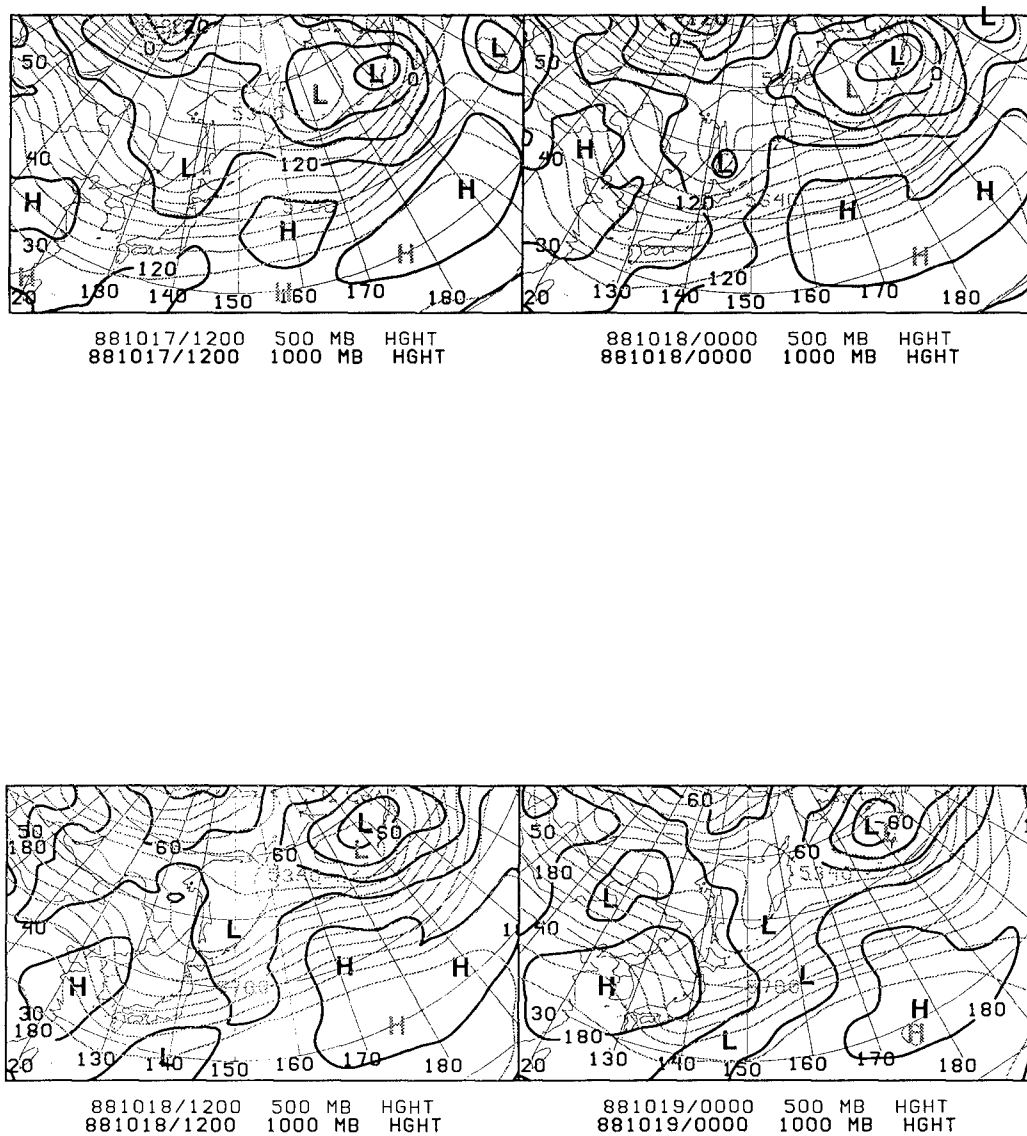


Fig. 6.2. The 1000mb heights (black) and 500 mb heights (gray) for (upper left) 881017/1200, (upper right) 881018/0000, (lower left) 881018/1200, and (lower right) 881019/0000. Contour interval for both fields is 60 m.

formed at the 500 mb pressure level. Inspection of corresponding tropopause maps to be shown in section 4 will justify selection of 1800 UTC 17 October as the initial time of the mobile trough.

The mobile trough attains its greatest strength based on geostrophic vorticity on 881019/0000 (Fig. 6.1f) as it crosses Honshu. Then, the mobile trough begins to merge with another mobile trough situated just to the south of Kamchatka Peninsula at 1200 UTC 19 October. This coupling can be seen by following the merger of the vorticity patterns of the two separate mobile troughs. Higher values of vorticity are seen farther north after the merger (see Fig. 6.1g). After the merger, the mobile trough moves to the northeast where it eventually disappears over the Aleutian Islands on 1800 UTC 23 October (not shown).

Cyclogenesis was not associated with the development of this mobile trough (Fig. 6.2). A trough off the east coast of Japan develops ahead of the mobile trough, but a cyclone never develops. A cyclone formed north of the mobile trough, but the development was in association with a different mobile trough.

2. Basic state and perturbation fields

In this case study, 437 mb will be the focal point of the investigation. The 437 mb level contained the greatest values of QGPV, and correspondingly the greatest influence on 500 mb heights. Figure 6.3 shows total QGPV fields and the partitioning of QGPV into perturbation and basic state QGPV fields for four different times.

The base state field consists of QGPV decomposed into spherical harmonic wavenumbers (0-5) zonal and (0-8) total with a time-mean component of the small-scale wavenumbers (up to 15) averaged over the lifetime of the mobile trough (881017-

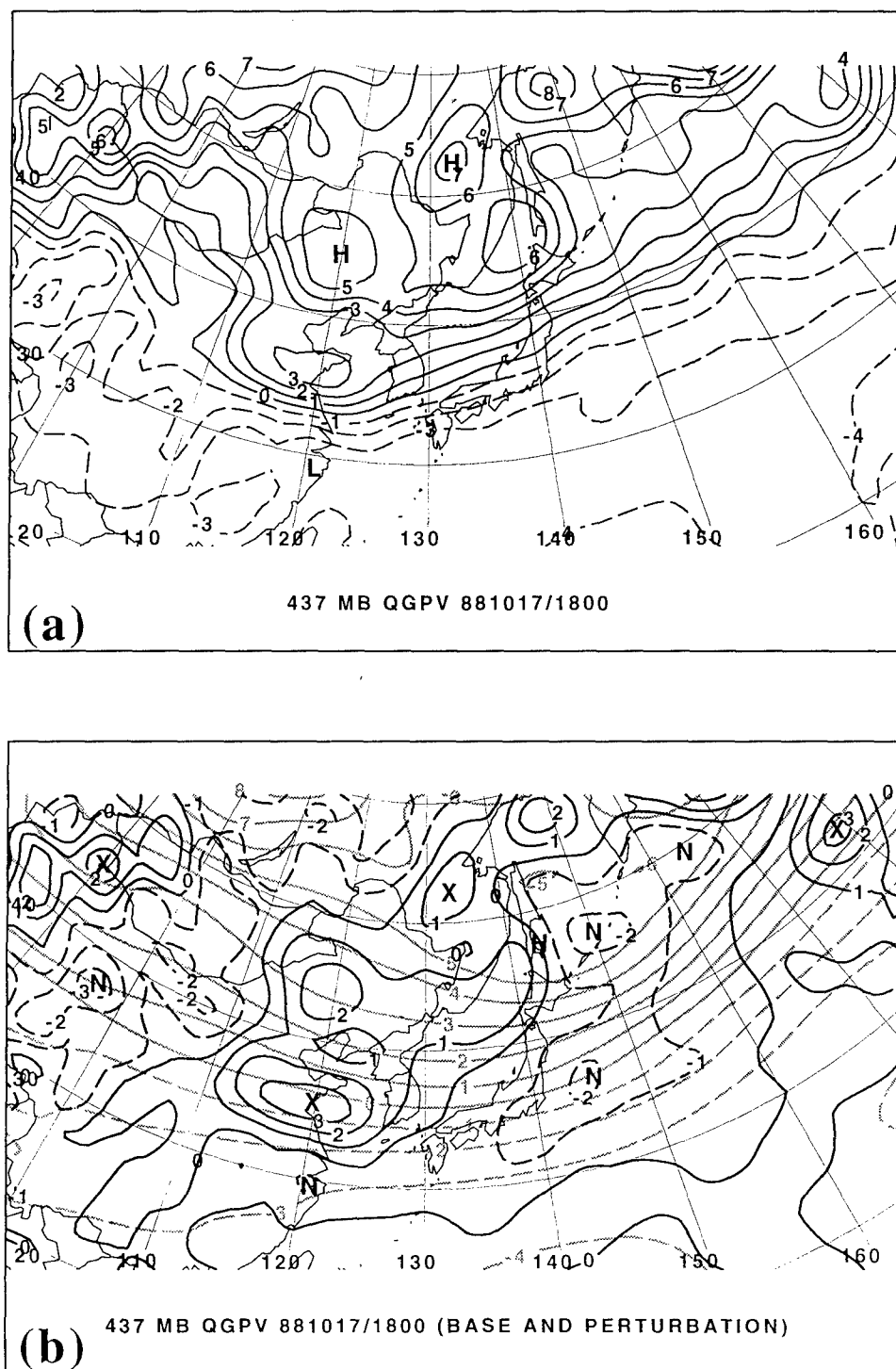


Fig 6.3. (a) 437 mb QGPV ($\times 10^{-4} \text{ s}^{-1}$) for 1017/1800; (b) 437 mb QGPV base state (gray, $\times 10^{-4} \text{ s}^{-1}$) and perturbation 437 mb QGPV (black, $\times 10^{-4} \text{ s}^{-1}$) for 881017/1800; (c) same as (a) except for 881018/1800, (d) same as (b) except for 881018/1800; (e) same as (a) except for 881019/0600; (f) same as (b) except for 881019/0600; (g) same as (a) except for 881019/0600; (h) same as (b) except for 881019/1800. Positive and negative QGPV anomalies in (b), (d), (f), and (h) are marked with X's and N's, respectively.

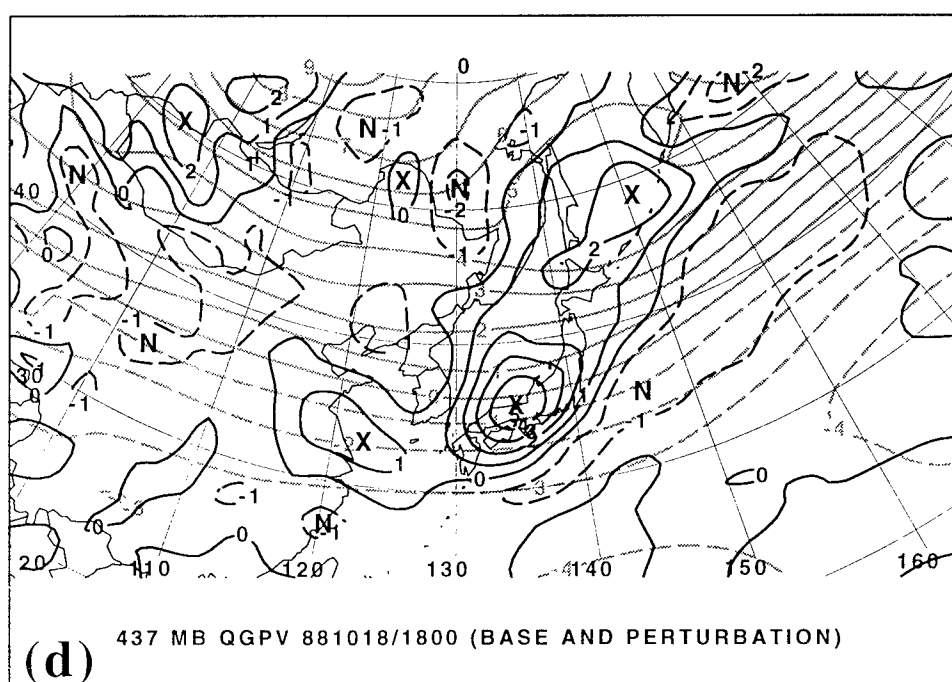
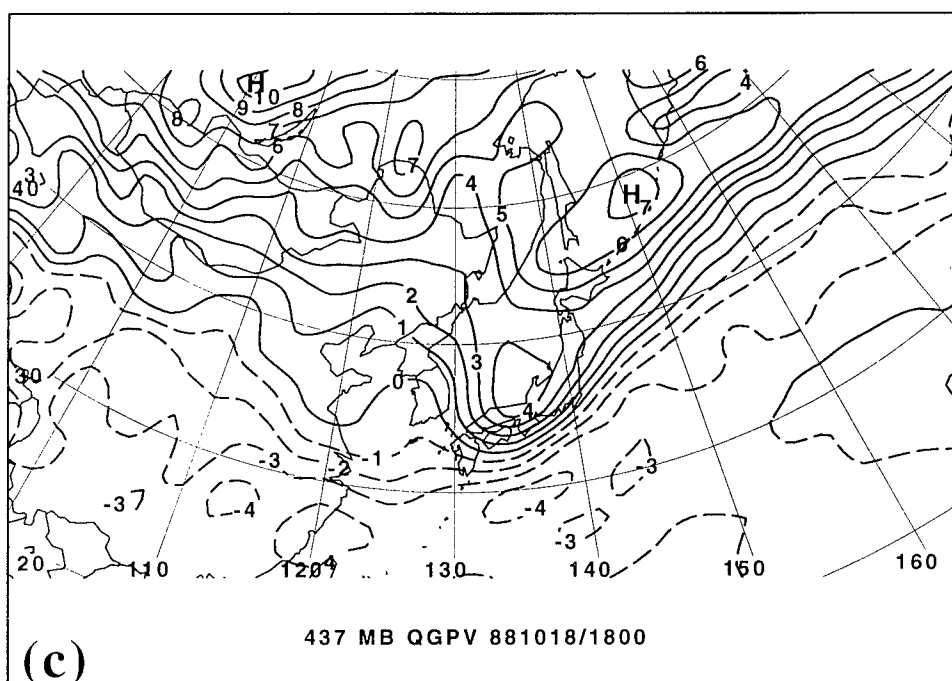


Fig. 6.3, continued.

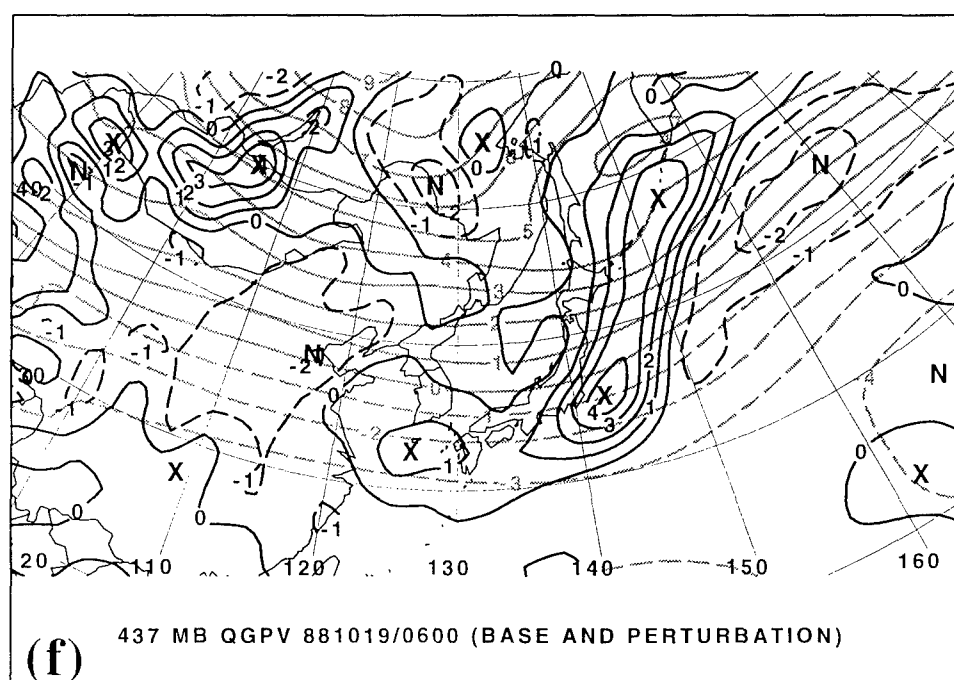
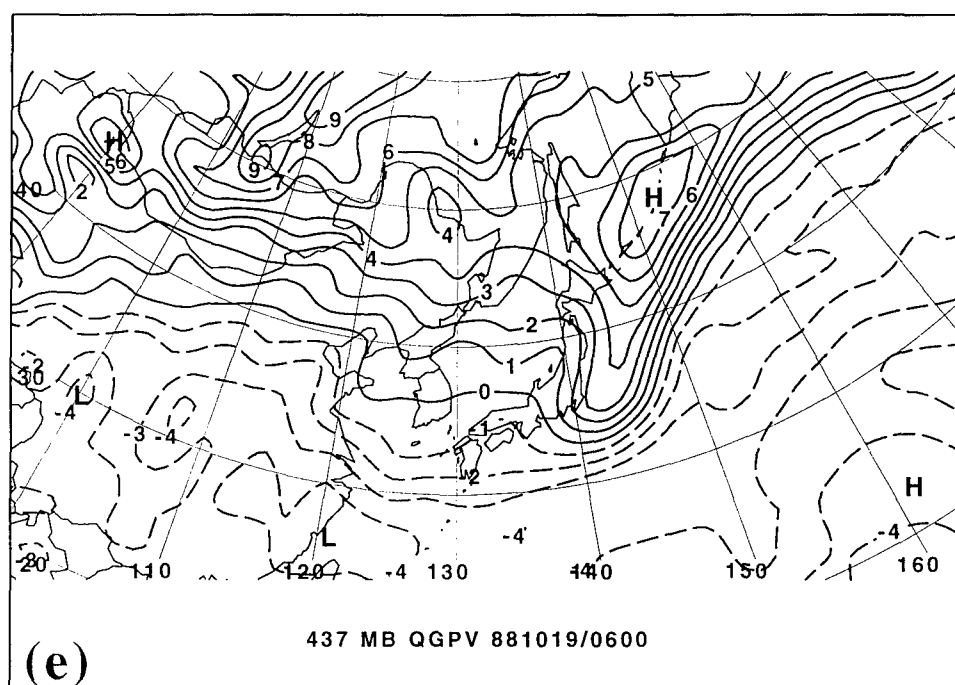


Fig. 6.3, continued.

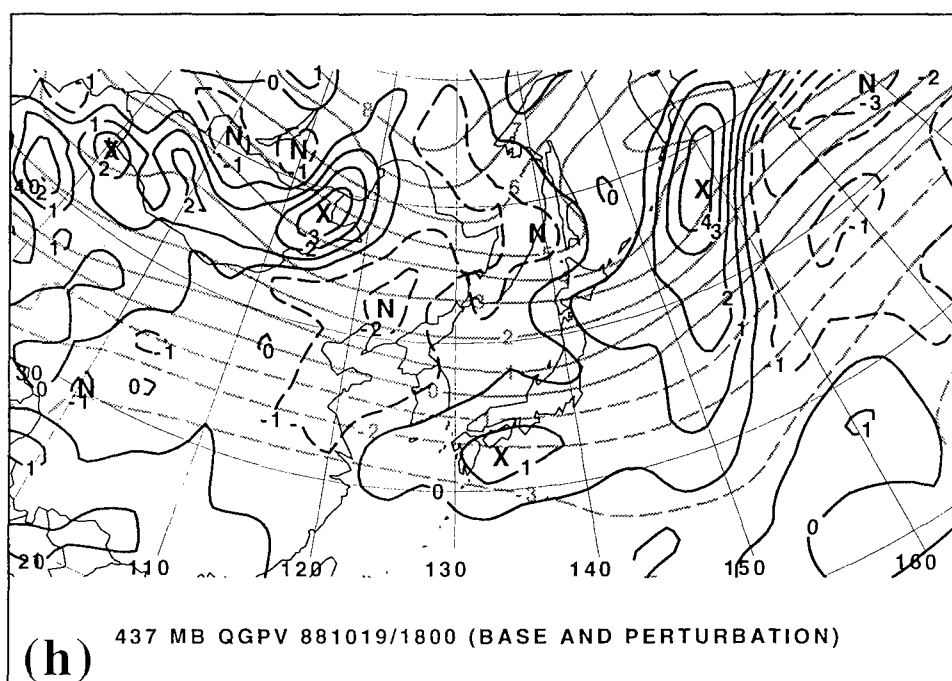
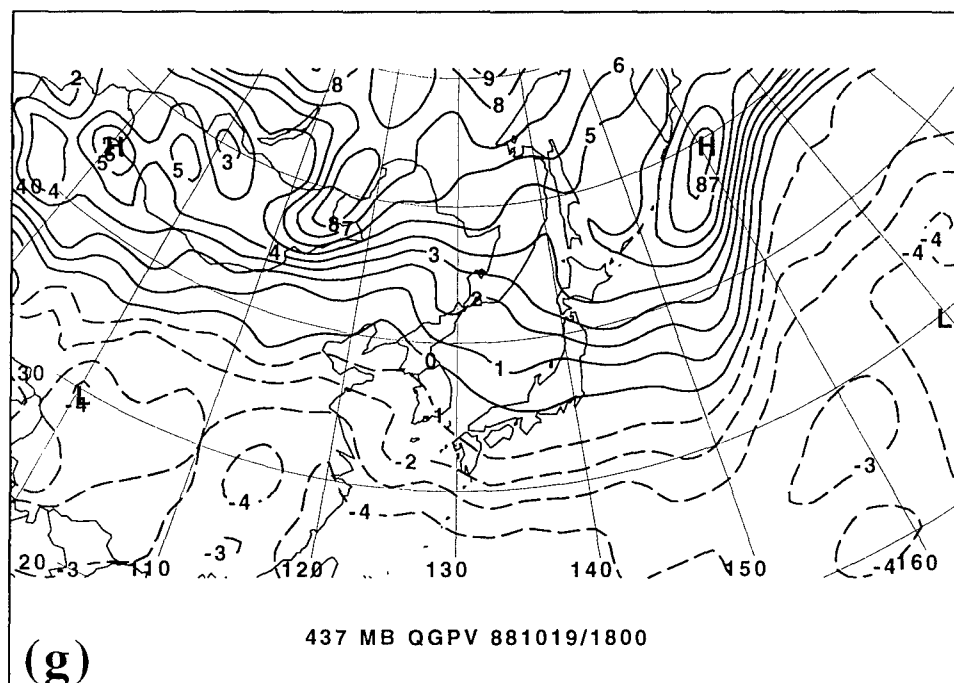


Fig. 6.3, continued.

881023). The base state selection was predicated on the desire to put the upstream ridge, a wavenumber 6 phenomenon, in the perturbation field. This upstream ridge had a direct influence in the development of the mobile trough as we will see in the tropopause map charts.

The perturbation QGPV fields are commensurate to the spatial and temporal evolution of the case study mobile trough. At 881017/1800, the QGPV anomaly associated with the mobile trough is located on the Yellow Sea coast of China (Fig. 6.3b). The anomaly is elongated in the east-west direction.

The wave in the full QGPV field which is associated with the mobile trough strengthens and narrows as the mobile trough grows (Fig. 6.3c). Figure 6.3d shows that the positive QGPV anomaly centered over southern Honshu has grown in strength and changed its shape as well.

The trough merger process can also be shown in the QGPV fields. Figure 6.3e show that the contours of QGPV off the coast of Japan are connected. The perturbation field (Fig. 6.3f) shows the two anomalies are now linked by a $3 \times 10^{-4} \text{ s}^{-1}$ contour. The troughs have merged by 1019/1800, and there is only one positive QGPV anomaly located just to the south of Kamchatka Peninsula (Fig. 6.3h).

Figure 6.4 illustrates the time evolution of the perturbation and base state height fields. The base state heights was computed in the same manner as the QGPV fields. The 437 mb perturbation height fields (associated with the upper-level perturbation potential vorticity) capture both the mobile trough and a mobile trough to its northeast (see Fig. 6.1a). The combination of two troughs into one height perturbation does not pose a

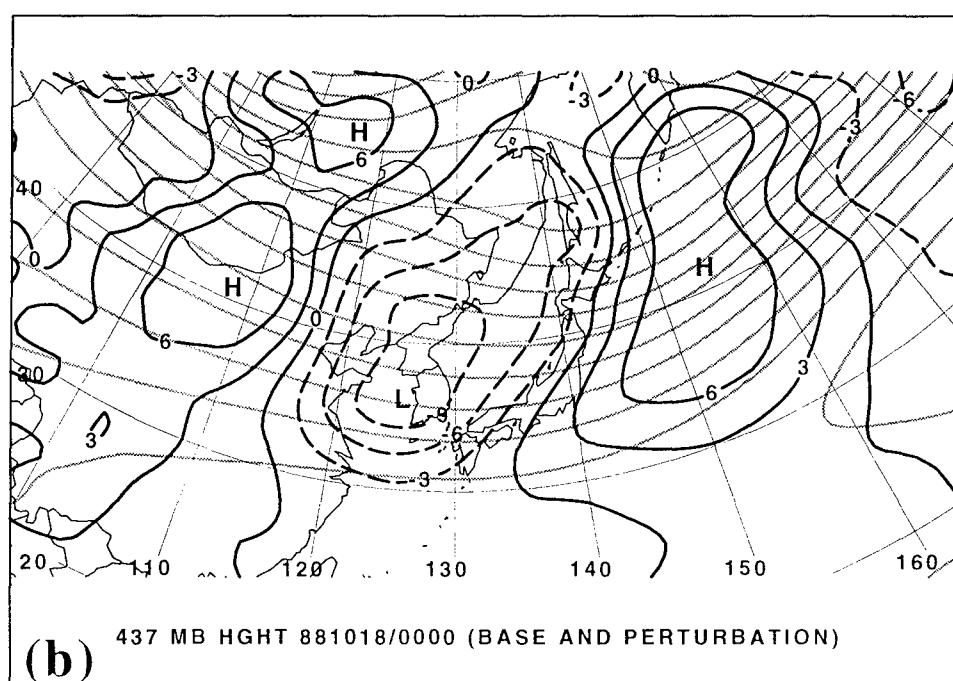
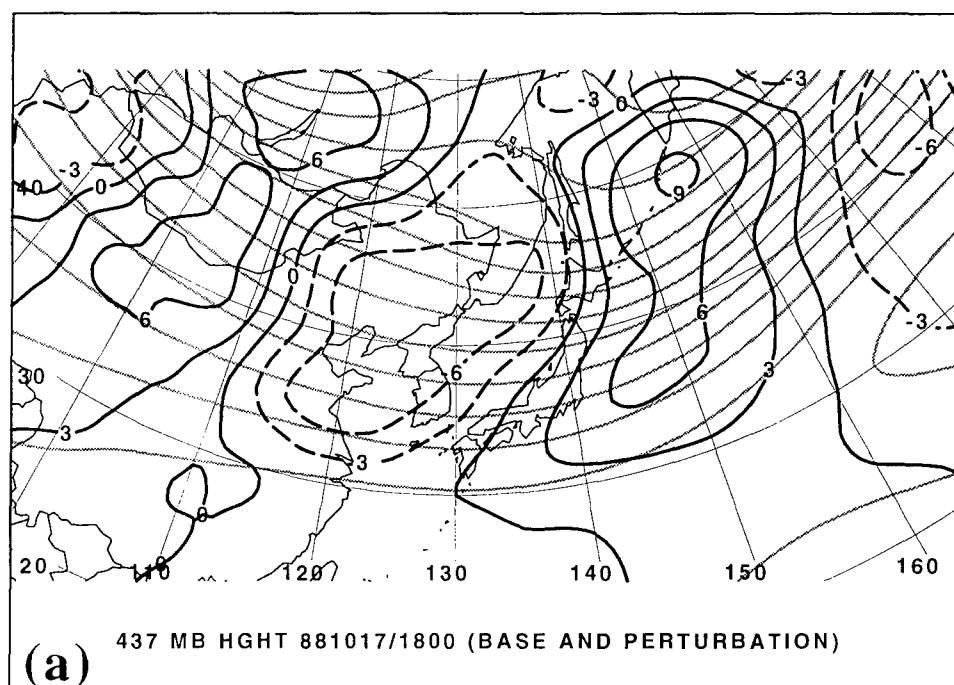


Fig. 6.4. Basic state 437 mb height (gray, contour interval 6 dam) and perturbation 437 mb height (black, contour interval 3 dam) for (a) 881017/1800, (b) 881018/0000, (c) 881018/1200, (d) 881019/0000, (e) 881019/0600, (f) 881019/1200.

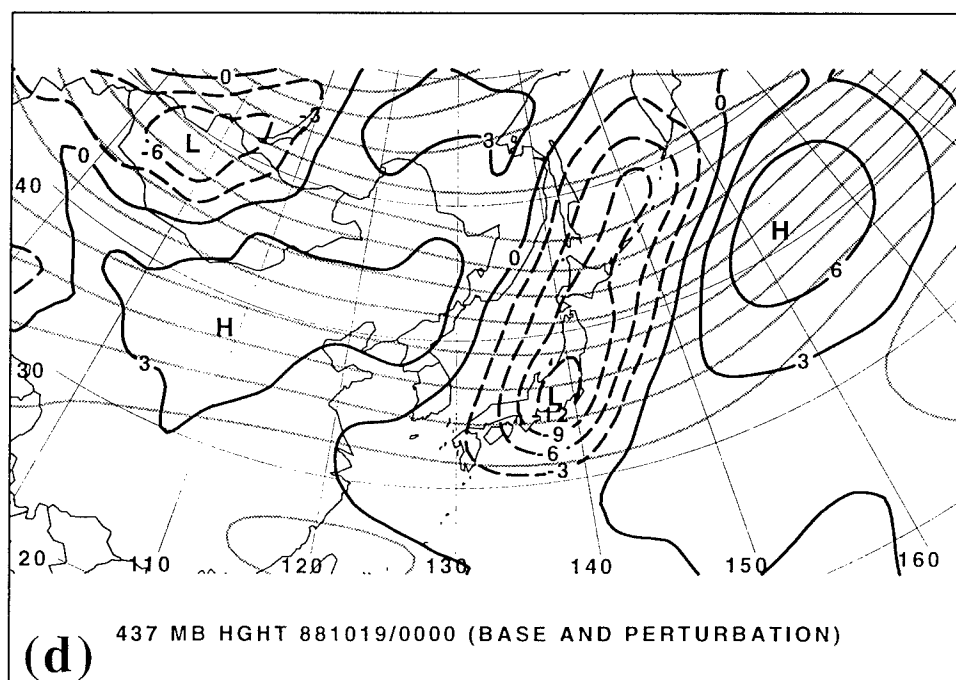
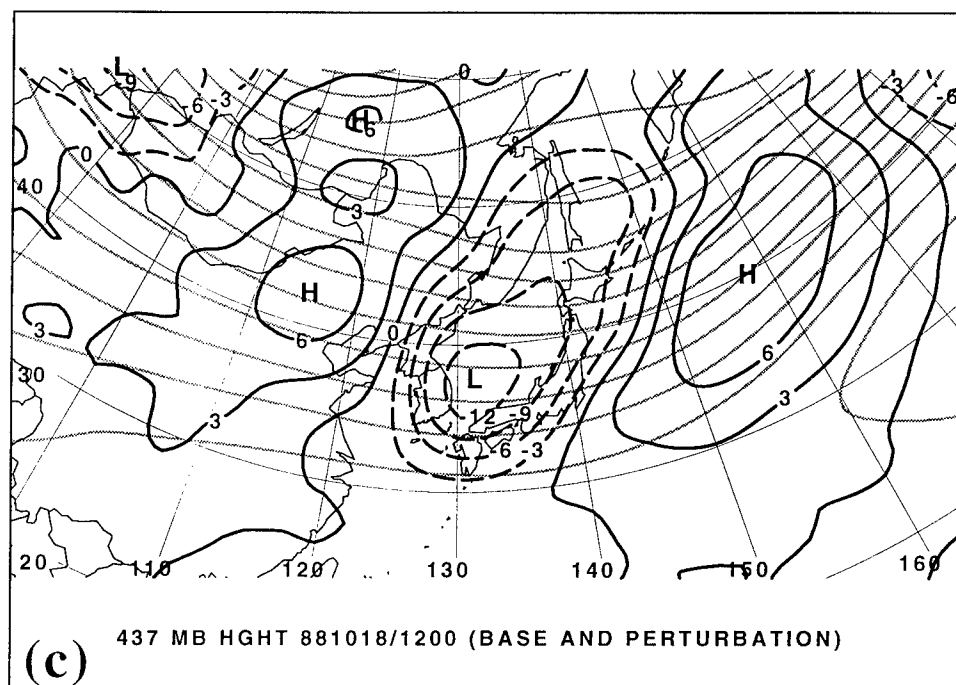


Fig. 6.4, continued.

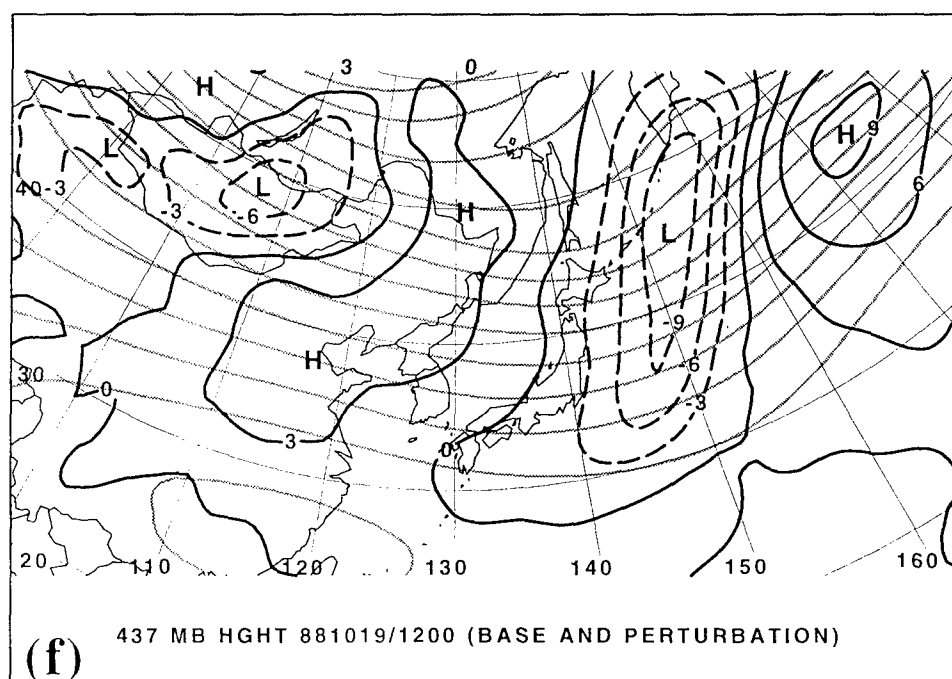
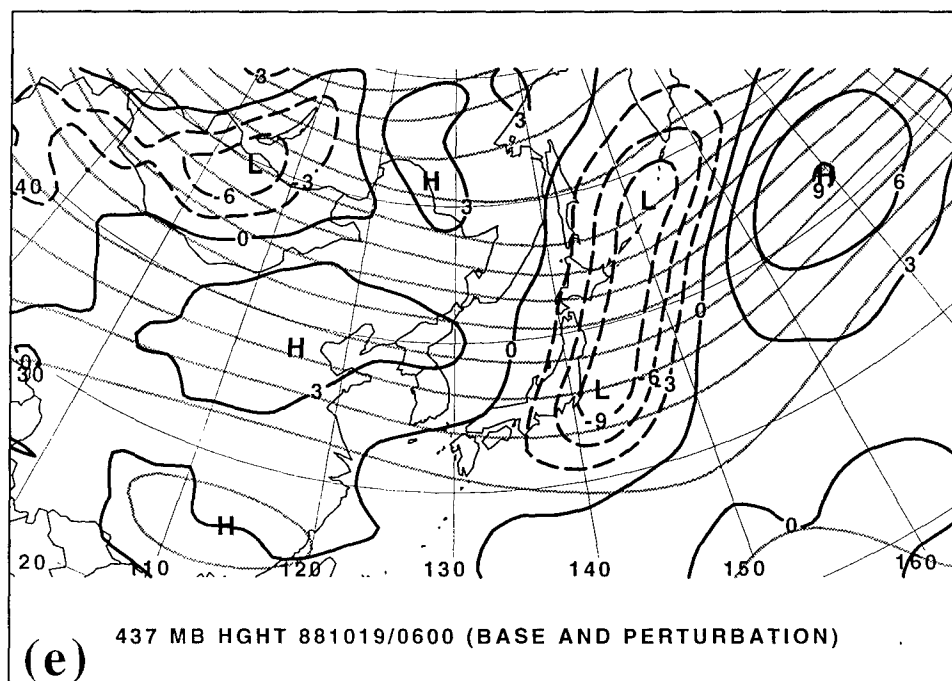


Fig. 6.4, continued.

problem for the diagnostics because the local minimum of height corresponds to our mobile trough throughout.

Figures 6.4a-b show the formation of the trough as the initiation of a local height minimum over the central Yellow Sea. Over the next 24 hours, the height perturbation associated with the mobile trough moves eastward with the mean flow and becomes elongated in the north-south direction (Fig. 6.4c-d).

The trough merger process is seen in figures 6.4e-f. Two height minima are present at 1019/0600, one just to the east of Tokyo, and one south of Kamchatka Peninsula. Six hours later, only one height minimum is present.

The partitioning scheme I used was able to give insight into the complex evolution of the case study mobile trough as it formed over the Yellow Sea and then interacted with another mobile trough.

3. QGPV tendencies

The QGPV and observed tendencies from the first three and one-half days are investigated (1017/1800-1021/0000) to ascertain what mechanisms were most important in the genesis and subsequent intensification of the mobile trough. Figure 6.5 shows a comparison of tendencies between those of the QGPV height tendency equation (4.10) and those from the upper-level height perturbation calculated by centered finite differencing.

TENDENCY COMPARISON OCTOBER 1988 CASE

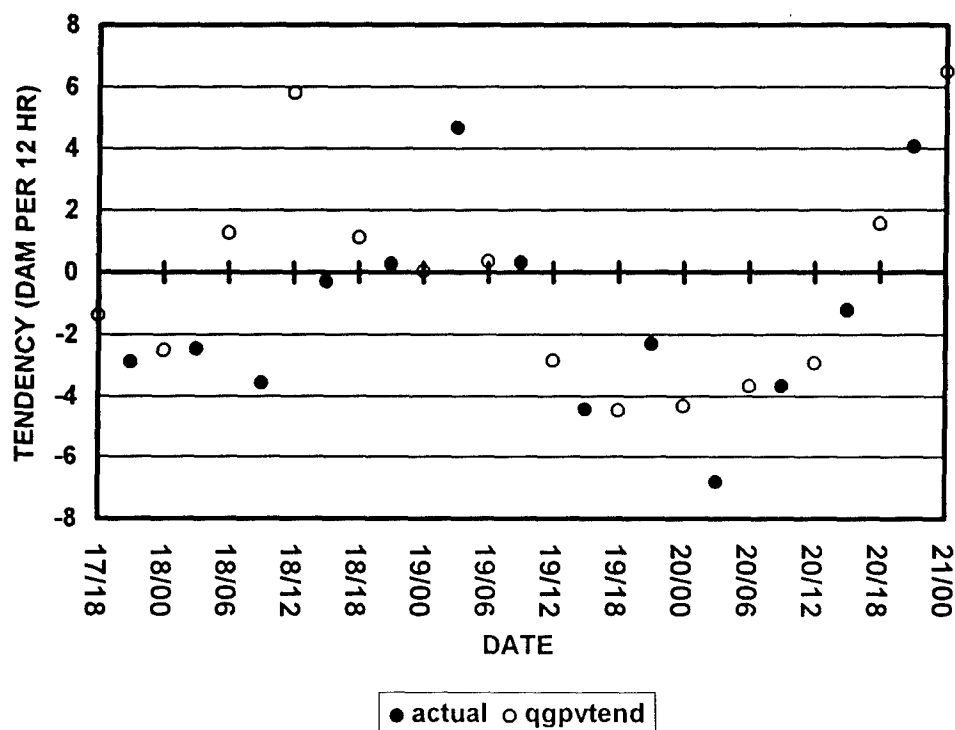
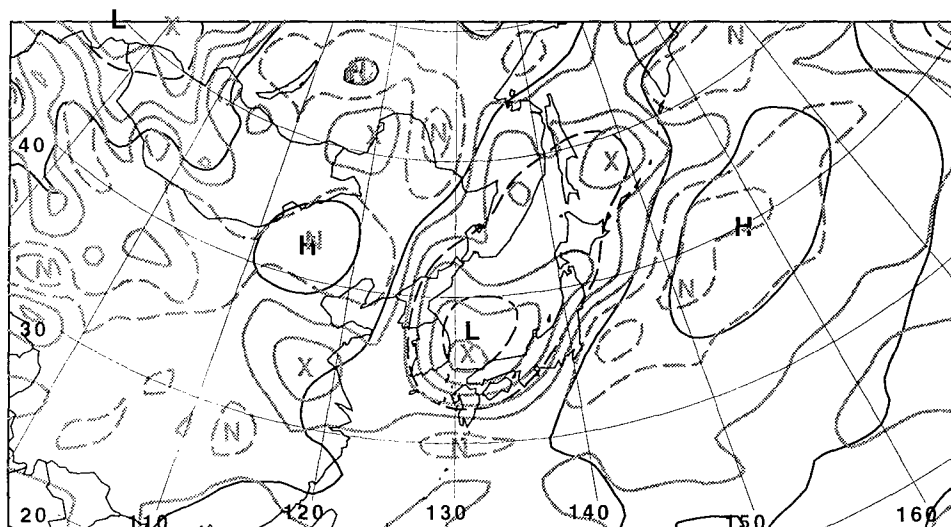


Fig. 6.5. Comparison of observed intensification of trough associated with upper-level small-scale QGPV (filled circles; computed as a 6-hour finite difference of minimum heights) with intensification rate computed from the quasigeostrophic height tendency equation (4.10) (open circles; defined as instantaneous height tendency at location of minimum height). Chart is similar to figure 5.5, except for 17 October 1988 case.

The two tendencies are comparable but with two notable exceptions. The QGPV tendencies predict filling at 06 and 12 UTC on 18 October while the trough is observed strengthening. Also, the trough weakens between 00 UTC and 06 UTC on 19 October



437 MB PERTURBATION HEIGHT & QGPV 881018/1200

Fig 6.6. Perturbation height (black, contour interval 6 dam) and perturbation QGPV (gray, $\times 10^{-4} \text{ s}^{-1}$) at 437 mb for 881018/1200.

while the QGPV tendencies are near zero, completely missing the filling episode. A possible source of error may be the geographical discrepancy between the center of the perturbation height minimum and the center of the positive QGPV perturbation (Fig. 6.6). Since the effect of QGPV is linear in nature, one would expect a maximum of perturbation QGPV to correspond spatially to a minimum of perturbation height. However, the spatial patterns of diagnosed and actual tendencies due to the full fields over the region are similar in position and magnitude. This suggests that the partitioning scheme failed to adequately separate the mobile trough from the basic state. This explanation seems plausible; however, other partitioning schemes between the basic state and the perturbation showed similar discrepancies. For evaluation purposes at the times of 1200 UTC 18 October and 0600 UTC 19 October, the diagnosed tendencies will be discounted. However, the QGPV tendency compared favorably with the observed tendency after 0600 UTC 19 October with only minor differences noted.

4. Tropopause maps

This case will now be examined using dynamical tropopause maps. The complicated nature of the formation of waves in the upper troposphere can be greatly simplified using tropopause analysis. As with the previous case, these dynamical tropopause maps were constructed by interpolating atmospheric variables to the 1.5 PVU surface.

Figure 6.7 displays the evolution of the tropopause before and during the formation of the mobile trough. The maps show the distribution of potential temperature and wind on the dynamical tropopause. The major feature seen on these charts is a concentrated set of potential temperature contours extending across the east Asian

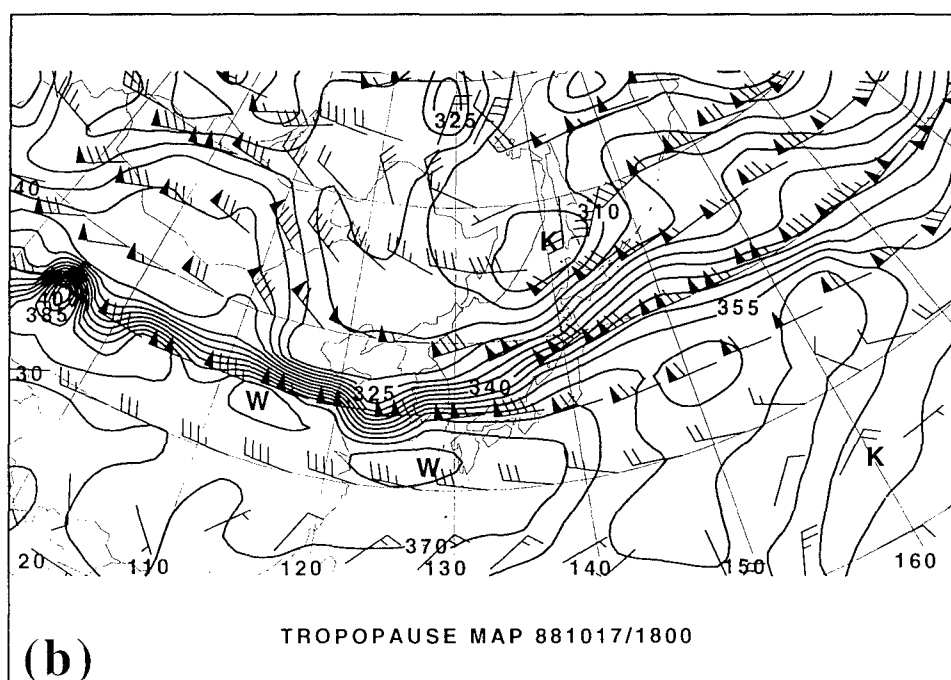
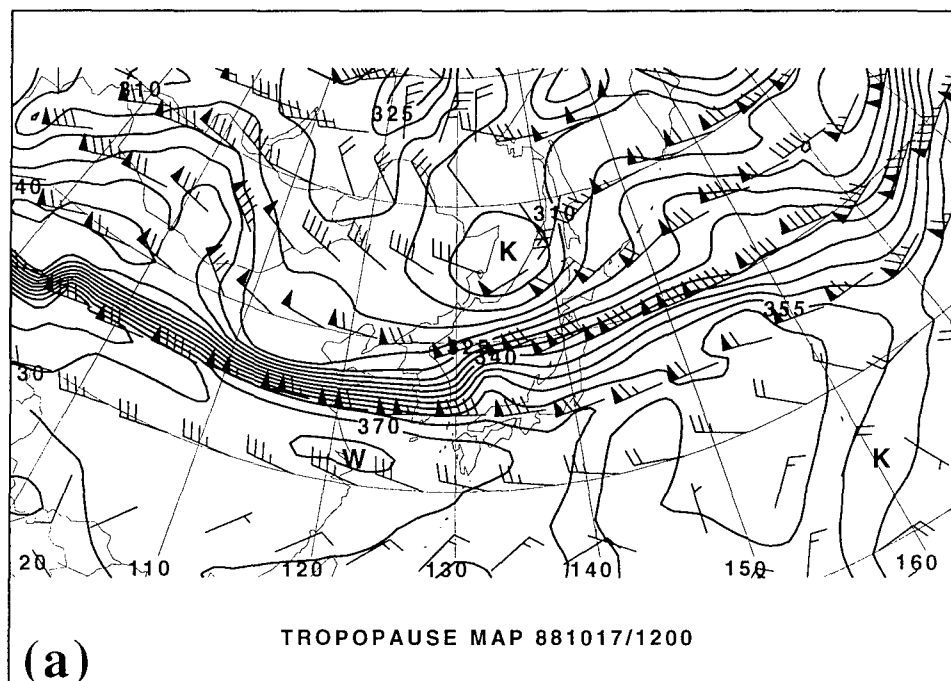


Fig. 6.7. Maps of tropopause potential temperature (contour interval 5K) and winds (with one pennant, full barb, and half barb denoting 25, 5, 2.5 m s⁻¹, respectively) for (a) 1200 UTC 17 Oct. 1988, (b) 1800 UTC 17 Oct. 1988, (c) 0000 UTC 18 Oct. 1988, (d) 1200 UTC 18 Oct. 1988.

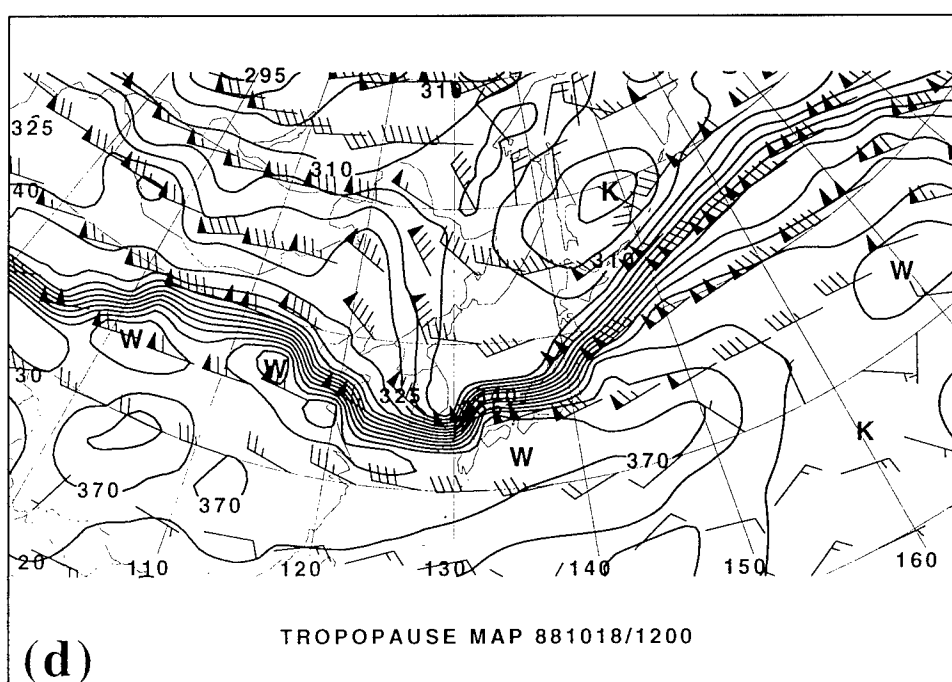
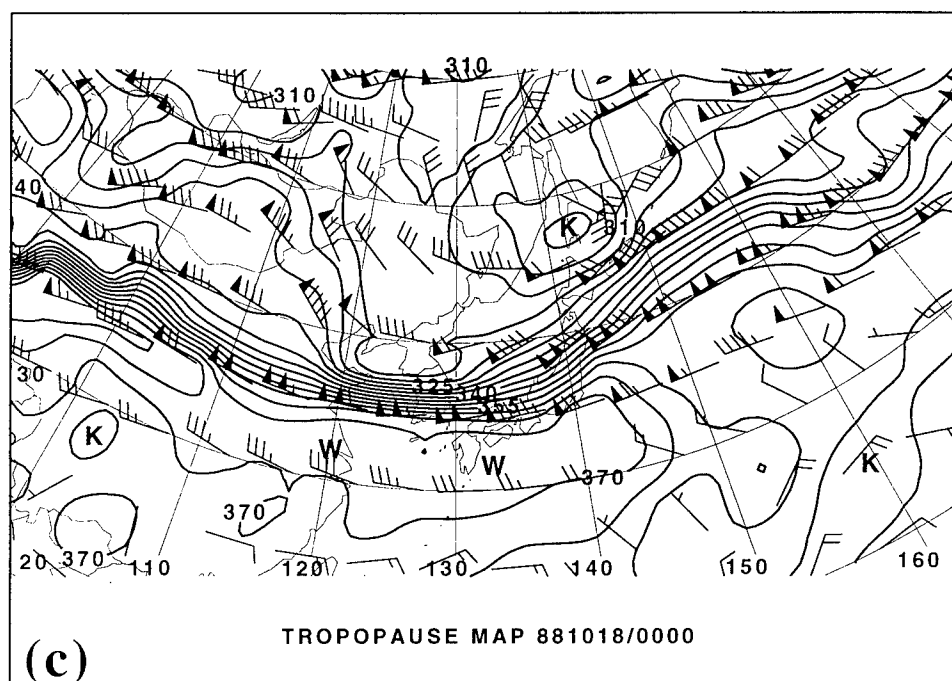


Fig. 6.7, continued.

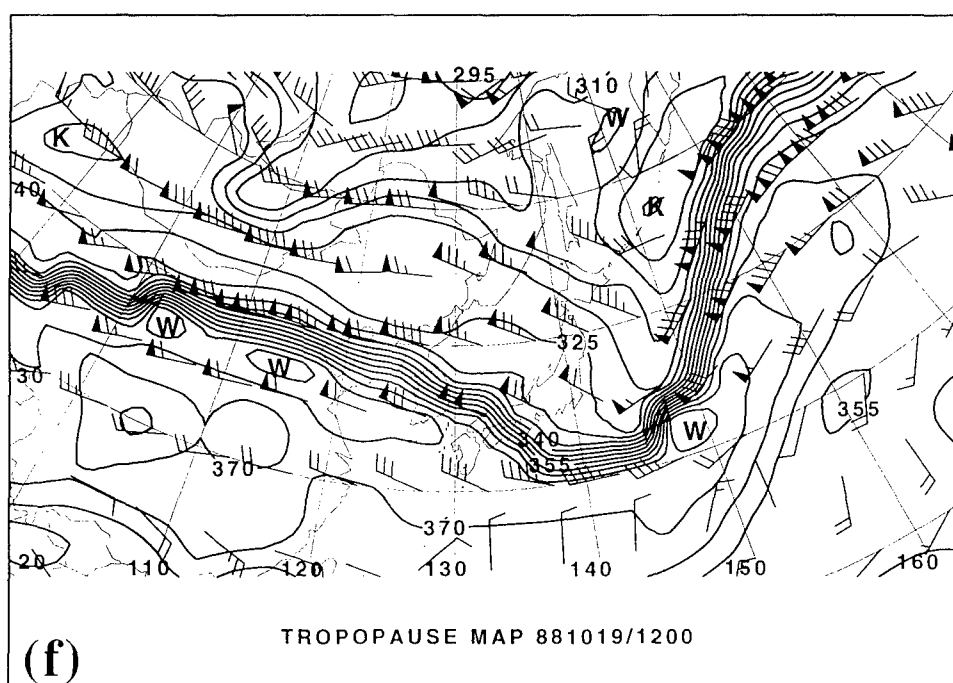
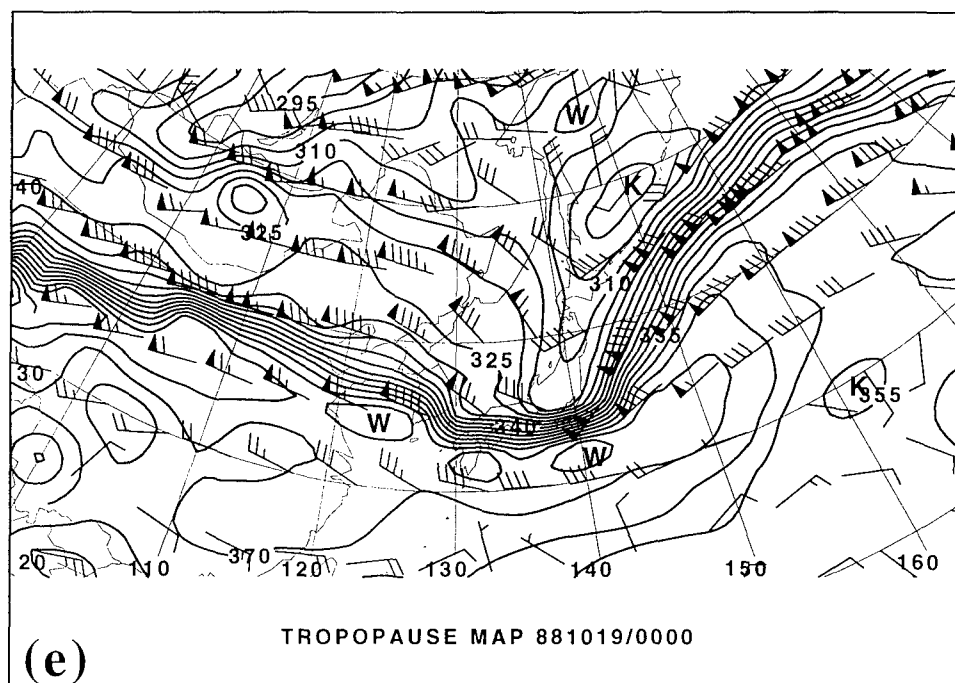


Fig. 6.7, continued.

continent and Japan. This gradient (consisting of temperatures from approximately 330K to 350K) is associated with a very strong subtropical jet stream with wind speeds up to 80 m s^{-1} . The polar gradient (consisting of temperatures from 310K to 325K) is less prominent throughout the analysis.

Figure 6.7a shows a well-developed wave at the tropopause over northern China and Mongolia upstream of the area where the mobile trough formed at 500 mb. Note that this precursor wave system is associated with the polar gradient (310K to 325K) and not the subtropical gradient. The upstream ridge is inducing anticyclonic circulation. The northerlies associated with the ridge are causing significant cross-contour flow into the gradient associated with the subtropical jet stream.

Six hours later at 1800 UTC 18 October (Fig. 6.7b), a slight wave in the contours associated with the subtropical jet is evident over the southern part of the Yellow Sea where the mobile trough develops. Advection of potential temperature due to the upstream ridge continues; therefore, strengthening of the incipient mobile trough can be expected. Based on the development of the wave on the subtropical gradient, one can claim the formation of the mobile trough at this time.

Figure 6.7c shows the wave associated with the mobile trough developing further and extending over 45K. The polar jet and the subtropical jet have merged during the development of the wave. The wave is originally elongated in the along flow direction. Six hours later, the wave is stretched meridionally (Fig. 6.7d). The stretching continues for the next 24 hours (Fig. 6.7e-f) as the wave merges with an isolated vortex just to the east of Sakhalin Island. The upstream wave that generated the cross-contour flow has dramatically weakened.

The development of the wave on the tropopause which is associated with the 500 mb mobile trough appears to fit the pattern of downstream Rossby wave development. The northerlies associated with the upstream ridge provided the cross-contour flow that induced our trough. Deformation significantly changed the shape of the wave. A detailed analysis of the role of deformation, both horizontal and vertical, will be given in the next section.

5. Piecewise tendency diagnosis

Figure 6.8 shows the piecewise tendency contributions of the terms of (4.10). The fifth and sixth terms of (4.10) were combined in this figure and labeled as VORTEX-VORTEX terms.

a. Downstream development

The downstream development term, $L^{-1}(\mathbf{v}'_u \cdot \nabla \bar{q}_u)'$, provides the largest contribution in initiating the trough (-3.7 dam per 12 hr) at 1017/1800. The tendency due to this term hovers near zero through 1019/0000. It becomes strongly positive for the rest of the period investigated. The term contributes most to filling the trough on 1019/1800 (5.8 dam per 12 hr). However, other terms counteract the effects of the downstream development term.

Figures 6.9 and 6.10 illustrate how the downstream development process affected the trough. A negative QGPV anomaly over north-central China is causing significant positive QGPV advection into the trough. Strengthening occurs at the center of height minimum because advectons of base state QGPV are significantly more cross-contour to the west of the trough than to the east.

PIECEWISE TENDENCY DIAGNOSIS OCTOBER 88 CASE

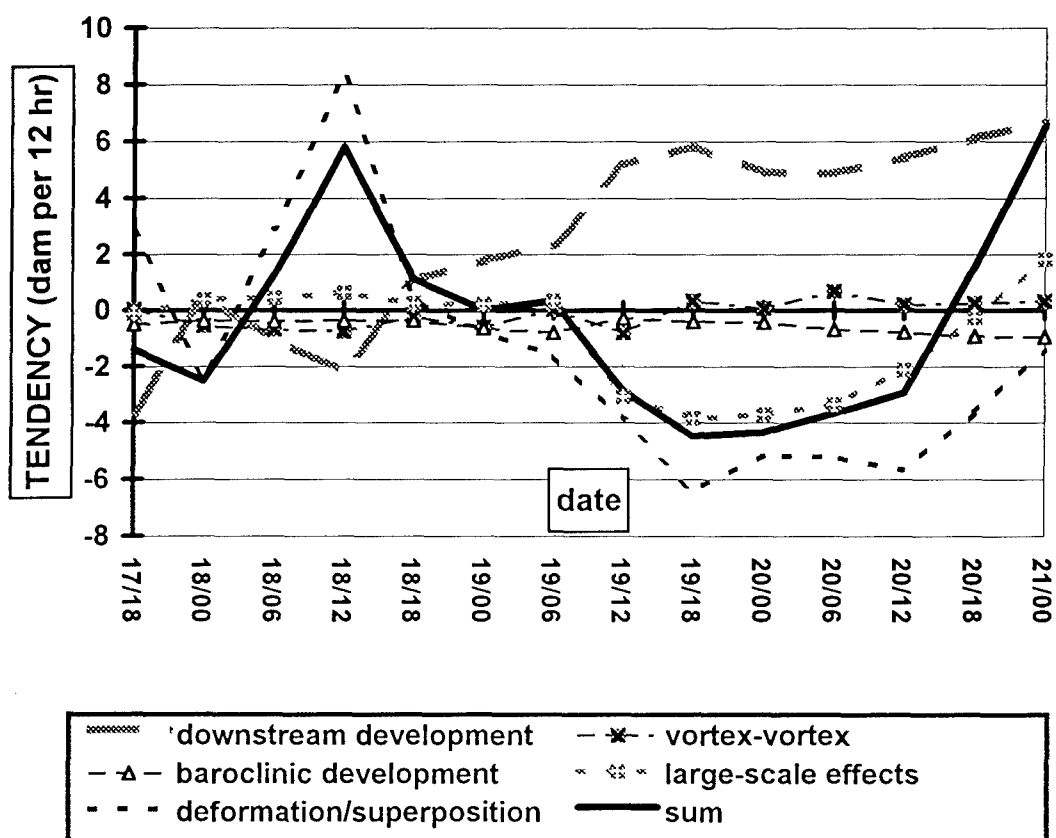


Fig. 6.8. Quasigeostrophic height tendencies associated with various dynamical processes during the development of the upper-level mobile trough, 1800 UTC 17 Oct. 1988 to 0000 UTC 21 Oct. 1988.

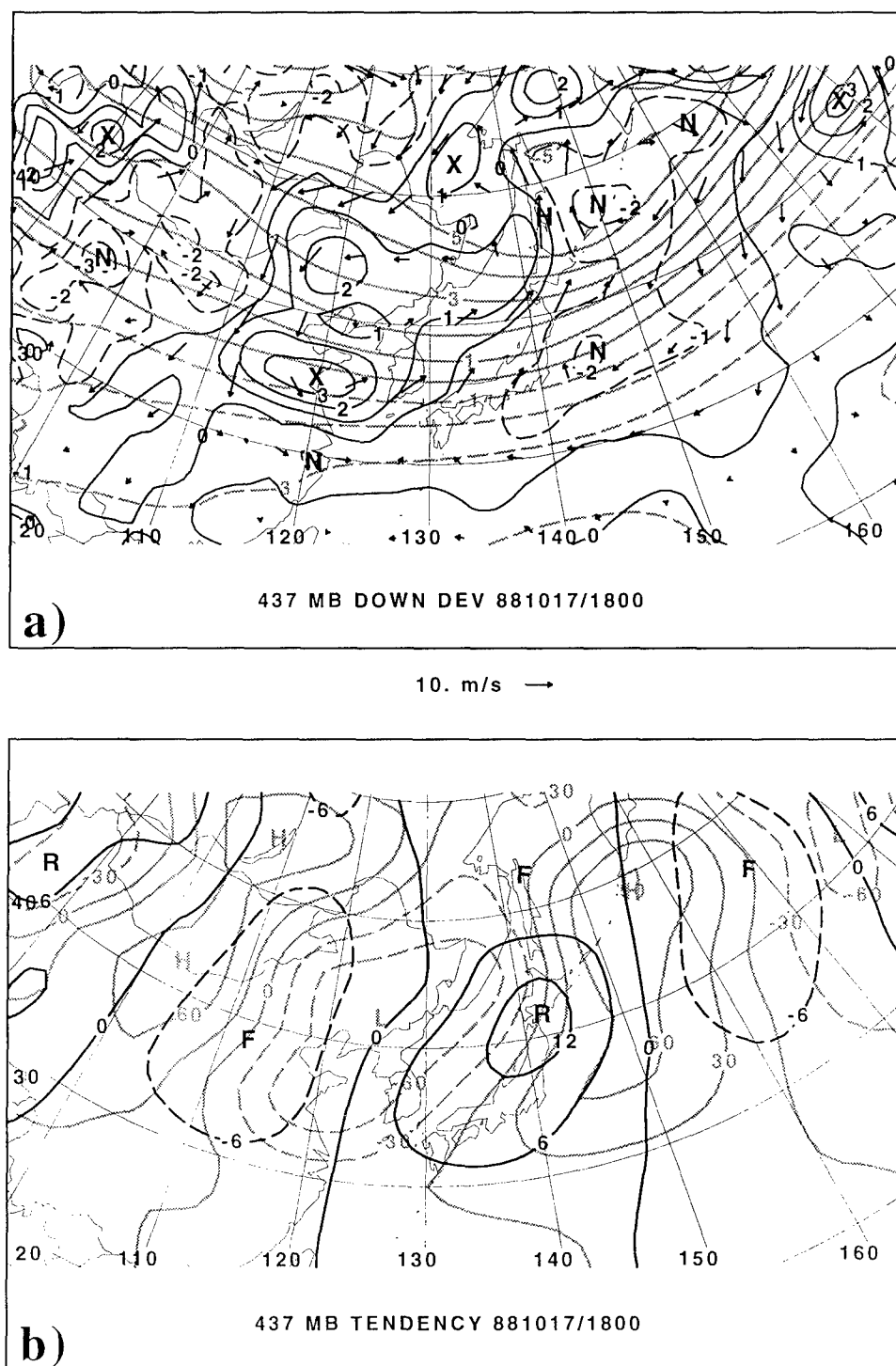
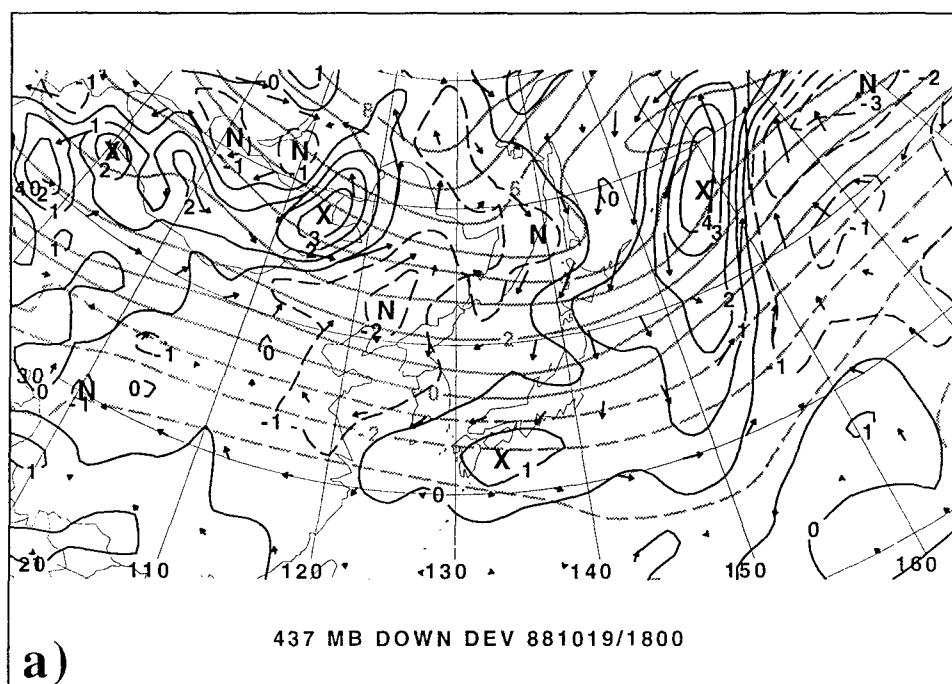


Fig. 6.9. Advections and tendencies associated with downstream development at 18 UTC 17 Oct. 1988. (a) Basic state 437 mb QGPV (black, $\times 10^{-4} \text{ s}^{-1}$); perturbation 437 mb QGPV (gray, $\times 10^{-4} \text{ s}^{-1}$); and 437 mb winds associated with upper-level perturbation QGPV. (b) Small-scale height tendencies associated with advection of upper-level large-scale potential vorticity by winds associated with upper-level perturbation QGPV (black, dam per 12 hr); and 437 mb heights associated with upper-level perturbation QGPV (gray, dam).



10. m/s →

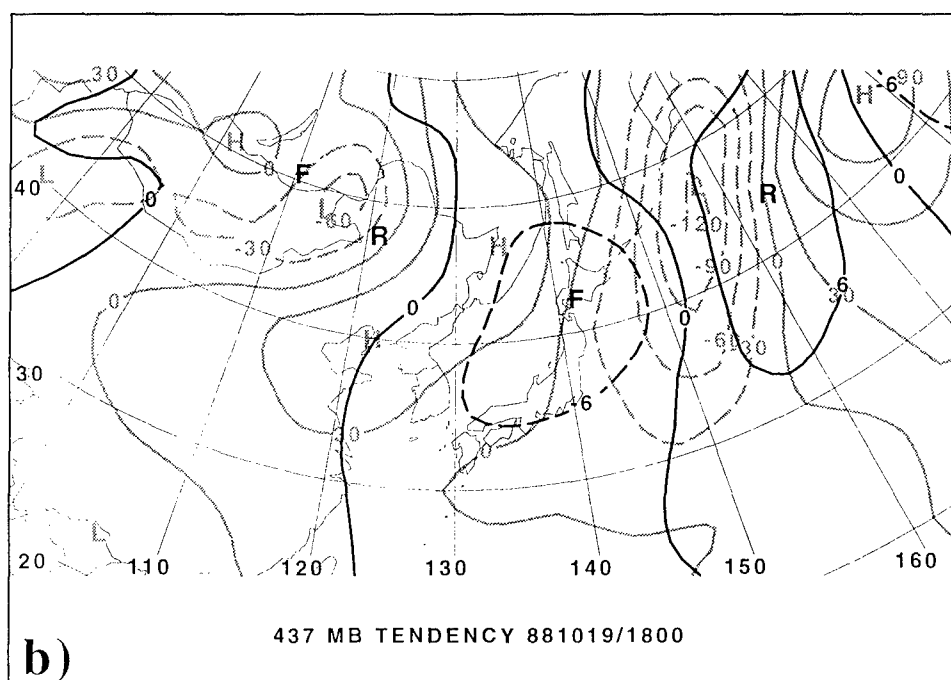


Fig. 6.10. Same as Fig. 6.9, except for 1800 UTC 19 Oct. 1988.

On 1019/1800 (Fig. 6.10), the downstream development process contributes strongly to trough filling. The southerlies associated with QGPV anomaly situated to the south of Kamchatka Peninsula dominate the advection patterns causing height rises over two-thirds of the height perturbation, attempting to weaken the trough (5.8 dam per 12hr). However, competing processes counteract the downstream development term and produce a net strengthening of the trough (-4.5 dam per 12 hr).

b. Deformation / superposition

This term, $L^{-1}(-\bar{v} \bullet \nabla q'_U)'$, may involve horizontal (barotropic) deformation and vertical deformation by the vertical wind shear of the basic state, or superposition. The contributions from this term were significant throughout the period of study of this trough.

In order to separate the total deformation into the horizontal deformation and deformation due to vertical shear, the same procedure that was described in Chapter V was used. For this case, the 437 mb level winds were used to advect all levels of QGPV to calculate the vertical superposition term. The vertical superposition term is the difference between the total deformation term and the horizontal deformation component.

Figure 6.11 displays the height tendencies from vertical superposition, barotropic deformation, and the total term. Initially, the term contributed weakly to strengthening the trough at 1018/0000. The total term was a factor in trough decay until 1019/0000. After that time, the total term was the significant contributor to trough development. Superposition contributed more to strengthening the trough throughout the study period than barotropic deformation.

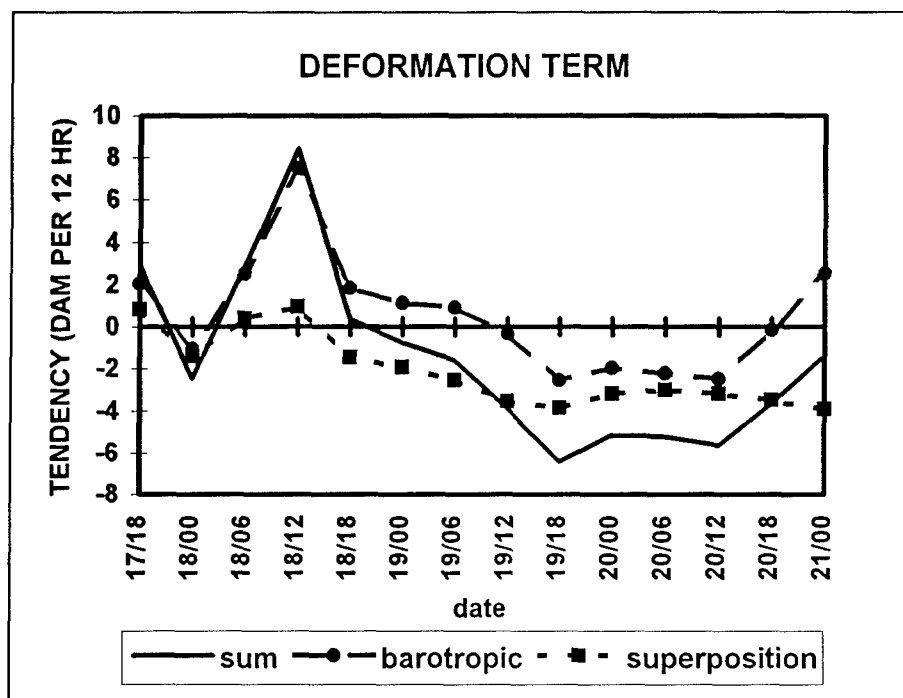


Fig. 6.11. Quasigeostrophic height tendency contribution (dam per 12hr) from barotropic (dots, dashed), superposition (squares, dotted line), and the sum of the two (second term of (4.10); black, solid line). See the text for the details on how these terms were calculated.

The trough was slightly strengthened due to barotropic deformation (-1.0 dam per 12 hr) on 1018/0000. Figure 6.12a shows the positive q' anomaly associated with the trough to be elongated along the mean flow over the Yellow Sea and the Korean peninsula. Basic state 437 mb heights and axes of dilatation due to the basic state winds are plotted to show the mechanism of strengthening. The axes of dilatation are oriented at a 60 degree angle to the major axis of the perturbation. The effect of the deformation is to stretch the anomaly along the minor axis. This results in weak height falls due to a compacting of the QGPV anomaly.

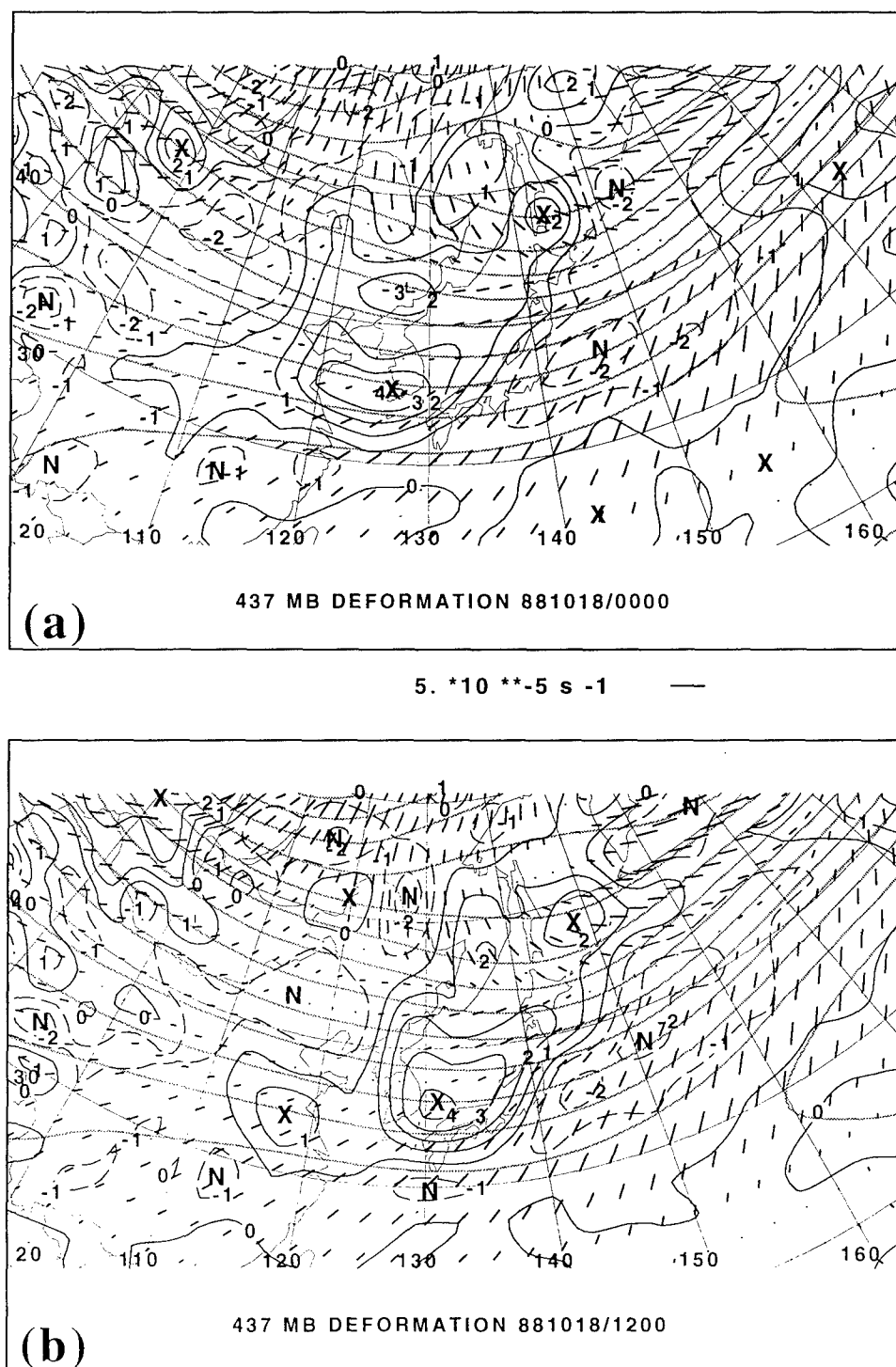


Fig. 6.12. Deformation associated with basic state upper-level flow at (a) 881018/0000 and (b) 881018/1200. Perturbation 437 mb QGPV (black, $\times 10^{-4} \text{ s}^{-1}$); basic state 437 mb heights (gray, contour interval 6 dam); and 437 mb axes of dilatation associated with basic state flow (lengths of axes are proportional to the magnitude of deformation, scale at center).

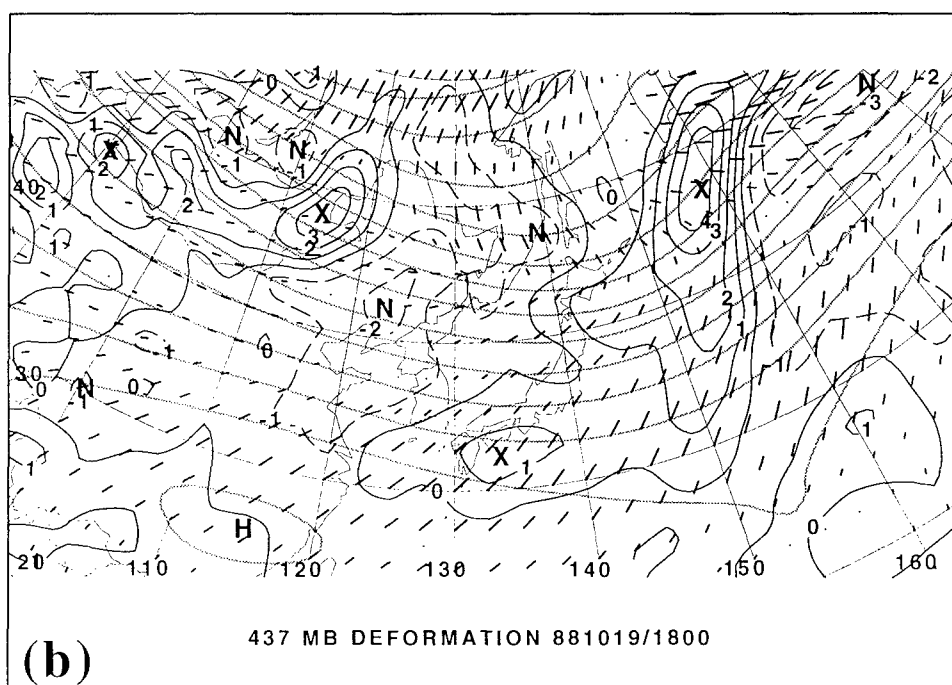
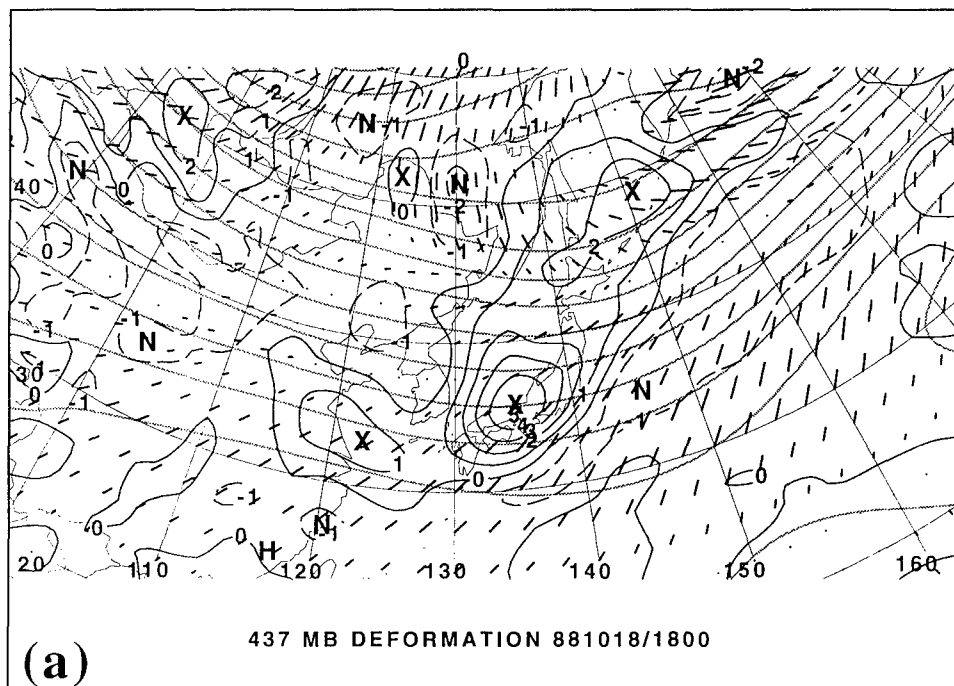


Fig. 6.13. Same as Fig. 6.12 except for (a) 881018/1800 and (b) 881019/1800.

At 12 UTC 18 October, the positive QGPV anomaly associated with the mobile trough is located in the southern part of the Sea of Japan (Fig. 6.12b). The QGPV anomaly is more circular, due to ongoing stretching by barotropic deformation. The axes of dilatation are now oriented along the major axis of the QGPV anomaly.

Six hours later, figure 6.13a shows that the stretching of the QGPV anomaly by the base state winds continues. The anomaly's shape is most circular at this time. Continued stretching by the deformation would weaken the trough, which in fact it does.

At 1019/1800, barotropic deformation has stretched the QGPV anomaly to the point that it is no longer distinguishable from the QGPV anomaly associated with the mobile trough to the north (Fig. 6.13b). This was the result of continued stretching of the anomaly along its major axis. It was interesting that this QGPV anomaly was initially elongated east-west along the mean flow and was strengthened by deformation by making the anomaly more circular. However, the stretching continued until the anomaly had become elongated out in the north-south direction, making it weaker once again. The dominant positive QGPV anomaly situated just to the south of Kamchatka Peninsula is again in a favorable deformation field. The axes of dilatation are now oriented along the minor axis of the elongated perturbation. Strengthening of the mobile trough by deformation resumes again as the large-scale flow attempts to stretch the QGPV anomaly into a more circular shape.

The superposition process can be described as the process when two anomalies at different levels become aligned in the vertical. For this case, recall from section 4 of this chapter that two jets became superimposed at the genesis of this mobile trough. Vertical superposition consistently contributed to trough development after 1018/1200.

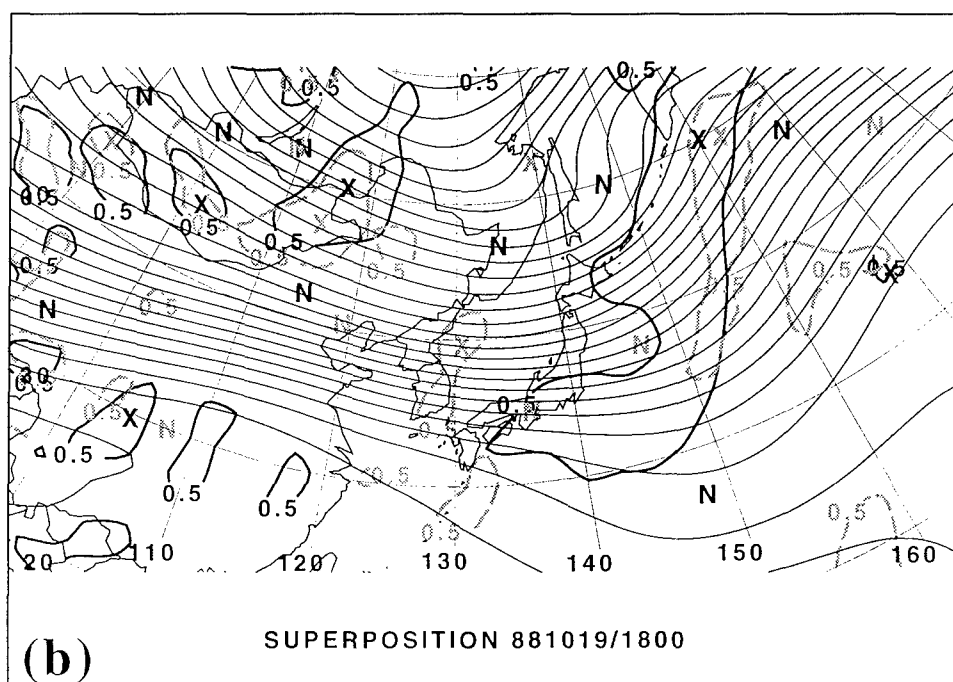
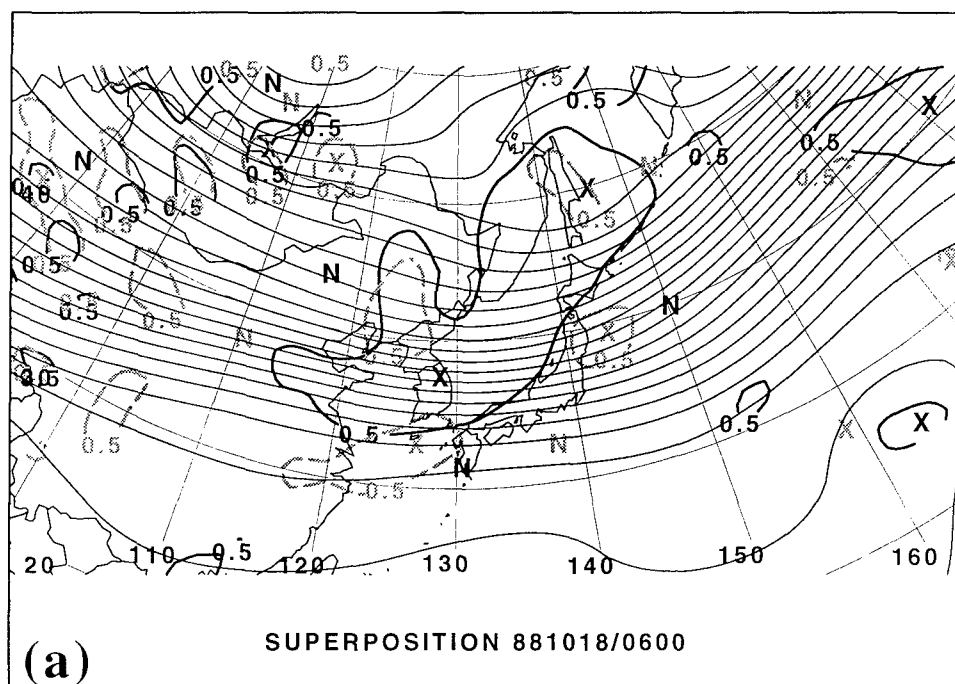


Fig. 6.14. Illustration of superposition process. (a) Basic state height thickness 297-507mb (thin black, contour interval 2 dam); 297 mb perturbation QGPV ($0.5 \times 10^{-4} \text{ s}^{-1}$ contour shown, thick, black); 507 mb perturbation QGPV ($0.5 \times 10^{-4} \text{ s}^{-1}$ contour shown, gray, dashed) for 881018/0600. (b) Same as (a) except for 881019/1800.

To illustrate the process of superposition, figure 6.14 displays the large-scale thickness (thin black, contour interval 20 m) between 297 mb and 507 mb and the $0.5 \times 10^{-4} \text{ s}^{-1}$ contour of perturbation QGPV at 297 mb (thick, black) and 507 mb (gray, dashed).

At 1018/0600, the superposition term is not significant in the development of the trough. The diagnosed contribution attributed to superposition is slightly positive. The trough is located at 37 N 129 E at this time. Figure 6.14a shows the shear to be westerly across the Korean peninsula. The perturbation QGPV at the two different levels are nearly vertically aligned. Thus, the vertical shear will attempt to decouple the QGPV perturbations and move the perturbation at 297 mb farther downshear (eastward).

At 1019/1800, the tendency due to the superposition term contributes most strongly to strengthening the trough. The center of the trough is located at 47N 153E. The contours of thickness are oriented southwest to northeast over the location of the trough (Fig. 6.14b). A large region of perturbation QGPV at 297 mb is located upshear of an elongated area of QGPV at 507 mb south of Kamchatka Peninsula. The vertical shear of the basic state will superimpose the two regions of QGPV, increasing the QGPV in the vertical column and strengthening the trough.

c. Large-scale interaction

The large-scale interaction term, $L^{-1}(-\bar{\mathbf{v}} \cdot \nabla \bar{q}_U)'$, represents the effect of the large-scale winds advecting the large-scale QGPV. This term becomes significant after 1019/0600. Figure 6.15a shows the large-scale heights and the large-scale QGPV at 1019/1800, and small-scale tendencies due to the base state interactions are shown in

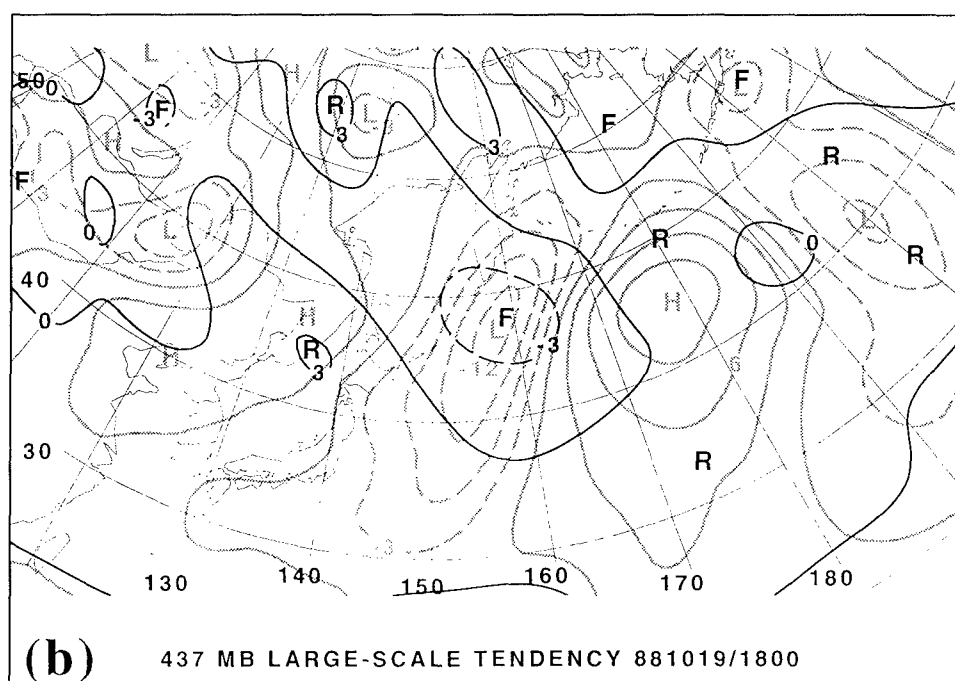
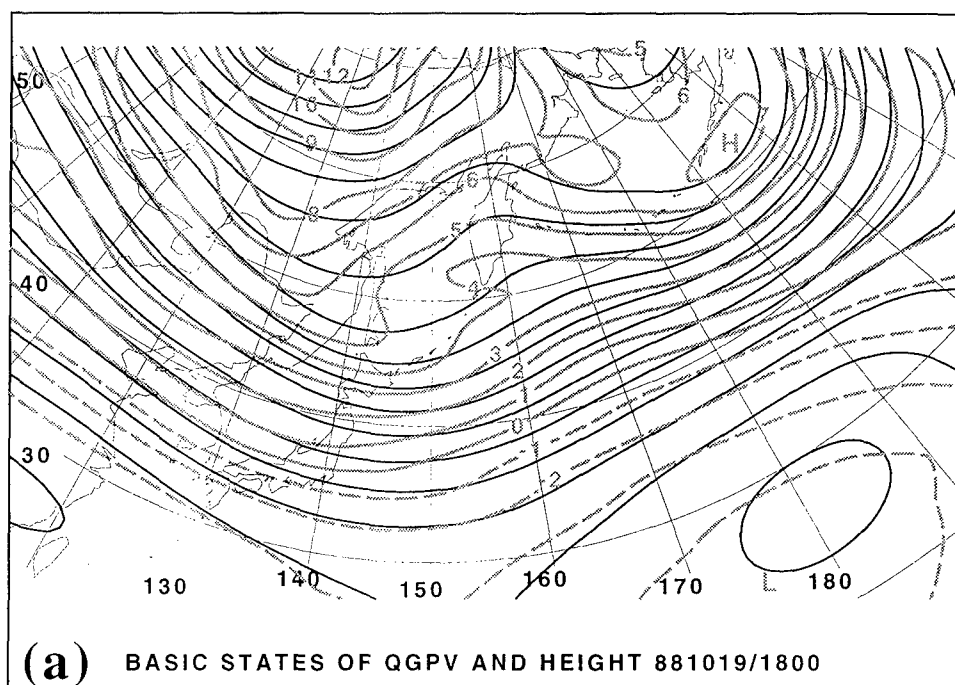


Fig. 6.15. Advections and tendencies of large-scale interactions for 1800 UTC 19 Oct 1988. (a) 437 mb base state heights associated with full inversion of QGPV (black, contour interval 6 dam) and 437 mb base state QGPV associated with inversion of upper-level QGPV (gray, $\times 10^{-4} \text{ s}^{-1}$); (b) 437 mb small-scale height tendencies associated with the advection of upper-level base state QGPV by winds associated with full inversion of base state QGPV (contour interval 3 dam per 12 hr), and 437 mb heights associated with upper-level perturbation QGPV (gray, dam).

figure 6.15b. The phase difference between the large-scale height and the large-scale QGPV can lead to positive QGPV advections in the vicinity of the trough. The geographical pattern of height falls due to this term remained nearly constant throughout the period of investigation. This same effect was detailed in the previous case of this research. The largest contribution to mobile trough development due to large-scale interactions was at 1019/1800 (-3.8 dam per 12 hr).

d. Baroclinic amplification

The baroclinic term, $L^{-1}(-v'_L \bullet \nabla \bar{q}_U)'$, slightly strengthens the mobile trough throughout the period of investigation. Figure 6.16 shows an example of the effects of the lower-level perturbation scale winds on upper-level basic state QGPV for 1017/1800. Throughout the evolution of the trough, the magnitude of the winds associated with inversion of lower-level QGPV advection is very small, no greater than 5 m s^{-1} . A low-level cyclone which developed in association with the trough to the north provided for little strengthening of the trough. A weak cyclonic circulation associated with the low levels can be detected over Honshu (Fig. 6.16a). A weak anticyclonic circulation can be seen just over the QGPV anomaly associated with our mobile trough. The advections due to the low-level potential vorticity aid the development of the trough by advecting higher values of QGPV into the anomaly; however, the effect was small (-0.5 dam per 12 hr). Furthermore, the baroclinic term provided strengthening no greater than 1 dam per 12 hr.

e. Vortex-vortex

The small-scale vortex-vortex interaction terms, $L^{-1}(-v'_L \bullet \nabla q'_U)'$, and $L^{-1}(-v'_U \bullet \nabla q_U)'$ were insignificant for this case. The tendencies due to these two terms

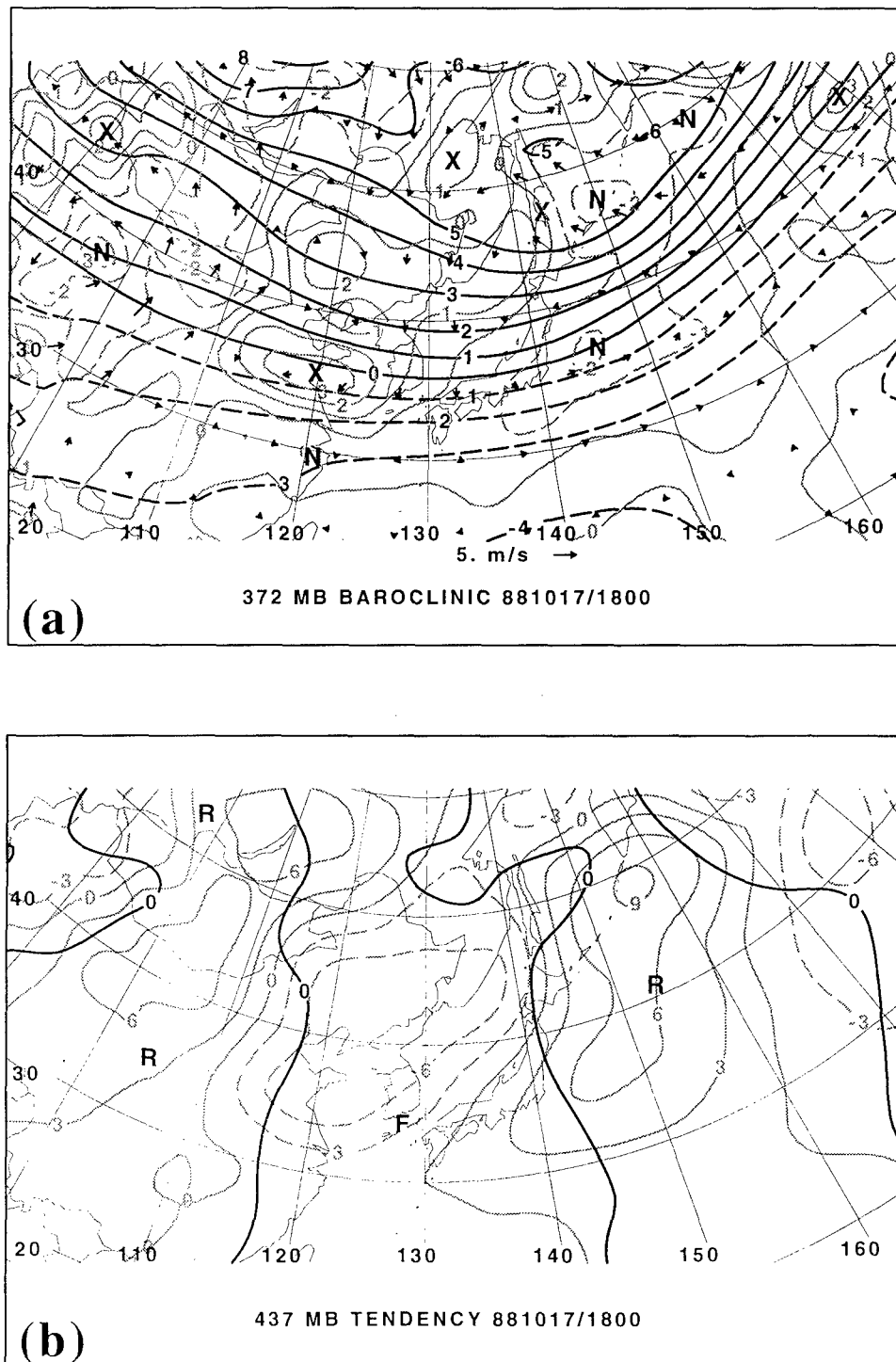


Fig. 6.16. Advections and tendencies associated with baroclinic amplification at 1800 UTC 17 Oct. 1988. (a) Base state 437 mb QGPV (black, $\times 10^{-4} \text{ s}^{-1}$); perturbation 437 mb QGPV (gray, $\times 10^{-4} \text{ s}^{-1}$); and 437 mb winds associated with lower-level perturbation QGPV. (Reference vector shown.) (b) Small-scale 437 mb height tendencies associated with advection of upper-level base state QGPV by winds associated with lower-level perturbation QGPV (black, contour interval 3 dam per 12 hr); and 437 mb heights associated with upper-level perturbation QGPV (gray, dam).

remained near zero. One might expect a larger contribution from these terms since two mobile troughs merge in this case. However, deformation by the large-scale flow appears to be responsible for the trough merger.

6. Summary

In summary, the formation of this mobile trough was assessed by using two methods: 1) piecewise tendency diagnosis on the QGPV height tendency equation, and 2) dynamical tropopause maps. It was found that downstream development was the primary mechanism responsible for the wave formation on the subtropical jet. Barotropic deformation and vertical superposition played a key role in modulating the later development of the mobile trough. Cyclogenesis was not associated with the formation of this mobile trough.

Analysis of dynamical tropopause maps also confirmed that the downstream development process was responsible for the formation of the mobile trough. Deformation played a key role in modulating the shape of the wave associated with the mobile trough. This downstream development mechanism was manifested as advection of potential temperature at the tropopause level, generating a trough downstream from a pre-existing one.

Barotropic deformation played a key role in modulating the strength of the trough by changing the shape of the associated QGPV anomaly. Also, as two jets merged over the mobile trough, vertical superposition of QGPV further aided the development of the trough.

CHAPTER VII

SUMMARY AND CONCLUSIONS

1. Summary

The purpose of this research was to understand the mobile trough genesis process over the Yellow Sea-East China Sea region. Mobile trough genesis events were selected from the objective climatology of mobile troughs by Lefevre and Nielsen-Gammon (1995). A detailed analysis was given of two mobile troughs which developed in two distinct large-scale flow regimes during the cold season.

Two methods were used to assess mobile trough genesis development. The first technique was based on the height tendency equation which uses the advection of quasigeostrophic potential vorticity (QGPV) as forcing. Piecewise tendency diagnosis (PTD) was used to quantitatively assess the role of individual dynamical processes. PTD uses piecewise potential vorticity inversion to produce height tendencies. The forcing terms in the quasigeostrophic height tendency equation are partitioned into potential vorticity advection associated with distinct dynamical processes. The basic state used in this research was an extension of the basic state used by Nielsen-Gammon and Lefevre (1996). The basic state used here was composed by low-pass filtering the spherical harmonic representation of QGPV plus a time-mean component of the perturbation scale. This partitioning method between the basic state and perturbation placed stationary small-scale features in the mid-latitudes into the basic state.

The second method used dynamical tropopause maps to examine the generation of waves, mobile troughs, at the tropopause level. The tropopause can be defined as a surface of constant Ertel's potential vorticity (EPV). Dynamical tropopause maps were created by interpolating wind and potential temperature to the 1.5 PVU surface. Theories of wave generation were confirmed using tropopause maps. Tropopause maps showed a simplified representation of the dynamics of the upper-levels of the atmosphere.

The first mobile trough formed on 0000 UTC 31 March 1987. According to both PTD and tropopause map analysis, downstream development due to the group velocity of Rossby waves appeared to initiate the mobile trough. A pre-existing upstream ridge provided for advection of potential temperature which developed a new mobile trough downstream. The PTD method showed downstream development to be the main contributor to trough development and also to trough decay at the end of its life. Baroclinic processes were present in lesser roles, but they were associated with a surface cyclone that developed in association with a downstream mobile trough. The surface cyclone developed prior to the initiation of the case study mobile trough. Large-scale processes which involved the interaction between the base states of QGPV and height provided for development later on in the life of the trough.

The second mobile trough formed on 1800 UTC 17 October 1988. Downstream development initiated the development of this mobile trough also, as confirmed by both PTD and tropopause map analysis. The mobile trough formed in a zonal flow regime. The development of this trough is also due to advection of potential temperature at the tropopause by an upstream pre-existing ridge. Barotropic deformation and vertical superposition processes were more important in modulating the strength of the trough

after its genesis. Barotropic deformation acted to change the shape of the associated QGPV perturbation which affected the strength of the trough. Vertical superposition processes became important as two jets became superimposed over the mobile trough later on in its development. Baroclinic processes were not significant as low-level development did not occur with the genesis of the trough.

2. Conclusions

The mounting evidence from this research and previous studies points to downstream development as the primary mechanism for generating new mobile troughs. Both case studies presented in this research showed that downstream development was significant in the early stages of mobile trough genesis. Baroclinic processes were expected to be more important over a more favorable environment such as our study region; however, the results presented in this research failed to show that. Type A cyclogenesis appears to be more rare than previously thought. Examination of more mobile trough genesis events that occur over the study region might help foster the hypothesis that Type A cyclone development, as envisioned in early theories, may not occur in the atmosphere.

The effect of strong jet streams should not be underestimated either. Barotropic deformation was shown in the second case to dramatically change the shape of the QGPV perturbation associated with the mobile trough. Deformation by the large-scale flow initially strengthened the trough, then weakened it with unfavorable stretching. Then, deformation strengthened the trough again as the stretching became favorable once more. Vertical superposition processes can be significant in this region when two jets at

different levels merge at the same location. The trough is strengthened by combining QGPV perturbations associated with each jet.

Both the downstream development mechanism and deformation by the large-scale flow were shown to be the most important factors in the development of these two mobile troughs. These findings confirm previous research which used QGPV to assess mobile trough development. Thus, further research into the interaction between the large-scale and mobile troughs should be undertaken. An investigation on the propagation of a *group* of Rossby waves is needed to ascertain the interactions that occur between the large scale and the mobile troughs. The development of a new mobile trough downstream due to a pre-existing trough appears to be closely related to the propagation of a group of Rossby waves.

REFERENCES

- Bjerknes, J., 1937: Theorie der aussertropischen Zyklonenbildung, *Meteor. Zeits.*, **54**, 462-466.
- Bosart, L. F., G. J. Hakim, K. R. Tyle, M. A. Bedrick, W. E. Bracken, M. J. Dickinson, and D. M. Schultz, 1996: Large-scale antecedent conditions associated with the 12-14 March 1993 cyclone ("superstorm '93") over eastern North America. *Mon. Wea. Rev.*, **124**, 1865-1891.
- Bretherton, F. P. 1966: Critical layer instability in baroclinic flows. *Quart. J. Roy. Meteor. Soc.*, **92**, 325-332.
- Carlson, T. N., 1991: *Mid-Latitude Weather Systems*. Harper Collins Academic, 507 pp.
- Chang, J. G., 1993: Downstream development of baroclinic waves as inferred from regression analysis. *J. Atmos. Sci.*, **50**, 2038-2053.
- Charney, J. G., 1947: The dynamics of long waves in baroclinic westerly current. *J. Meteor.*, **4**, 135-163.
- , and M. E. Stern, 1962: On the stability of internal baroclinic jets in a rotating atmosphere. *J. Atmos. Sci.*, **19**, 159-172.
- Chen, S., J. Kuo, Y. H. Zhang, and Q. F. Bai, 1991: Synoptic climatology of cyclogenesis over East Asia, 1958-1987. *Mon. Wea. Rev.*, **119**, 1407-1418.
- Davis, C. A., and K. A. Emanuel, 1991: Potential vorticity diagnostics of cyclogenesis. *Mon. Wea. Rev.*, **119**, 1929-1953.
- Eady, E. T., 1949: Long waves and cyclone waves. *Tellus*, **1**, 33-52.
- Gold, D., 1996: A quantitative analysis of baroclinic instability in extratropical cyclogenesis. M. S. thesis, Texas A&M University, 102 pp.
- Holopainen, E., and J. Kaurola, 1991: Decomposing the atmospheric flow using potential vorticity framework. *J. Atmos. Sci.*, **48**, 2614-2625.
- Holton, J. R., 1992: *An Introduction to Dynamic Meteorology*. Academic Press, 511 pp.
- Hoskins, B. J., and P. Berrisford, 1988: A potential vorticity perspective of the storm of 15-16 October 1987. *Weather*, **23**, 122-129.

- , M. E. McIntyre, and A. W. Robertson, 1985: On the use and significance of isentropic potential vorticity maps. *Quart. J. Roy. Meteor. Soc.*, **111**, 877-946.
- Kalnay, E., M. Kanamitsu, R. Kistler, W. Collins, D. Deaven, L. Gandin, M. Iredell, S. Saha, G. White, J. Woollen, Y. Zhu, M. Chelliah, W. Ebisuzaki, W. Higgins, J. Janowiak, K. C. Mo, C. Ropelewski, J. Wang, A. Leetmaa, R. Reynolds, R. Jenne, and D. Joseph, 1996: The NCEP/NCAR 40-year reanalysis project. *Bull. Amer. Meteor. Soc.*, **77**, 437-471.
- Kanamitsu, M., 1989: Description of the NMC global data assimilation and forecast system. *Wea. Forecasting*, **4**, 335-342.
- Kuo, H.-L. 1949: Dynamic instability of two-dimensional nondivergent flow in a barotropic atmosphere. *J. Meteor.* **6**, 105-122.
- Lefevre, R. J., 1995: Using the quasigeostrophic potential vorticity height tendency equation to diagnose the development of midtropospheric mobile troughs. Ph. D. dissertation, Texas A&M University, 220 pp.
- , and J. W. Nielsen-Gammon, 1995: An objective climatology of mobile troughs in the Northern Hemisphere. *Tellus*, **47A**, 638-655.
- Maddox, R. A., 1983: Large-scale meteorological conditions associated with mid-latitude mesoscale convective complexes. *Mon. Wea. Rev.*, **111**, 1475-1493.
- McEver, G. D., 1996: Mobile trough genesis over the Mongolian Plateau. M. S. thesis. Texas A&M University, 112 pp.
- Nielsen-Gammon, J. W., 1995: Dynamical conceptual models of upper-level mobile trough formation: Comparison and application. *Tellus*, **47A**, 705-721.
- , and R. J. Lefevre, 1996: Piecewise tendency diagnosis of dynamical processes governing the development of an upper-tropospheric mobile trough. *J. Atmos. Sci.*, **53**, 3120-3142.
- Orlanski, I., and E. K. M. Chang, 1993: Ageostrophic geopotential fluxes in downstream and upstream development of baroclinic waves. *J. Atmos. Sci.*, **50**, 212-225.
- , and J. Katzfey, 1991: The life cycle of a cyclone wave in the Southern Hemisphere. Part I: Eddy energy budget. *J. Atmos. Sci.*, **48**, 1972-1998.
- , and J. Sheldon, 1993: A case of downstream baroclinic development over western North America. *Mon. Wea. Rev.*, **121**, 2929-2950.

- Petterssen, S., 1955: A general survey of factors influencing development at sea level. *J. Meteor.*, **12**, 36-42.
- , and S. J. Smebye, 1971: On the development of extratropical cyclones. *Quart. J. Roy. Meteor. Soc.*, **97**, 457-482.
- Press, W. H., S. A. Teukolsky, W. T. Vetterling, and B. P. Flannery, 1992: *Numerical Recipes in FORTRAN: The Art of Scientific Computing*. Cambridge University Press, 963 pp.
- Rhea, J. O., 1966: A study of thunderstorm formation along drylines. *J. Appl. Meteor.*, **5**, 58-63.
- Rivest, C., C. A. Davis, and B. F. Farrell, 1992: Upper-tropospheric synoptic-scale waves. Part I: Maintenance and excitation of quasi-modes. *J. Atmos. Sci.*, **49**, 2108-2138.
- , and B. F. Farrell, 1992: Upper-tropospheric synoptic-scale waves. Part II: Maintenance and excitation of quasi-modes. *J. Atmos. Sci.*, **49**, 2120-2138.
- Rotunno, R., and M. Fantini, 1989: Petterssen's "Type B" cyclogenesis in terms of discrete, neutral Eady modes. *J. Atmos. Sci.*, **46**, 3599-3602.
- Sanders, F., 1986: Explosive cyclogenesis in the west-central North Atlantic Ocean, 1981-1984. Part I: Composite structure and mean behavior. *Mon. Wea. Rev.*, **114**, 1781-1794.
- , 1988: Life history of mobile troughs in the upper westerlies. *Mon. Wea. Rev.*, **116**, 2629-2648.
- Snyder, C. and R. S. Linden, 1988: Upper-level baroclinic instability. *J. Atmos. Sci.*, **45**, 2445-2459.
- Staley, D. O., 1988: Baroclinic instability in the upper troposphere. *J. Atmos. Sci.*, **45**, 3298-3302.
- Thorncroft, C. D., B. J. Hoskins, M. E. McIntyre, 1993: Two paradigms of baroclinic-wave life cycle behavior. *Quart. J. Roy. Meteor. Soc.*, **119**, 17-55.
- Wash, C. H., J. E. Peak, W. E. Calland, and W. A. Cook, 1988: Diagnostic study of explosive cyclogenesis during FGGE. *Mon. Wea. Rev.*, **116**, 431-451.

Whitaker, J. S., and A. Barcilon, 1992: Genesis of mobile troughs in the upper westerlies.
J. Atmos. Sci., **49**, 2097-2107.

APPENDIX

AN IMPROVED BASIC STATE FOR MOBILE TROUGH

RESEARCH

The basic state should represent the mean flow of the medium in which the evolving synoptic-scale waves are embedded. The success of piecewise tendency diagnosis, PTD, approach relies on using the central value of perturbation height as a measure of the intensity of the disturbance of interest. If the partitioning scheme does not isolate the perturbation from larger-scale features, then the intensity changes of the perturbation may not correspond closely to the intensification or weakening of the system.

A spherical harmonic wavenumber truncation has been used in previous mobile trough genesis research to partition the large-scale flow from the mobile troughs. This scheme partitions the desired features in the perturbation scale. However, some of the basic state make be placed in the perturbation field, as evidenced by persistent small-scale anomalies that reside where semi-permanent circulation features exist (e.g., subtropical highs, jet streams) To retain in the basic state small-scale features that move little with time, a time average of the perturbation field was calculated over the lifetime of the mobile trough.

Mathematically, the basic state used in this research can be written in the following manner:

$$\bar{\phi} = \bar{\phi}_{k=1,m} + \tilde{\phi}'_{k=(m+1),15} \quad (A1)$$

(Primes represent perturbations, and overbars represent basic states. The tilde represents

a time average.). The base state is composed of the spherical harmonic wavenumbers 1 to m plus a time-mean of the perturbation spherical harmonic wavenumbers m to 15, where m is defined as the cut-off for the large scale. This process was applied to geopotential height, QGPV, and their corresponding boundary conditions.

A comparison of the two basic states shows that the basic state used in this research (in black contours) contains a more robust subtropical ridge and a more concentrated height gradient over the location of the jet stream in the October 1988 mobile trough genesis case study (Fig. A1a). The time-mean component of the perturbation scale wavenumbers up to 15 is seen in figure A1b.

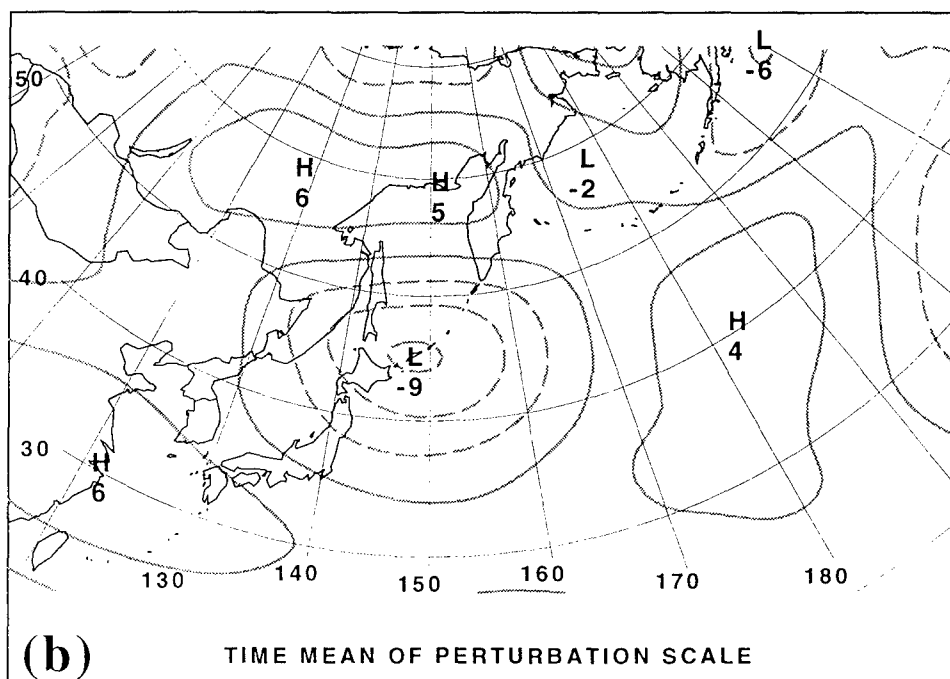
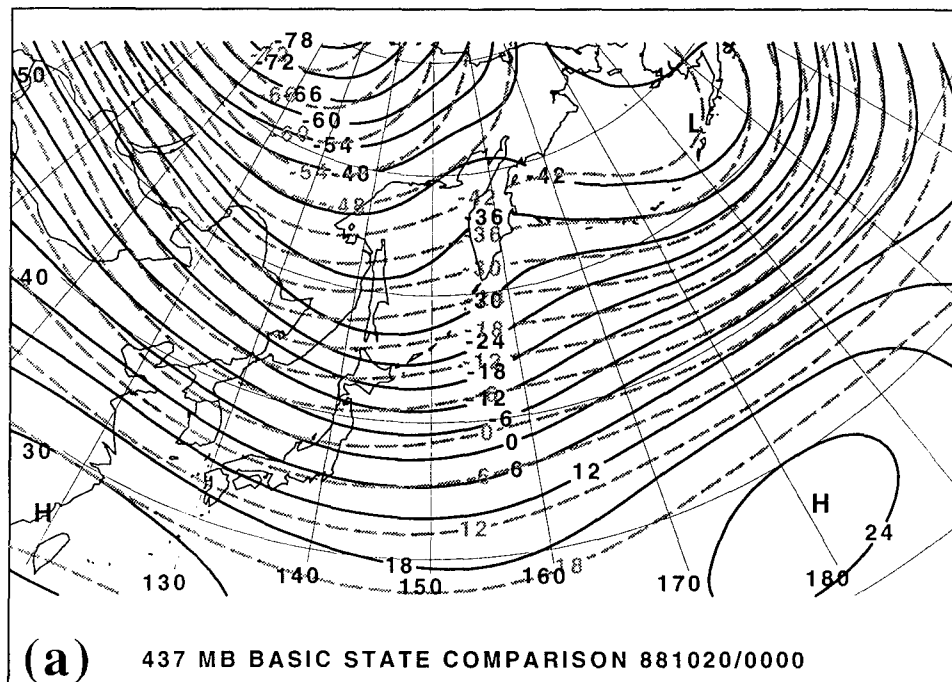


Fig. A1. Basic state comparison for 0000 UTC 20 October 1988. (a) Basic state 437 mb height field (gray, dashed) containing only large-scale total wavenumbers 0-8, and same basic state plus a time-mean component of total wavenumbers 9-15 (black) (contour interval for both fields, 6 dam); (b) 437 mb height (contour interval 3 dam, negative contours dashed) time-mean component of total wavenumbers 9-15.

~~Wichita, Texas 76001~~